

Elucidating 2-deoxy-2-fluoro-D-glucose translocation, metabolism, and application in plants

Dissertation

To Fulfill the
Requirements for the Degree of
„Doctor rerum naturalium“ (Dr. rer. nat.)

**Submitted to the Council of the Faculty of Biology and Pharmacy
of the Friedrich Schiller University Jena**

**by Fatangare, Amol Bhagirath (M.Sc. & M.Tech. in Biotechnology)
born on 30th Sept 1985 in Sangamner, India.**

Reviewers:

1. Prof. Dr. Jonathan Gershenzon

Director, Department of Biochemistry, Max Planck Institute-Chemical ecology, Hans-Knöll-Straße 8, D-07745 Jena, Germany

Phone: +49 3641 57 1300 E-mail: gershenzon@ice.mpg.de

2. Prof. Dr. Ulrich Schurr.

Forschungszentrum Jülich, IBG-2, Wilhelm-Straße Johnen, 52428 Jülich. Germany

phone: +49 2461 61 3073 E-mail: u.schurr@fz-juelich.de

3. Prof. Dr. Hans Peter Saluz

Head, Cell and Molecular Biology, Hans Knöll Institute, Beutenbergstr. 11a,D-07745 Jena, Germany

Phone: +49 3641 532 1201 E-mail: hanspeter.saluz@leibniz-hki.de

Date of Defense: 25th June 2015

Table of contents

1. Introduction	1
1.1 Isotopes as tracers in the study of chemical processes	1
1.2 Radiotracer imaging	2
1.3 Radiotracers in imaging	3
1.4 2-Deoxy-2-fluoro-D-glucose (FDG)	4
2.1 FDG in plant imaging	5
2.2 FDG metabolism in plants	7
2.3 FDG to study carbon allocation in plants after herbivore attack	8
2. Overview of Manuscripts.....	11
2.1 FDG in plant imaging	11
2.2 FDG metabolism in plants	12
2.3 FDG to study carbon allocation in plants after herbivore attack	13
3. Research Chapter I	15
Comparing 2-deoxy-2-[¹⁸ F]fluoro-D-glucose and [⁶⁸ Ga]gallium-citrate translocation in <i>Arabidopsis thaliana</i>	
4. Research Chapter II.....	29
Unravelling 2-deoxy-2-fluoro-D-glucose metabolism in <i>Arabidopsis thaliana</i>	
5. Research Chapter III	71
Using 2-deoxy-2-[¹⁸ F]fluoro-D-glucose to study carbon allocation in plants after herbivore attack	
5. General Discussion	97
6. Summary	109
7. Zusammenfassung.....	111
8. References	115
9. Acknowledgement	127
10. Curriculum Vitae	129
11. Eigenständigkeitserklärung.....	131

Abbreviations:

¹⁸ FDG	2-Deoxy-2[¹⁸ F]-fluoro-D-glucose
¹⁹ FDG	2-Deoxy-2[¹⁹ F]-fluoro-D-glucose
FDG	2-Deoxy-2-fluoro-D-glucose (¹⁸ FDG/ ¹⁹ FDG)
<i>Arabidopsis</i>	<i>Arabidopsis thaliana</i>
<i>Nicotiana</i>	<i>Nicotiana attenuata</i>
<i>M. sexta</i>	<i>Manduca sexta</i>
F	Fluorine
Radiotracer	Radioisotope labeled compound
MS	Mass spectrometry
MS/MS	Tandem mass spectrometry
NMR	Nuclear magnetic resonance spectroscopy
UHPLC	Ultra high performance liquid chromatography
PET/CT	Positron emission tomography/computed tomography
t _{1/2}	Radioactive half life
⁶⁸ Ga-citrate	⁶⁸ Gallium citrate
IP	Photostimulable phosphor-coated imaging plate
PPIS	Planar positron imaging system
MRI	Magnetic resonance imaging
FDG-6-P	FDG-6-phosphate
FDG-1-P	FDG-1-phosphate
F-gluconic acid	2-deoxy-2-fluorogluconic acid
F-maltose	2-Deoxy-2-fluoromaltose
FDM	2-Deoxy-2-fluoro-D-mannose
UDP	Uridine diphosphate
FDG-1,6-biP	FDG-1,6-biphosphate
JA	Jasmonic acid
Me-JA	Methyl-jasmonate
JA-Ile	JA-isoleucine
<i>irCOII</i>	invert repeat-CORONATINE INSENSITIVE 1 <i>Nicotiana</i> line
DPE2	cytosolic glucosyltransferase disproportionating enzyme 2
FACs	Fatty acid-amino acid conjugates
ABA	Abscissic acid
CK	Cytokinin
GA	Gibberellic acid
IAA	Indole acetic acid
ATP	Adenosine triphosphate

Introduction

My research elucidates the translocation and metabolism of 2-deoxy-2-fluoro-D-glucose (FDG), a radioactive glucose analogue, in model plant species *Arabidopsis thaliana* (*Arabidopsis*). In this work, I showed that FDG radioactivity distribution in plants was specific to the chemical nature of the supplied radiotracer and [F] radioactivity was mainly translocated via phloem with its distribution closely matching with photoassimilate distribution. Furthermore, to explore its applicability in *in vivo* plant imaging, I successfully demonstrated PET/CT imaging measurement using preclinical micro-PET/CT scanner. Secondly, I characterized FDG metabolism in *Arabidopsis* leaves using combination of MS and NMR spectroscopy techniques to shed light on metabolic fate of FDG in plants. Finally, I showed that FDG could be employed to study carbon allocation dynamics in *Nicotiana attenuata* (*Nicotiana*) plants after specialist herbivore- *Menduca sexta* (*M. sexta*) attack.

1. General Introduction

1.1 Isotopes as tracers in the study of chemical processes

"If you are worth your salt, you separate radium D from all that nuisance of lead." These were the words of Professor Ernest Rutherford to young chemist 'George de Hevesy' who was tasked with the responsibility of separating radioactive lead (Pb-210) from its admixture non-radioactive lead [Myers W. G., 1979]. Hevesy tried for two year to separate radioactive Pb-210 from its counterpart but failed. However, he did not fail to recognize the remarkable sensitivity of physical methods to detect infinitesimally small amounts of radioactive Pb-210 which makes it excellent radiotracer to trace non-radioactive Pb in chemical and biochemical processes. This was reflected in his 1923 paper about tracing the absorption and translocation of lead in *Vicia faba* plants. This was the start and it culminated in the foundation of very important field - Nuclear medicine and imaging. Hevesy was awarded "the 1943 Nobel Prize in Chemistry" in 1944 for his work on the use of isotopes as tracers in the study of chemical processes [www.nobelprize.org].

In the field of observation, Chance favors the prepared mind. Loius Pasteur (7 December 1854) [www.en.wikiquote.org].

1.2 Radiotracer imaging

Field of radiotracer imaging involves application of radioisotopes to analyze uptake and distribution of radioisotope labeled compounds (radiotracers) which could help in understanding underlying physiology or diagnostics. In actual experimental application, radioisotope is integrated or combined with compound of interest to form radiotracer. This radiotracer is then can be administered into organisms either plant or animal. Administered radiotracer is distributed via circulation or vascular system and taken up in various tissues depending upon the physiology of an organism. After allowing sufficient time for distribution, one can localize radiotracer using radiotracer detection techniques. High sensitivity of radiotracer detection techniques allows differentiating the subtle changes in the uptake, circulation and distribution pattern of fed radiotracer. These changes are analyzed to unravel the various aspects of actual physiology of the organism based on cellular functions related to the fed radiotracer. This way, radiotracers have been employed to assess particular biochemical or disease process in the body, based on the cellular function and physiology relevant to applied radiolabeled compound. Radiotracer imaging has been extensively used in clinical or animal studies involving tumor diagnostics, evaluating disease progression, functional brain imaging and studying physiological and biochemical pathways [Barrio et al, 1990; Alavi et al, 1982; Phelps ME, 2004; Schieferstein and Ross, 2013].

Radiotracer imaging is also being adapted to the new discipline of molecular medicine as it involves application of various radiotracers that are specific for particular biochemical or disease processes. Imaging probes (diagnostics) and drugs (therapeutics) share common concepts in structural design and principle of action as they target the same enzymes, receptors, and pathways [Som et al, 1977; Lampidis et al, 2006; Phelps ME, 2004; Zissen et al, 2011]. Thus, these radiotracers are aimed at not only to detect the underlying disease processes but also to target the relevant enzymes or receptors which could help restore normal physiology [Lampidis et al, 2006; Conrad et al, 2007; Zissen et al, 2011]. Developing new radiotracer agents, discovering novel applications for pre-existing radiotracers, and improving radiotracer imaging techniques have a tremendous impact in medicine and biology especially in the discipline of clinical diagnostics. Thus, development of new radiotracers, radiotracer validation, and establishing their applications in diagnostics or imaging are major thrust areas in current radiotracer research.

1.3 Radiotracers in imaging:

An isotope tracer is a chemical compound in which one or more atoms have been replaced by a corresponding isotope so by virtue of its physico-chemical properties such as differential mass, vibrational mode, or radioactive decay, it can be used to trace that isotope labeled compound. They can be divided into two categories mainly stable isotope (^2H , ^{13}C , ^{15}N , ^{18}O , ^{19}F etc.) labeled tracers and radioisotope (^3H , ^{11}C , ^{13}N , ^{14}C , ^{18}F , ^{32}P etc.) labeled tracers [Matwiyoff and Ott, 1973; Wolfe and Chinkes, 2005; Phelps ME, 2004]. Among the isotope tracers, radiotracers could allow for non-invasive detection in tissue owing to radioactive decay. However, most of the long-lived radiotracer (eg. ^{14}C , ^{32}P , ^{35}S etc) emits low energy β^- particles which cannot penetrate thick tissue. It necessitates destructive harvesting for analysis of radioisotope distribution [Dickson et al, 1990; Margolis et al, 1991]. Thus, these radiotracers are rarely used to examine the *in vivo* radiotracer dynamics in an organism. *In vivo* imaging is rather achieved using positron-emitting radioisotope (like ^{11}C , ^{13}N , ^{15}O , ^{68}Ga , ^{18}F etc) labeled compounds (PET-radiotracers or simply radiotracers) [Kiser et al, 2008; Jahnke et al, 2009; De Schepper et al, 2013; Converse et al, 2013]. Overview of such PET-radiotracer imaging process has been depicted in Fig. 1. A positron-emitting radioisotope emits a positron, which gives rise to two antiparallel high energy gamma ray photons upon its impact with and consequential annihilation by an electron [see inset, Fig. 1]. The resultant gamma photons are able to penetrate thick tissue and allow for the detection of a radioisotope without destructive tissue harvesting. Several characteristics make PET-radiotracers as radiotracers of choice. These positron radioisotope labeled compounds can be prepared with high specific activity. They can be detected in infinitesimally low concentrations and in a quantitative manner with the help of highly sensitive modern detectors. The short half-lives of these radioisotopes result in measureable radioactive decay time course permitting their application in highly dynamic processes such as measurement of substrate concentrations, reaction rates and ligand-receptor binding. Also, radioactivity disappears from subject tissue in short time so it's amenable to use in human studies.

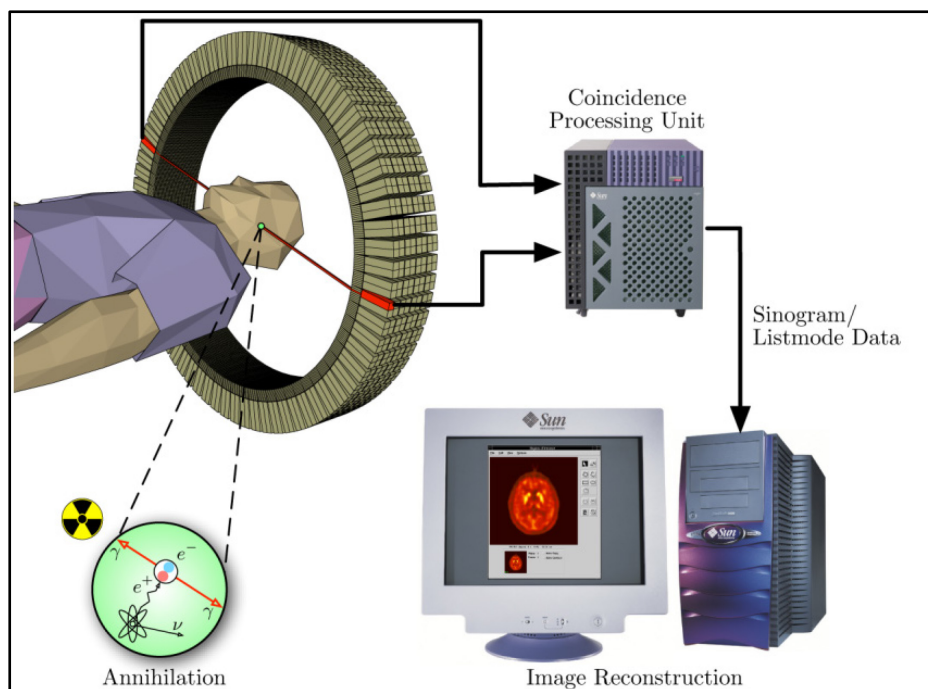


Fig. 1 Overview of PET imaging (wikimedia.org)

1.4 2-deoxy-2- ^{18}F fluoro-D-glucose (^{18}F FDG/FDG):

One of the above mentioned PET radioisotopes, ^{18}F , is most routinely used isotope to provide labeled substrate analogs (e.g., ^{18}F FDG, 5-fluorouracil) [Heidelberger et al, 1957; Som et al, 1980; Zissen et al, 2011] or pharmacological agents (e.g., ^{18}F -spiperone, fluoro-L-DOPA) [Barrio et al, 1989; Barrio et al, 1990] to trace biochemical or pharmacological processes in clinical diagnosis. ^{18}F has commonly been used to replace $-\text{H}$ or $-\text{OH}$ on a molecule of interest. Fluorine has small atomic size and the $\text{C}-\text{F}$ bond strength is comparable to that of $\text{C}-\text{H}$ and $\text{C}-\text{OH}$ bond. Small atomic radius of fluorine does not impose any structural constraints in the molecule. Thus, resulting fluorinated species is a structural analog of molecule of interest which is still be able to conjugate with the target compound with minimal steric hindrances. Moreover, fluorine is not known to occur naturally in compounds of biological origin so fluorine substitution in biological compound may block, with target enzymes, the biochemical pathway [Phelps ME, 2004].

^{18}F FDG is ^{18}F -labeled glucose analog in which $-\text{OH}$ group at C2' position of glucose has been replaced by ^{18}F [Fig. 2]. ^{18}F FDG chemically and structurally mimics glucose and its uptake and distribution is found to be similar to that of glucose in animal system [Som et al, 1977; Som et al, 1980]. ^{18}F FDG is commonly used as a radioactive glucose surrogate in medical

diagnostics and animal studies to trace uptake and metabolism of glucose in metabolically active tissue such as brain tissue or cancer cells [Som et al, 1980; Alavi et al, 1982; Ung et al, 2007]. ^{18}F has a radioactive half life ($t_{1/2}$) of 109.8 min [www.nndc.bnl.gov/chart/]. Consequently, ^{18}F FDG owing to its longer half life time, compared to other PET radiotracers, is more suitable radiotracer (for eg: ^{11}C , $t_{1/2}$ = 20.4 min) [www.nndc.bnl.gov/chart/] for *in vivo* imaging studies spanning over several hours. In addition, the mean dispersion range of emitted positron is shortest of all thus allowing resolution in mm range [Sanchez-Crespo et al, 2004].

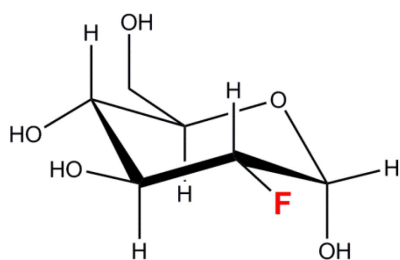


Fig. 2 2-deoxy-2- ^{18}F fluoro-D-glucose (^{18}F FDG)

2. Exploring FDG as a radiotracer for plant imaging

In this section, I will provide short introduction to subsequent chapters of my thesis which deals with

2.1 FDG in plant imaging.

2.2 FDG metabolism in plants

2.3 FDG to study carbon allocation in plants after herbivore attack

2.1 FDG in plant imaging

The application of ^{18}F FDG as a radiotracer for glucose has been well established in animal system but it has rarely been used in the plant imaging experiments. ^{18}F FDG application in plant imaging started when Tsuji et al (2002) first reported ^{18}F FDG uptake and distribution in tomato plants [Tsuji et al, 2002]. Later, Hattori et al (2008) described ^{18}F FDG translocation in intact *Sorghum* plant and suggested that it could be used as a tracer for photoassimilate translocation in plants [Hattori et al, 2008]. Recently, ^{18}F FDG has been used to study glycoside biosynthesis in plants as a measure of plant response to defense induction [Ferrieri et al,

2012]. There is growing evidence that ^{18}F FDG could also be used in plant imaging studies to trace sugar dynamics. However, to confirm this hypothesis, it was necessary to show that the observed [^{18}F] radioactivity translocation and distribution in an intact plant is an outcome of the chemical nature of the introduced radiotracer and not of the plant vascular architecture or radiotracer introduction method.

To prove this, we employed two chemically distinct radiotracers, ^{18}F FDG and ^{68}Ga Gallium citrate (^{68}Ga -citrate) for plant imaging. Here, ^{18}F FDG is a known glucose analog whereas Ga-citrate is a radiotracer whose chemical nature is similar to Aluminum (Al) or Iron (Fe) citrate. ^{68}Ga was chelated with citrate to maintain its solubility. Gallium (Ga) is a rare element that has no known biological role in plants; however, a positron emitting radioisotope [^{68}Ga] ($t_{1/2}=67.7$ min) [www.nndc.bnl.gov/chart/] is readily available in Ga. It has been shown that Ga could be taken up by the roots and transported to shoot [Wheeler and Power, 1995]. To show that the observed [^{18}F] radioactivity translocation and distribution pattern differs according to the chemical nature of introduced radiotracer, we introduced ^{18}F FDG and ^{68}Ga -citrate, in the model plant species *Arabidopsis* through leaf. We monitored corresponding radioactivity distribution pattern as an outcome of chemical nature of supplied radiotracer. We also established translocation route for [^{18}F] radioactivity by performing imaging experiments with stem girdled plants.

In plant radiotracer imaging experiments, radiotracer localization is generally monitored using a photostimulable phosphor-coated imaging plate (IP) to obtain static image of radiotracer distribution [Thorpe et al., 2007; Hattori et al., 2008; Ferrieri et al., 2012]. Recently, planar positron imaging system (PPIS) [Kume et al., 1997; Uchida et al., 2004; Matsushashi et al., 2006] or positron emission tomography (PET) scanner have been employed to obtain dynamic radiotracer distribution [Jahnke et al, 2009; De Schepper et al, 2013; Converse et al, 2013; Partelová et al, 2014]. Unlike IP or PPIS, positron emission tomography (PET) scanner could capture 3-dimensional radiotracer distribution over time. In *in vivo* imaging, radiotracer dynamics information is complemented with corresponding anatomical information to provide spatial distribution of metabolic or biochemical activity which is precisely aligned with underlying tissue. Anatomical information could be acquired using techniques like magnetic resonance imaging (MRI) [Borisjuk et al, 2012; Jahnke et al., 2009] or X-ray computed tomography (CT) [Dhondt et al., 2010]. Jahnke et al (2009) demonstrated a MRI-PET co-registration system which combined the anatomical information

of plants structures obtained from MRI with [^{11}C] radioactivity information obtained from PET. We used a bi-functional PET/CT modality which coupled the morphological information of a plant derived from CT with the corresponding radioactive signal derived from PET to generate 4-dimensional radiotracer dynamics. In this study, we report the first bi-functional PET/CT imaging of plants and discuss its potential applications in plant biology.

2.2 FDG metabolism in plants

Unraveling ^{18}F FDG translocation and metabolism in plants are crucial aspects of establishing ^{18}F FDG as potential radiotracer for plant imaging. Previous literature reported [^{18}F] radioactivity translocation and distribution pattern in plants however did not provide comprehensive picture of ^{18}F FDG metabolism in plant cells [Tsuji et al, 2002; Hattori et al., 2008; Ferrieri et al., 2012; Partelová et al, 2014]. FDG metabolism in plant cells is not characterized but rather presumed to be similar to FDG metabolism in animal tissue. FDG uptake and metabolism has been extensively studied in animal cells [McSheehy *et al.*, 2000; Kaarstad *et al.*, 2002; Southworth *et al.*, 2003]. Being glucose analogue, FDG is transported into animal cells via same transporters as glucose [Higashi et al, 1998; Brown et al, 1999; Yen et al, 2004]. Upon intracellular uptake, FDG is phosphorylated to FDG-6-phosphate (FDG-6-P) by the action of hexokinase [Sols and Crane, 1954; Bessell et al, 1972; Smith TA, 2001]. It was assumed that FDG-6-P underwent no further metabolism and simply accumulated inside the cell [Miller and Kiney, 1981; Reivich et al, 1985; Bessell and Thomas, 1973; Suolinna et al, 1986].

FDG metabolism in plants might be quite different than in animal cells as plants are specialist in sugar metabolism. Plants fix atmospheric CO_2 through photosynthesis. Fixed carbon is transformed to various sugars such as glucose, fructose, maltose, sucrose, and starch etc. as per the metabolic needs of the plant. These various sugars are then transported via numerous sugar transporters towards specialized organelles like plastids, vacuoles or organs like fruits, tubers for storage or utilization. Intrinsic complexity of biochemical pathways pertaining to sugar metabolism makes it harder to envisage the metabolic fate of FDG in plants. Thus, unraveling the FDG metabolism in plants is most logical step to follow after the ^{18}F FDG radiotracer imaging studies.

In present study (chapter 2), we analyzed FDG metabolism in *Arabidopsis* leaf tissue using 2-Deoxy-2- ^{19}F fluoro-D-glucose (^{19}F FDG) which contains stable ^{19}F fluorine isotope. ^{19}F FDG is

virtually similar to ^{18}F FDG in its chemical properties. Thus, its results could be extrapolated to ^{18}F FDG metabolism in *Arabidopsis*. We applied ^{19}F FDG to *Arabidopsis* leaf and analyzed leaf extract for fluorine-metabolites using MS and NMR. We demonstrated that FDG metabolism in plant cells is considerably different than animal cells and goes beyond FDG-6-P.

2.3 FDG to study carbon allocation in plants after herbivore attack

Photoassimilate allocation and partitioning are the key factors controlling plant growth and productivity [Zamski and Schaffer, 1996]. Along with current metabolic needs of the plant, numerous abiotic (light, temperature, CO_2 , water/salt stress etc.) and biotic factors (microbes, parasites, parasitic plants etc.) affect photoassimilate partitioning in plants [Lemoine et al, 2013]. Growth rate and biomass productivity in plants is highly influenced by such photoassimilate dynamics. Thus, there has been considerable interest in studying dynamics of photoassimilate allocation and partitioning under various environmental conditions [Babst et al, 2005; Ferrieri et al, 2013; Nour-eldin and Halkier 2013] and stress treatments, especially herbivory as one of them.

Upon wounding or herbivore attack plants divert resources in production of secondary defence metabolites, into storage tissue away from attack, or into growth processes. These processes are important to elucidate evolution of resistance and tolerance strategies of plants [Schwachtje and Baldwin, 2008]. Plant defenses are costly to invest in as it primary resources are redirected into defense pathways [Heil and Baldwin, 2002; Zavala and Baldwin, 2006; Bolton MD, 2009; Ferrieri et al, 2013]. Jasmoic acid (JA) and JA-conjugates such as methyl-jasmonate (Me-JA) or JA-isoleucine (JA-Ile) play important role in induction of defense responses in plants [Kang et al, 2006; De Geyter et al, 2012; Ferrieri et al, 2013]. Although, induction of defense pathways protect plant from herbivory, their activation can limit the availability of resources required for plant growth [Redman et al, 2001; Heil and Baldwin, 2002; Halitschke and Baldwin, 2003; Schwachtje and Baldwin, 2008; Meldau et al, 2012]. Instead of investing resources into defense compounds, plants may redirect resources away from affected tissue, often towards storage organs, such as roots [Holland et al, 1996; Babst et al, 2005; Schwachtje et al, 2006; Gomez et al, 2012]. The direction of resource re-allocation can change with environmental conditions and plant ontogeny.

Nicotiana attenuata a wild tobacco species that is native to western North America. It is a host plant for *Manduca sexta*, commonly known tobacco hornworm. *M. sexta*, a facultative

specialist, is able to tolerate nicotine, an antiherbivore chemical produced by *Nicotiana* plants. *M. sexta* can severely defoliate *Nicotiana* in its native habitat [Steppuhn and Baldwin, 2007]. In such case, the herbivory-induced activation of both defense and tolerance responses is predicted to alter resource assimilation and source-sink relationships [Schwachtje and Baldwin, 2008]. However, it is not known, how the herbivory induced-JA pathway regulates carbon allocation balancing the trade-off between plant growth and defence. It is demonstrated that simulated herbivory increases partitioning of recently assimilated carbon to roots of *Nicotiana* plants [Schwachtje et al, 2006]. In contrast, Machado et al (2013) showed that simulated *M. sexta* herbivory decreased sugar and starch concentrations in the roots and reduced regrowth from the rootstock and flower production [Machado et al, 2013]. In present study (Chapter 3), we used ^{18}F FDG in simulated herbivory experiments to analyze carbon allocation in the root system. JA perception is found to be important in carbon allocation processes thus, we also assessed the role of the JA in herbivore-induced ^{18}F FDG distribution by using transgenic plants insensitive to JA (*irCOII*). In this plant line, CORONATINE INSENSITIVE 1 (COI1) is silenced by transformation with an inverted repeat construct [Paschold et al, 2007]. *irCOII* plants are insensitive to JA and could not up-regulate JA-mediated defenses upon wounding or herbivory [Paschold et al, 2007]. In *irCOII* plants, we observed that carbon allocation to roots is decreased significantly only in leaf wounding treatment but not in simulated herbivory. Thus, independent of JA-mediated defenses, JA perception is found to be important in carbon allocation processes.

In summary, this thesis describes FDG translocation, metabolism in plants and demonstrates its application to study carbon allocation dynamics under various biotic stresses. We hope, this will further our understanding of FDG metabolism in plants and expand the scope of applications of FDG in plant imaging.

Chapter 1

Comparing 2-deoxy-2-[^{18}F]fluoro-D-glucose and [^{68}Ga]gallium-citrate translocation in *Arabidopsis thaliana*

Amol Fatangare[#], Peter Gebhardt, Hanspeter Saluz, Aleš Svatoš^{*}

[#] *First author*

^{*} *Corresponding author*

2-Deoxy-2-[^{18}F]fluoro-D-glucose (^{18}FDG /FDG) is a glucose surrogate commonly used in clinical or animal imaging but rarely in plant imaging to trace glucose metabolism. In present work, we compared distribution of ^{18}FDG to that of [^{68}Ga]gallium citrate (^{68}Ga -citrate) in *Arabidopsis thaliana* plants to show that the corresponding radioactivity distribution pattern depends on the chemical nature of the fed radiotracer.

Autoradiography results showed that the radioactivity distribution pattern and translocation route observed after ^{18}FDG feeding is markedly different from that of ^{68}Ga -citrate. [^{18}F] radioactivity accumulated mostly in roots and young growing parts such as the shoot apex, which are known sinks for photoassimilate. [^{18}F] radioactivity translocation, in this case, occurred *via* phloem. [^{68}Ga] radioactivity, on the other hand, was translocated to neighboring leaves and its translocation occurred via both xylem and phloem. PET/CT modality was able to capture the dynamic radiotracer distribution and its results corroborated well with the autoradiography imaging. In summary, we demonstrated that radiotracer distribution did differ according to the chemical nature of the supplied radiotracer.

Built on idea conceived by: Amol Fatangare, Peter Gebhardt, Hans Peter Saluz, Aleš Svatoš

Experiments designed and performed by: Amol Fatangare, Peter Gebhardt.

Manuscript written by: Amol Fatangare, Peter Gebhardt, Hans Peter Saluz, Aleš Svatoš.

Published in Journal of Nuclear Medicine and Biology (2014) Oct;41(9):737-43.

<http://dx.doi.org/10.1016/j.nucmedbio.2014.05.143>.

Chapter 2

Unravelling 2-deoxy-2-fluoro-D-glucose metabolism in *Arabidopsis thaliana*

Amol Fatangare[#], Christian Paetz, Bernd Schneider, Hans Peter Saluz, Aleš Svatoš^{*}

[#] *First author*

^{*} *Corresponding author*

FDG's application in plant imaging necessitates successful FDG tracer kinetics model which could only be established after unraveling FDG translocation and its metabolism in plants. Yet, there were no reports on FDG metabolism in plants to back the FDG imaging studies. Here, we elucidated FDG metabolism in *Arabidopsis thaliana* leaf tissue. We fed 2-deoxy-2-[¹⁹F]fluoro-D-glucose (¹⁹FDG/FDG) which contains stable fluorine [¹⁹F] isotope, to *Arabidopsis* leaves and later extracted and analyzed the leaf tissue for end product of ¹⁹FDG metabolism using liquid chromatography coupled to mass spectrometry and nuclear magnetic resonance spectroscopy. We found 2-deoxy-2-fluorogluconic acid, FDG-6-phosphate, 2-deoxy-2-fluoromaltose, and uridine diphosphate-FDG as four major end products of FDG metabolism in *Arabidopsis* leaf tissue. Our results demonstrate that FDG metabolism in plant tissue goes beyond FDG-6-phosphate and is considerably different than that of animal cells.

Built on idea conceived by: Amol Fatangare, Hans Peter Saluz, Aleš Svatoš

Experiments designed and performed by: Amol Fatangare, Christian Paetz, Aleš Svatoš

Manuscript written by: Amol Fatangare, Christian Paetz, Aleš Svatoš

Manuscript in preparation.

Chapter 3

Using 2-deoxy-2-[^{18}F]fluoro-D-glucose to study carbon allocation in plants after herbivore attack

Stefan Meldau^{#*}, Melkamu Woldemariam[#], Amol Fatangare, Aleš Svatoš, Ivan Galis

First author

** Corresponding author*

Herbivory induced activation of both defense and tolerance response is predicted to alter resource allocation in plants. JA-signalling is also known to play a role in this process. Here, we investigated changes in recently assimilated carbon allocation using 2-deoxy-2-[^{18}F]fluoro-D-glucose (^{18}FDG /FDG) in *Nicotiana* roots following wounding and simulated leaf herbivory. Upon simulated herbivory, but not wounding alone, carbon partitioning specifically to the root tips was reduced. In jasmonate (JA) signalling-deficient *irCOII* plants, the wound-induced allocation of ^{18}FDG to the roots was decreased, while more ^{18}FDG was transported to young leaves, demonstrating an important role of the JA pathway in regulating the wound-induced carbon partitioning between shoots and roots. Our data highlight the use of ^{18}FDG to study stress-induced carbon allocation responses in plants.

Built on idea conceived by: Stefan Meldau, Melkamu Woldemariam, Amol Fatangare, Aleš Svatoš, Ivan Galis.

Experiments designed and performed by: Stefan Meldau, Melkamu Woldemariam, Amol Fatangare, Ivan Galis

Manuscript written by: Stefan Meldau, Melkamu Woldemariam, Amol Fatangare, Aleš Svatoš, Ivan Galis.

Manuscript submitted to BMC Research Notes (2014).

Chapter 1

Comparing 2-deoxy-2-[^{18}F]fluoro-D-glucose and [^{68}Ga]gallium-citrate translocation in *Arabidopsis thaliana*

Amol Fatangare[#], Peter Gebhardt, Hanspeter Saluz, Aleš Svatoš^{*}

[#] *First author*

^{*} *Corresponding author*



Contents lists available at ScienceDirect

Nuclear Medicine and Biology

journal homepage: www.elsevier.com/locate/nucmedbioComparing 2-[¹⁸F]fluoro-2-deoxy-D-glucose and [⁶⁸Ga]gallium-citrate translocation in *Arabidopsis thaliana*Amol Fatangare ^{a,1}, Peter Gebhardt ^b, Hanspeter Saluz ^{b,c}, Aleš Svatoš ^{a,*}^a Mass spectrometry/Proteomics research Group, Max Planck Institute for Chemical Ecology, Hans-Knöll-Straße 8, D-07745 Jena, Germany^b Department of Cell and Molecular Biology, Leibniz Institute for Natural Product Research and Infection Biology – Hans Knöll Institute, Beutenbergstr. 11a, D-07745 Jena, Germany^c Friedrich-Schiller-University Jena, D-07737 Jena, Germany

ARTICLE INFO

Article history:

Received 3 April 2014

Received in revised form 27 May 2014

Accepted 27 May 2014

Keywords:

Imaging

PET/CT

Plant

Photoassimilate

Translocation

ABSTRACT

2-[¹⁸F]fluoro-2-deoxy-D-glucose (¹⁸FDG) is a glucose surrogate commonly used in clinical or animal imaging but rarely in plant imaging to trace glucose metabolism. Recently, ¹⁸FDG has been employed in plant imaging for studying photoassimilate translocation and glycoside biosynthesis. There is growing evidence that ¹⁸FDG could be used as a tracer in plant imaging studies to trace sugar dynamics. However, to confirm this hypothesis, it was necessary to show that the observed ¹⁸FDG distribution in an intact plant is an outcome of the chemical nature of the introduced radiotracer and not of the plant vascular architecture or radiotracer introduction method.

Methods: In the present work, we fed ¹⁸FDG and [⁶⁸Ga]gallium-citrate (⁶⁸Ga-citrate) solution through mature *Arabidopsis thaliana* leaf and monitored subsequent radioactivity distribution using positron autoradiography. The possible route of radioactivity translocation was elucidated through stem-girdling experiments. We also employed a bi-functional positron emission tomography/computed tomography (PET/CT) modality to capture ¹⁸FDG radiotracer dynamics in one of the plants in order to assess applicability of PET/CT for 4-D imaging in an intact plant.

Results: Autoradiography results showed that [¹⁸F] radioactivity accumulated mostly in roots and young growing parts such as the shoot apex, which are known to act as sinks for photoassimilate. [¹⁸F] radioactivity translocation, in this case, occurred mainly via phloem. PET/CT results corroborated with autoradiography. [⁶⁸Ga] radioactivity, on the other hand, was mainly translocated to neighboring leaves and its translocation occurred via both xylem and phloem.

Conclusion: The radioactivity distribution pattern and translocation route observed after ¹⁸FDG feeding is markedly different from that of ⁶⁸Ga-citrate. [¹⁸F] radioactivity distribution pattern in an intact plant is found similar to the typical distribution pattern of photoassimilates. Despite its limitations in quantification and resolution, PET/CT could be a useful tool to elucidate *in vivo* dynamics of [¹⁸F] radioactivity in intact plants.

© 2014 Elsevier Inc. All rights reserved.

1. Introduction

Photoassimilate allocation and partitioning are the key factors controlling plant growth and productivity [1]. Photoassimilate translocation occurs via phloem and its partitioning is highly dynamic process. Along with current metabolic needs of the plant, numerous abiotic (light, temperature, CO₂, water/salt stress etc.) and biotic

factors (microbes, parasites, parasitic plants etc.) affect photoassimilate partitioning in plants [2]. Growth rate and biomass productivity in plants is highly influenced by such photoassimilate dynamics. Thus, there has been considerable interest in studying *in vivo* dynamics of photoassimilate translocation and partitioning under various environmental conditions [3–5].

Photoassimilate translocation and partitioning in plants has been studied using long-lived ¹⁴C radioisotope labeling [6–8]. However, detection of ¹⁴C distribution necessitates destructive harvesting of plant tissue (e.g., phenolics) [9]. Thus, ¹⁴C radiotracers are rarely used to study the photoassimilate translocation in an intact plant. *In vivo* imaging in plants has been achieved using a positron-emitting radioisotope (like ¹¹C, ¹³N, ¹⁵O and ¹⁸F) labeled compounds (radiotracers) [10]. Previously, ¹¹C radiotracers had been used to study carbon allocation in plants [11–14]. However, ¹¹C has the half-life (t_{1/2}) of 20.3 min [15] which limits its applicability to short time-scale experiments.

Abbreviations: AIDA, Advanced image data analyzer; ¹⁸FDG, 2-[¹⁸F]fluoro-2-deoxy-D-glucose; ⁶⁸Ga-citrate, [⁶⁸Ga]gallium citrate; [¹⁸F] radioactivity, ¹⁸FDG and/or its metabolites; [⁶⁸Ga] radioactivity, ⁶⁸Ga-citrate and/or its metabolites; IP, Imaging plate; PET, Positron emission tomography; CT, Computed tomography; CPS, Counts per second; MRI, Magnetic resonance imaging; Bq, Becquerel (SI unit of radioactivity); 4-D, 4-dimensional space; β⁺, Beta particles; OSEM 3D, Three-dimensional ordered subset expectation maximization algorithm; ROI, Region of interest; PSL, Photostimulated luminescence; FOV, Field of view.

* Corresponding author. Tel.: +49 3641571700; fax: +49 3641571701.

¹ First author.

<http://dx.doi.org/10.1016/j.nucmedbio.2014.05.143>

0969-8051/© 2014 Elsevier Inc. All rights reserved.

2-[^{18}F]fluoro-2-deoxy-D-glucose (^{18}FDG) is a radioactive glucose surrogate with a half-life of 109.8 min [15]. It is commonly used in medical diagnostics and animal studies to trace uptake and the metabolism of glucose in metabolically active tissue such as brain tissue or cancer cells [16] but rarely in plant imaging studies. Tsuji *et al* (2002) first reported ^{18}FDG uptake and distribution in tomato plants [17]. Later, Hattori *et al* (2008) described ^{18}FDG translocation in intact sorghum plants and suggested that it could be used as a tracer for photoassimilate translocation in plants [18]. Recently, ^{18}FDG has been used to study glycoside biosynthesis in plants as a measure of plant response to defense induction [19]. There is growing evidence that ^{18}FDG could also be used in plant imaging studies to trace sugar dynamics. To confirm this hypothesis, it was necessary to show that the observed ^{18}FDG distribution in an intact plant is an outcome of the chemical nature of the introduced radiotracer and not of the plant vascular architecture or radiotracer introduction method.

In the present work, we compared ^{18}FDG distribution with that of another chemically distinct radiotracer ^{68}Ga citrate (^{68}Ga -citrate). Here, ^{68}Ga was chelated with citrate to maintain its solubility. Gallium (Ga) is a rare element that has no known biological role in plants; however, a positron emitting radioisotope [^{68}Ga] ($t_{1/2} = 67.7$ min) is readily available in Ga [15]. The chemistry of Ga is very similar to that of aluminum (Al) and Iron (Fe). It has been shown that Ga could be taken up by the roots and transported to shoot [20]. Like Al, Ga is also known to cause plant toxicity [21]. Al toxicity is reversed by chelating it with organic acids and thus excluding it from entering the plant cell [22]. Citrate forms the one of the stable complexes with Al [23] and Al-citrate (1:1) does not show phytotoxicity [24]. With this logic, we assume that ^{68}Ga -citrate will be non-toxic to plant cells and can be used as radiotracer for plant imaging experiments. We introduced ^{18}FDG and ^{68}Ga -citrate, in the model plant species *Arabidopsis thaliana* through leaf and monitored radioactivity distribution pattern as an outcome of chemical nature of supplied radiotracer. With the help of stem-girdling experiments, we elucidated a possible route of [^{18}F] radioactivity translocation through plant vasculature.

Metabolite dynamics and distribution in an intact plant can be studied using non-invasive techniques which combine the morphological information of a plant with information about the distribution of its metabolites (e.g. combination of magnetic resonance imaging (MRI) and positron emission tomography (PET)) [25,26]. X-ray computed tomography (CT) is one of the imaging techniques which provides morphological and anatomical information about a plant [27]. PET is a radiotracer-imaging technique which captures radiotracer distribution in an intact plant [25,26,28]. We used a bi-functional PET/CT modality which coupled the morphological information of a plant derived from CT with the corresponding radioactivity signal derived from PET to generate 4-D radiotracer dynamics. PET/CT has been routinely used for animal or clinical imaging but not for plant imaging. In this article, we report PET/CT imaging of *Arabidopsis thaliana* plant to explore the applicability of PET/CT in plant imaging and discuss its potential applications in plant biology.

2. Materials and methods

2.1. Plant material and growth conditions

Arabidopsis thaliana Col-0 plants were used for all the experiments. *A. thaliana* seeds were stratified for 3 days at 4 °C and grown either in soil or hydroponically. In hydroponics, seeds were grown using Araponics™ system (www.araponics.com). We used a hydroponic medium [29] which consisted of 0.75 mM MgSO_4 , 1.5 mM Ca (NO_3)₂, 0.075 mM Na_2MoO_4 , 0.1 mM Na_2SiO_3 , 0.5 mM KH_2PO_4 , 1.25 mM KNO_3 , 0.072 mM FeCl_3 in EDTA, 0.002 mM ZnSO_4 , 0.01 mM MnSO_4 , 0.015 mM CuSO_4 , 0.05 mM H_3BO_3 , 0.05 mM KCl. Root aeration was provided by an air-pump (Rena 200) equipped with an air stone made up of mineral sand. For soil-grown plants,

vernalized seeds were placed in 10 cm round pots containing wet soil which consisted of 80% Fruhstorfer Nullerde™, 10% vermiculite, and 10% sand, fertilized with Triabon (1 g L⁻¹) and Osmocote Exact Mini (1 g L⁻¹) and treated with *Steinernema feltiae*. Plants were placed in a controlled environment growth chamber at 21 °C temperature and 60% humidity under long-day conditions. Light of intensity 190–220 $\mu\text{mol m}^{-2} \text{s}^{-1}$ was provided for 16 hours followed by 8 hours of dark. Hydroponically grown plants are used for all experiments unless otherwise mentioned.

2.2. ^{18}FDG imaging

^{18}FDG was ordered from the cyclotron facility at the Department of Nuclear Medicine, Bad Berka, Germany. On the day of the experiment, 4 week old plants were transferred from growth chamber to radiolaboratory. Radiotracer was externally fed to plants through mature rosette leaf. One of the mature rosette leaves was pricked at three spots, one on midrib and two on leaf lamina on either side of midrib, with micropipette tip and radiotracer solution was applied on pricked spots. Radiotracer solution was applied to leaf in the time frame of 8.00–10.00 am and it is noted as experiment start time. Plants were kept under normal laboratory room light and temperature conditions during the experimental period. Plants were harvested and autoradiographed 6 hours after radiotracer application.

2.3. ^{68}Ga -citrate imaging

^{68}Ga radioisotope is produced at the laboratory using $^{68}\text{Ge}/^{68}\text{Ga}$ generator by milking the generator one time to wash out the stable $^{68}\text{Zn}^{2+}$ as a decay product before the use of the second eluate for the radiotracer solution [30]. 200 μl of citric acid (0.05 M) and 50 μl of sodium acetate (1.1 M) were added as a buffer to the generator eluate. ^{68}Ga -citrate tracer solution was adjusted to pH 5 with sodium carbonate (2 M). Radiotracer was fed to plants as described previously. However, in case this case, considering the short half-life of [^{68}Ga] radioisotope, plants were harvested and autoradiographed 4 hours after radiotracer application.

2.4. Cauline leaf uptake

Four-to-five-week old soil grown plants with well-developed stems were selected. ^{18}FDG solution was fed to plant through cauline leaf as described previously.

2.5. Heat-girdling

Four-to-five-week old soil grown plants with well-developed stems were selected for the hot air stem girdling. The part of the stem above the intended girdling region was supported by a wooden support to retain the original plant architecture. The stem was heat-girdled by passing a hot air stream of 90 °C through an air nozzle held 2 cm from the stem and gradually revolving the nozzle for 20–30 sec [31]. Radiotracer was fed to plants as described previously. Above ground shoot was harvested and autoradiographed 4 hours after radiotracer application.

2.6. Autoradiography using IPs and radioactivity quantification

Plants were cut to various parts like shoot, rosette, radiotracer fed leaf and root. Plant parts were placed between 2 thin plastic sheets and autoradiographed using IP (BAS-MS2040, Fuji Film, Tokyo, Japan). IPs were scanned on FLA-3000 scanner (Fuji Film, Tokyo, Japan) at a spatial resolution of 50 μm . IP images were further edited and exported using advanced image data analyzer (AIDA) (<http://www.raytest.com>; software version 3.11.002). Raw IP data were analyzed using AIDA 2D-densitometry functionality to quantify the relative

radioactivity in each plant part. Region of interest (ROI) was defined for each plant part manually on the basis of radioactivity spread seen in IP image. Cumulative photostimulated luminescence (PSL) intensity in plant part was calculated by summing up the PSL intensities in corresponding ROI at each pixel. Background PSL intensity was calculated for a squared region on the same IP where it was not exposed to any plant part. Background PSL intensity was area corrected and subtracted from the cumulative intensity of a particular ROI to calculate net PSL intensity in that particular plant part. Similarly, intensities in different plant parts were measured and related as percentage of total plant radioactivity. The percentage allocation of [^{18}F] and [^{68}Ga] radioactivity in each plant part was compared using one-way ANOVA.

2.7. 4-D PET/CT imaging

PET/CT imaging of intact plant was performed using a Siemens Inveon PET/CT (Siemens Medical Solutions USA, Inc., Malvern, Pennsylvania, USA). This PET/CT system consists of two independently operating PET and CT modalities. The PET module has an effective transaxial field of view (FOV) of approximately 10 cm and an axial FOV of 12.7 cm and provides resolution better than 1.5 mm in the FOV [32,33]. The CT module consists of a cone beam micro X-ray source (50 μm focal spot size) and a 2048 \times 3072 pixel X-ray detector. A CT detector provides a FOV of 10 \times 10 cm (low resolution mode).

A. thaliana plant with stem heights of 3–5 cm was selected so as to fit into the PET/CT scanner. Plant was fixed vertically on a Styrofoam platform with roots immersed in 2 mL of aqueous solution. ^{18}F FDG was fed to one of the rosette leaves according to the method described previously. Plants were placed inside the thin plastic cylinder to minimize leaf movement due to air currents inside the scanner. The whole assembly was mounted on a PET/CT bed as shown in Supplemental Fig. 3A and B. First, computed tomography was performed, followed by PET data acquisition over a period of 6 hours. Micro-CT imaging was performed with 80 kV at 500 μA , 360° of rotation and 200 projections per bed position. The micro-CT images were reconstructed using a COBRA software package (http://www.exxim-cc.com/products_cobra.htm). All images were visualized and analyzed using IRW Software 2.2 (Inveon Research Workplace, Preclinical Solutions, Siemens Medical Solutions USA, Inc., Malvern, Pennsylvania, United States).

The PET data acquisition was carried out with default settings of the coincidence timing window of 3.4 ns and energy window of 350–650 keV. Attenuation was corrected on the basis of the CT measurements. The PET image was reconstructed using Fourier rebinning and the three-dimensional ordered subset expectation maximization (OSEM 3D) algorithm. The image matrix size was 256 \times 256 \times 159 and the requested resolution was 1.635 mm. A threshold was used to draw ROI, in order to scout for the small structures of the plant in the PET image. In case of the whole plant and ^{18}F FDG fed leaf, best scouting results were obtained using a threshold of 5–100% of maximum activity. For the roots and plant shoots, best scouting results obtained using a threshold of 50–100%. The ROIs defined using a threshold approach gave a very rough estimate of the volume and radioactivity of the given ROI.

3. Results

3.1. ^{18}F FDG imaging

The ^{18}F FDG uptake and distribution in plants ($n = 4$) were limited. PSL quantification data suggested that, on average, 20% of the net fed radioactivity was translocated to other plant parts (Fig. 1) while remaining radioactivity was retained in the radiotracer-fed leaf (Fig. 1). Intense radioactivity signal was visible in the leaf lamina and petiole of the ^{18}F FDG fed leaf (Fig. 2B), producing an overexposed

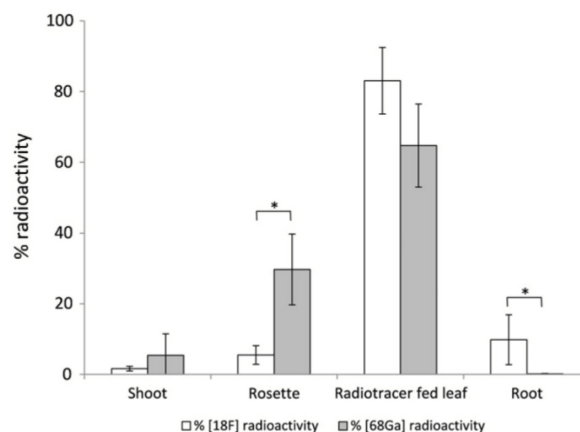


Fig. 1. Percentage radioactivity accumulated in each plant part. ^{18}F FDG or ^{68}Ga -citrate was fed to the plant ($n = 4$ for each radiotracer) through mature rosette leaf. 6 hours (in case of ^{18}F FDG) or 4 hours (in case of ^{68}Ga -citrate) after the feeding, plant were cut into shoot, rosette, radiotracer fed leaf, root and autoradiographed on phosphor imaging plate (IP). IP images were analyzed using AIDA 2-D densitometry to quantitate the percentage radioactivity accumulated in each plant part. Region of interest (ROI) was defined for each plant part manually. Net photostimulated luminescence (PSL) intensity in plant part was calculated by summing up the background corrected PSL intensities in corresponding ROI. Intensities in different plant parts were measured and related as percentage of total plant radioactivity. Bars represent percentage radioactivity in each plant part. Error bars represent mean \pm S.D. The percentage allocation of [^{18}F] and [^{68}Ga] radioactivity in each plant part was compared using one-way ANOVA and significant differences were denoted by * ($P < 0.05$). The differences in percentage allocation of [^{18}F] and [^{68}Ga] radioactivity for rosette and root were statistically significant.

region on the imaging plate. Translocated radioactivity distribution greatly varied from plant to plant due to varied plant morphology but nearly half of the translocated radioactivity accumulated in the roots, while the rest was partitioned into rosette leaves and shoot (Fig. 1). Radioactivity signal in shoot was more intense as compared to the mature leaves of the rosette (Fig. 2B). When ^{18}F FDG was fed through the cauline leaf, radioactivity was seen both above and below the portion of the stem to which the ^{18}F FDG-fed cauline leaf was attached (Fig. 3B). Radioactivity was seen partitioned to the other branches at nodal junctions (Fig. 3B).

3.2. ^{68}Ga -citrate imaging

When ^{68}Ga -citrate was fed to plants ($n = 4$) through one of the rosette leaves, about 35% of the net radioactivity was translocated to other plant parts (Fig. 1). Most of the translocated radioactivity translocated to the rosette leaves adjacent to radiotracer fed leaf irrespective of the developmental stages of the neighboring leaves (young or mature) (Fig. 2D). Radioactivity signal in these leaves was evenly spread across leaf lamina. The radioactivity signal in root was less intense compared to the radioactivity signal seen in mature or young leaves located near the ^{68}Ga -citrate fed leaf (Fig. 2D). Differences in relative accumulation of [^{18}F] and [^{68}Ga] radioactivity in rosette and shoot parts were significant ($P < 0.05$) (Fig. 1). When ^{68}Ga -citrate was fed through the cauline leaf, radioactivity was transported bi-directionally in the stem (Supplemental Fig. 3D).

3.3. Radiotracer transport across girdled regions of the stem

The application of hot air immediately causes the stem to turn pale blue and its diameter to shrink. Hot air girdling disrupts phloem transport, although xylem transport remains relatively unaffected [31]. In stem-girdled plants, when ^{18}F FDG was fed through one of the rosette leaves, radioactivity signal was distinctly observed until the girdled region (depicted by an arrow in Fig. 4A) on the stem but not

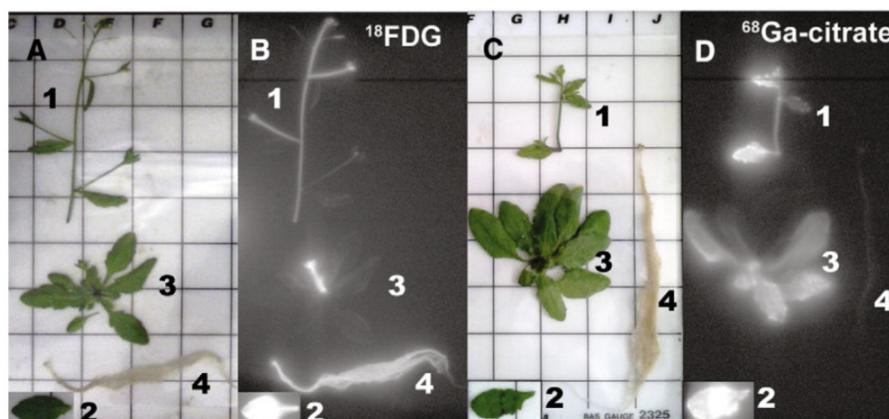


Fig. 2. Radiotracer uptake through leaf and subsequent radioactivity distribution in plant. (A) In ^{18}F -FDG imaging, one of the rosette leaves is pricked with a micropipette tip and ^{18}F -FDG was fed at the spots on the leaf (2); after 6 hours, plant was cut into shoot (1), radiotracer fed leaf (2), rosette (3) and root (4) and autoradiographed on imaging plate (IP). (B) depicts the corresponding ^{18}F -FDG autoradiogram. (C) In ^{68}Ga -citrate imaging, one of the rosette leaves is pricked with a micropipette tip and ^{68}Ga -citrate solution was fed at the spots on the leaf (2). Plant parts were cut and autoradiographed as mentioned previously. (D) depicts corresponding ^{68}Ga -citrate autoradiogram. In all autoradiograms, brightness marks the high radioactivity present in that area. All experiments were repeated at least three times and the representative data are shown.

beyond (Fig. 4B). In few cases, low intensity radioactivity signal was seen beyond girdled region. The radioactivity translocation was hindered at the girdled region but not completely inhibited as observed in few cases. Similar results were obtained where ^{18}F -FDG

was fed through the cauline leaf (Supplemental Fig. 3B). When ^{68}Ga -citrate was fed through one of the rosette leaves, radioactivity was seen beyond the girdled region (Fig. 4D) and was not hindered at the girdled region (depicted by an arrow in Fig. 4C). Similar results were obtained for the plants in which ^{68}Ga -citrate was fed through the cauline leaf (Supplemental Fig. 3D).

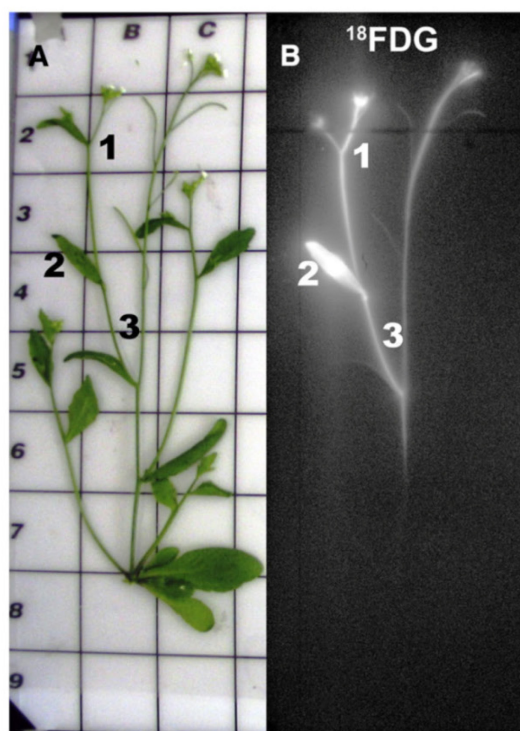


Fig. 3. ^{18}F -FDG uptake through the cauline leaf and subsequent radioactivity distribution above and below parts of the stem. (A) ^{18}F -FDG was fed through a cauline leaf (1) and after 6 hours, the plant stem bearing the cauline leaf was cut and autoradiographed using an imaging plate. (B) depicts the corresponding ^{18}F -FDG autoradiogram showing that radioactivity was seen both above and below the part of the stem to which the cauline leaf was attached. In autoradiogram, brightness marks the high radioactivity present in that area. All experiments were repeated at least three times and the representative data are shown.

3.4. 4-Dimensional radiotracer dynamics achieved using PET/CT

Fig. 5 shows a series of snapshots taken from the PET/CT dynamic imaging of a plant ($n = 1$) which was fed with ^{18}F -FDG through one of the rosette leaves. PET/CT measurements captured the dynamic tracer distribution in an intact plant as shown in Supplemental video file 1. Plant morphological information was obtained through CT measurements at a resolution of $367\ \mu\text{m}$. Low X-ray absorption and soft nature of plant tissue resulted in poor contrast CT picture. The overall plant architecture, leaf boundaries and thick parts like midribs were visible but it was not possible to visualize internal structures. PET provided the information on radiotracer dynamics in an intact plant at a resolution of $1.64\ \text{mm}$. PET imaging of the root parts produced distinct radioactivity image compared to aerial parts. The water in which roots were immersed acted as dense material for positron attenuation reducing positron travel distance before its annihilation. High radiotracer amounts in the aerial plant parts, on the other hand, produced blurred radiotracer distribution image due to phenomenon of positron escape from thin leaf structure. This was particularly evident in the radiotracer-fed leaf. Initially, radioactivity was localized in the ^{18}F -FDG fed spots of the leaf, but later spread throughout the leaf lamina. Radioactivity signal observed in petiole of ^{18}F -FDG fed leaf increased over time. Radioactivity was visible in roots and the stem within the first 30 min of radiotracer application (Fig. 5). Radioactivity in roots and plant shoot showed a linear increase over time (Supplemental Fig. 2C and E). A high radioactivity signal accumulated in roots over a period of time (Fig. 5). Mature leaves did not show a visible radioactivity signal during the experimental time-scale. Radioactivity was seen in the stems and shoot apices of plants but it was masked by the halo effect resulting from the intense radioactivity present in the ^{18}F -FDG fed leaf.

4. Discussion

^{18}F -FDG is a positron-emitting radiotracer which would allow for *in vivo* imaging in plants. There is great interest in exploring and

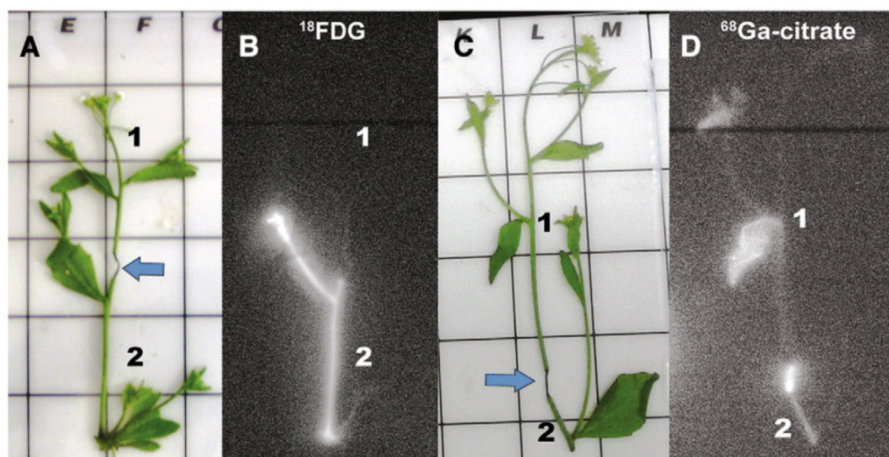


Fig. 4. Radiotracer uptake through leaves and the subsequent translocation of radioactivity across the girdled region on the stem. (A) the stem of *A. thaliana* was girdled by passing hot air over the stem (girdled region shown by arrow). In ^{18}F -FDG imaging, ^{18}F -FDG was fed on the rosette leaf (not shown). After 4 hours, the plant stem was cut and autoradiographed using an imaging plate. (B) depicts corresponding ^{18}F -FDG autoradiogram. (C) In ^{68}Ga -citrate imaging, the stem of *A. thaliana* was girdled (girdled region shown by arrow) and ^{68}Ga -citrate solution was fed on the plant rosette leaf (not shown). After 4 hours, the plant stem was cut and autoradiographed using an imaging plate. (D) depicts the corresponding ^{68}Ga -citrate autoradiogram. In all autoradiograms, brightness marks the high radioactivity present in that area. All experiments were repeated at least three times and the representative data are shown.

establishing novel applications of ^{18}F -FDG in plant. However, lack of a suitable radiotracer introduction method is one of challenges in plant imaging experiments. Unlike animals, plants possess different vasculature systems: phloem and xylem. The complexity of vascular bundles in plant stems makes it difficult to introduce radiotracer directly into either xylem or phloem. Introducing radiotracer into the plant through cut leaf [18], cut leaf petiole [19] had been reported in previous studies. We implemented slightly modified method for radiotracer-feeding in which we applied radiotracer solution to pricked spots on the leaf lamina and midrib. This method is less invasive and involves both direct and indirect delivery of radiotracer to vascular tissue. When the radiotracer is applied on the midrib, it comes into direct contact with the midrib vascular tissue. This might explain the rapid appearance of radioactivity in root within 30 min of ^{18}F -FDG introduction through leaf (Fig. 5). On the other hand, radiotracer applied on the leaf lamina has to travel via the symplastic and/or apoplastic pathway(s) in order to reach leaf vascular tissue and therefore may take longer time for translocation to other plant parts.

In case of ^{18}F -FDG imaging, ^{18}F -FDG fed spots on the leaf lamina appeared as circular zones of high radioactivity. This might be a result of localized uptake or the accumulation of ^{18}F -FDG by the leaf tissue. Our preliminary experiments showed that *Arabidopsis thaliana*

suspension cells could take up ^{18}F -FDG from the external nutrient solution and its uptake process is inhibited by HgCl_2 (Supplemental Fig. 1). It has been already shown that plant leaf cells could take up glucose from the external solution [34,35], an uptake process which is sensitive to HgCl_2 [36]. ^{18}F -FDG being a glucose analog, we think that similar mechanism might be involved in ^{18}F -FDG uptake by leaf cells. ^{18}F -FDG metabolism in plant cells is not completely understood. However, our preliminary ^{19}F -FDG (non-radioactive FDG) metabolism studies suggest that ^{19}F -FDG is taken up by the plant cells and metabolized to ^{19}F -FDG-6-phosphate, ^{19}F -disaccharide, Uridine-di-phosphate- ^{19}F -FDG etc. The localized uptake and intracellular conversion of ^{18}F -FDG to other metabolites may hinder the efflux of the [^{18}F] radioactivity out of the plant cells which could explain why high amount of radioactivity resided in the ^{18}F -FDG fed leaf. AIDA 2D-densitometry results suggested that nearly 80% radioactivity was retained in ^{18}F -FDG fed leaf. However, this might be an underestimation as high radioactivity levels in ^{18}F -FDG fed leaf often resulted in over-exposure. The resultant PSL intensity in over-exposed area might get saturated and lead to underestimation the radioactivity in that area. Moreover, the large background spread of such intense radioactivity signal makes it difficult to define ROI for ^{18}F -FDG fed leaf, which further leads to error in quantification. Similar errors also apply to [^{68}Ga] radioactivity quantification. These quantification errors

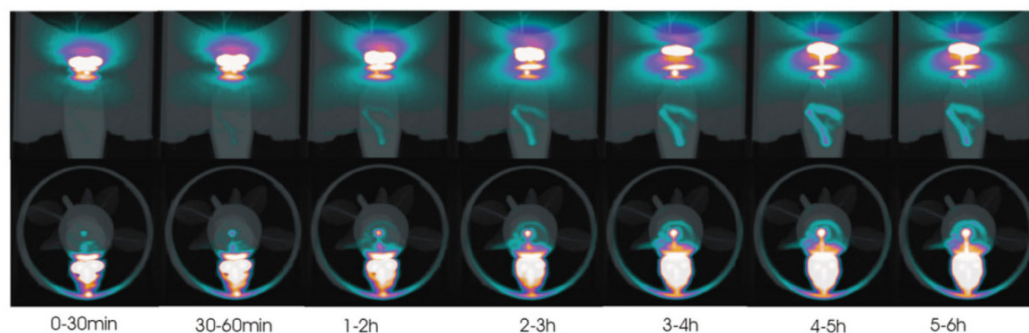


Fig. 5. Positron emission tomography/computed tomography (PET/CT) imaging. ^{18}F -FDG solution was fed on a rosette leaf (2), and radioactivity dynamics were monitored using PET/CT over 6 hours. (A) represents the series of PET/CT snapshots taken from side at sequential time frames. (B) represents the series of PET/CT snapshots taken from the top at sequential time frames. The brightness marks the high radioactivity present in that area. White, red, brown, yellow, green, blue colors represent diminishing concentrations of radioactivity.

would be less pronounced in other plant parts due to low level of radioactivity in those parts. IP images showed high radioactivity signal in apical inflorescence, root and young leaves (Fig. 2B), which are known active sinks for photoassimilate [37]. Mature rosette leaves, which are known to be sources for photoassimilate [37], accumulated less radioactivity compared to other plant parts. Plant stage, plant size, orthostichy and sectoriality also might have influenced the observed radioactivity distribution [19,26]. Like photoassimilate, [^{18}F] radioactivity also translocated through phloem and its passage is blocked by girdling. However, in few cases, radioactivity was seen across girdled region. This may result from minute fraction of [^{18}F] radioactivity getting mixed with and translocated in xylem stream. The observed [^{18}F] radioactivity distribution is similar to photoassimilate partitioning in plants explored using $^{11}\text{CO}_2$ radiotracer feeding [4,13,14,38]. The radioactivity distribution pattern observed after ^{18}F FDG feeding differed markedly from that of ^{68}Ga -citrate. No accumulation specificity was observed for different plant parts in case [^{68}Ga] radioactivity distribution. [^{68}Ga] radioactivity translocation was bi-directional and was not blocked at girdled region. So, [^{68}Ga] radioactivity must be able to flow in and across both xylem and phloem. Chemistry of ^{68}Ga is very similar to Al or Fe. Thus, [^{68}Ga] radioactivity may resemble Al or Fe in its translocation or distribution pattern in plants. We hypothesize that ^{68}Ga is rendered non-toxic to plant cells due to chelation with citrate. However it's *in vivo* behavior in leaf cells is hard to comment upon due to lack of necessary biochemical data regarding ^{68}Ga -citrate metabolism. If $^{68}\text{Ga}(\text{III})$ behave similar to $\text{Fe}(\text{III})$ then its translocation through apoplast may occur in its original $^{68}\text{Ga}(\text{III})$ intact form however its uptake in leaf cells and passage through symplast will require necessary transporters [39]. Also, $^{68}\text{Ga}(\text{III})$ translocation through phloem will necessitates its chelation with nicotinamine as Ga -citrate will tend to precipitate at neutral pH of phloem [40,41]. These postulations could only be verified after elucidating the metabolism of ^{68}Ga -citrate in leaf cells and the chemical form in which [^{68}Ga] radioactivity translocated through phloem.

So far, our findings are in accordance with the hypothesis that the observed radioactivity distribution and its translocation pathway differed as per the different chemical nature of the fed radiotracer compounds. This hypothesis should be further substantiated by establishing the chemical form in which corresponding radioactivity translocated. [^{18}F] radioactivity distribution pattern is similar to the distribution pattern of photoassimilate so ^{18}F FDG seems to be a good candidate for tracing photoassimilate in plants. However, it is premature to infer so, solely on ^{18}F FDG imaging experiments. *Arabidopsis* plants photosynthesize sucrose as photoassimilate and it is the main sugar component translocated in phloem. It had been reported that ^{18}F FDG persist as an intact sugar molecule during its translocation to other plant parts [19]. This is contradictory to the literature that only sugars such as sucrose, raffinose and sugar alcohol such as galactinol have been known to be translocated in *Arabidopsis thaliana* phloem [42,43]. Translocation of photoassimilate in plants had been studied by labeling leaves with $^{11}\text{CO}_2$ radiotracer gas either in pulse labeling or as a continuous labeling manner [4,14,38]. As PET is a non-invasive imaging technique, it could allow for the comparison of radioactivity distributions in a single plant using both $^{11}\text{CO}_2$ and ^{18}F FDG as radiotracers. This comparison will prove whether the [^{18}F] radioactivity distribution after ^{18}F FDG feeding is similar to photoassimilate distribution or not.

4.1. Applications of PET/CT in plant imaging

Photoassimilate flux in plant is influenced by a plant's external environment factors [2,44]. Unraveling the *in vivo* dynamics of photoassimilate in an intact plant under natural conditions or with respect to biotic and abiotic stresses is an important research aspect in modern plant biology. The distribution of photoassimilate and other metabolites in an intact plant have been analyzed using 2-D planar

positron imaging systems [14,45]. 2-D imaging systems suit well for planar plant structures such as leaves but could not be extended for plants with 3-D morphology (like rosette leaves or extensive branching). Converse *et al* (2013) have demonstrated the use of a microPET scanner to obtain radiotracer dynamics in plants [28], but the method lacked corresponding morphological information of a plant. A combination of magnetic resonance imaging (MRI) and positron emission tomography (MRI/PET) have been successfully used to obtain radiotracer distribution along with morphological information [25,26]. In this method, MRI provided the information on plant anatomical features which was later combined with radiotracer dynamics obtained from PET [25]. To use the MRI/PET modality, however, one had to transfer plants from the MRI instrument to the PET scanner, which alters the external environment of the plants during the experiment. Here, we used integrated PET/CT modality which effectively addressed above mentioned problems to achieve 4-D dynamics of radiotracer distribution in *A. thaliana* plants. Both PET and CT scanners were embedded in the same instrument and thus the position of the plant on the bed remained unchanged. The external environment of the plant remained same throughout the experiment. Due to stationary positioning of the plant on the instrument bed, the fusion of PET and CT data was also possible in easy and effective manner.

Thorpe *et al.* showed that [^{11}C] photoassimilate translocation from $^{11}\text{CO}_2$ labeled leaf petiole to roots occurred within 40 minutes [13,38]. Our PET/CT results showed that [^{18}F] radioactivity was seen in roots within 30 minutes of ^{18}F FDG application. In our case, the direct introduction of ^{18}F FDG through a pricked midrib might have reduced the arrival time of ^{18}F FDG radiotracer into the roots. The quantification of radioactivity that had been translocated to various plant parts was difficult due to high background noise and a halo effect arising from intense radioactivity in the radiotracer-fed leaf. The thin and flat nature of leaves cause most of the positrons to escape the leaf before annihilation. The phenomenon of positron escape and errors caused by partial volume averaging for thin leaf structure lead to large errors in estimation of radiotracer concentration [46]. The FOV of the instrument limits the dimensions of the plant that could be measured. However, this limitation could be resolved to some extent by using an instrument with bigger FOV or by placing the plant horizontally over the PET/CT bed. High resolution X-ray CT techniques could be employed to improve the CT contrast [27]. We hope that, with above problems addressed, PET/CT could prove useful in plant imaging and widen the scope of problems that could be addressed using the PET radiotracers to elucidate the source-sink relationship, perform flux analysis of metabolites or study long-distance transport in an intact plant in response to various biotic and abiotic stresses.

5. Conclusion

This study explores the applicability of ^{18}F FDG and ^{68}Ga -citrate in plant imaging using IP and PET/CT imaging techniques. The radioactivity distribution observed after ^{18}F FDG feeding is significantly different than another radiotracer like ^{68}Ga -citrate. This implies that the mechanism of ^{18}F FDG radiotracer uptake and its radioactivity distribution must be different from that of ^{68}Ga -citrate. ^{18}F FDG can be taken up and sequestered by the plant cells. ^{18}F FDG is also metabolized by the plant cells however its complete fate remains to be elucidated. [^{68}Ga] radioactivity translocated to other plant parts but showed no differential accumulation specificity for different plant parts. Further study will be necessary to establish whether it mimics Al or Fe distribution. Our results showed that [^{18}F] radioactivity distribution pattern is similar to the distribution pattern of photoassimilate and it is mainly transported through phloem so ^{18}F FDG seems to be a good candidate for tracing photoassimilate in plants. Ferrieri *et al.* (2012) reported that [^{18}F] radioactivity translocate through plant vasculature in its intact chemical form as ^{18}F FDG. This is contradictory to fact that

typically sucrose is the major photoassimilate sugar known to be translocated in phloem of *Arabidopsis thaliana* owing to its less reactive non-reducing nature. ^{18}F FDG being a monosaccharide glucose analogue, it's difficult to comment on its possible loading mechanism into phloem without understanding its uptake mechanism and metabolic fate in plant leaf tissue. We will investigate these aspects of ^{18}F FDG metabolism in plant tissue in our further research. PET/CT allows dynamic radiotracer imaging in plants but also has several limitations particularly with respect to absolute quantification and PET resolution. However, being the non-invasive technique, PET/CT could be used to compare the radioactivity distribution in a single plant after feeding $^{11}\text{CO}_2$ or ^{18}F FDG through the same leaf in two independent experiments. This comparative imaging experiment and additional evidence from biochemical side, particularly with regard to the ^{18}F FDG uptake mechanism and metabolism in plant cells, will be necessary to conclusively prove that ^{18}F FDG can be used as a true proxy for photoassimilate translocation in plants.

Supplementary data to this article can be found online at <http://dx.doi.org/10.1016/j.nucmedbio.2014.05.143>.

Acknowledgments

We thank A. Weber and the greenhouse team of MPI-Chemical Ecology for growing the *A. thaliana* plants; Klaus Gase for providing imaging plates for autoradiography experiments; Thomas Opfermann for setting up initial PET/CT experiments and Emily Wheeler for editorial assistance. We thank Dr. Stefan Meldau for his guidance and fruitful discussions. We are also grateful to the Hans Knöll Institute for permission to use the PET/CT facility; the Max Planck Society for a stipend to Amol Fatangare and for financial support.

References

- [1] Zamski E, Schaffer AA. Photoassimilate distribution in plants and crops: source-sink relationships. Marcel Dekker Inc.; 1996.
- [2] Lemoine R, La Camera S, Atanassova R, Dédaldéchamp F, Allario T, Pourtau N, et al. Source-to-sink transport of sugar and regulation by environmental factors. *Front Plant Sci* 2013;4:272.
- [3] Babst BA, Karve AA, Judt T. Radio-metabolite analysis of carbon-11 biochemical partitioning to nonstructural carbohydrates for integrated metabolism and transport studies. *Plant Cell Physiol* 2013;54:1016–25.
- [4] Ferrieri AP, Agtuca B, Appel HM, Ferrieri RA, Schultz JC. Temporal changes in allocation and partitioning of New carbon as ^{11}C elicited by simulated herbivory suggest that roots shape aboveground responses in *Arabidopsis*. *Plant Physiol* 2013;161:692–704.
- [5] Nour-Eldin HH, Halkier BA. The emerging field of transport engineering of plant specialized metabolites. *Curr Opin Biotechnol* 2013;24:263–70.
- [6] Webb JA, Gorham PR. Translocation of photosynthetically assimilated C in straight-necked squash. *Plant Physiol* 1964;39:663–72.
- [7] Geiger DR, Saunders MA, Cataldo DA. Translocation and accumulation of translocate in the sugar beet petiole. *Plant Physiol* 1969;44:1657–65.
- [8] Fisher DB. Kinetics of C-14 translocation in soybean I. Kinetics in the stem. *Plant Physiol* 1970;45:107–13.
- [9] Margolis HA, Delaney S, Vézina L-P, Bellefleur P. The partitioning of ^{14}C between growth and differentiation within stem-deformed and healthy black spruce seedlings. *Can J Bot* 1991;69:1225–31.
- [10] Kiser MR, Reid CD, Crowell AS, Phillips RP, Howell CR. Exploring the transport of plant metabolites using positron emitting radiotracers. *HFSP J* 2008;2:189–204.
- [11] Moorby J, Ebert M, Evans N. The translocation of ^{11}C -labelled photosynthate in the soybean. *J Exp Bot* 1963;14:210–20.
- [12] Thorpe M, Minchin P. Continuous monitoring of fluxes of photoassimilate in leaves and whole plants. *J Exp Bot* 1991;42:461–8.
- [13] Thorpe M, Walsh K, Minchin P. Photoassimilate partitioning in nodulated soybean I. ^{11}C methodology. *J Exp Bot* 1998;49:1805–15.
- [14] Matsuhashi S, Fujimaki S, Uchida H, Ishioka NS, Kume T. A new visualization technique for the study of the accumulation of photoassimilates in wheat grains using ^{11}C CO₂. *Appl Radiat Isot* 2006;64:435–40.
- [15] Valk PE, Bailey DL, Townsend DW, Maisey MN. Positron emission tomography: basic science and clinical practice. London: Springer-Verlag; 2003.
- [16] Phelps ME. PET: molecular imaging and its biological applications. New York: Springer; 2004.
- [17] Tsuji AUH, Yamashita T, Matsuhashi S, Ito T, Mizuniwa C, Ishioka NS, et al. Uptake of ^{18}F FDG and $^{15}\text{NO}_3$ in tomato plants. *TIARA Annu Rep* 2001, 035. Japan: Japan Atomic Energy Research Institute; 2002. p. 103–4.
- [18] Hattori E, Uchida H, Harada N, Ohta M, Tsukada H, Hara Y, et al. Incorporation and translocation of 2-deoxy-2- ^{18}F fluoro-d-glucose in *Sorghum bicolor* (L.) Moench monitored using a planar positron imaging system. *Planta* 2008;227:1181–6.
- [19] Ferrieri AP, Appel H, Ferrieri RA, Schultz JC. Novel application of 2- ^{18}F fluoro-2-deoxy-n-glucose to study plant defenses. *Nucl Med Biol* 2012;39:1152–60.
- [20] Wheeler D, Power I, Edmeades D. Effect of various metal ions on growth of two wheat lines known to differ in aluminium tolerance. *Plant Soil* 1993;155:489–92.
- [21] Wheeler D, Power I. Comparison of plant uptake and plant toxicity of various ions in wheat. *Plant Soil* 1995;172:167–73.
- [22] Barcelo J, Poschenrieder C. Fast root growth responses, root exudates, and internal detoxification as clues to the mechanisms of aluminium toxicity and resistance: a review. *Environ Exp Bot* 2002;48:75–92.
- [23] Smith R, Martell A, Motekaitis R. NIST standard reference database 46. NIST Critically selected stability constants of metal complexes database ver 2003; 2003 2.
- [24] Kochian LV. Cellular mechanisms of aluminum toxicity and resistance in plants. *Annu Rev Plant Biol* 1995;46:237–60.
- [25] Jahnke S, Menzel M, Van Dusschoten D, Roeb GW, Bühler J, Minwuyet S, et al. Combined MRI–PET dissects dynamic changes in plant structures and functions. *Plant J* 2009;59:634–44.
- [26] De Schepper V, Bühler J, Thorpe M, Roeb G, Huber G, van Dusschoten D, et al. ^{11}C -PET imaging reveals transport dynamics and sectorial plasticity of oak phloem after girdling. *Front Plant Sci* 2013;4:200.
- [27] Dhondt S, Vanhaeren H, Van Loo D, Cnudde V, Inzé D. Plant structure visualization by high-resolution X-ray computed tomography. *Trends Plant Sci* 2010;15:419–22.
- [28] Converse A, Ahlers E, Bryan T, Williams P, Barnhart T, Engle J, et al. Positron emission tomography (PET) of radiotracer uptake and distribution in living plants: methodological aspects. *J Radioanal Nucl Chem* 2013;297:241–6.
- [29] Gibeau DM, Hulett J, Cramer GR, Seemann JR. Maximal biomass of *Arabidopsis thaliana* using a simple, low-maintenance hydroponic method and favorable environmental conditions. *Plant Physiol* 1997;115:317–9.
- [30] Gebhardt P, Opfermann T, Saluz H. Computer controlled ^{68}Ga milking and concentration system. *Appl Radiat Isot* 2010;68:1057–9.
- [31] Jeannette E, Reyss A, Gregory N, Gantet P, Prioul JL. Carbohydrate metabolism in a heat-girdled maize source leaf. *Plant Cell Environ* 2000;23:61–9.
- [32] Constantinescu CC, Mukherjee J. Performance evaluation of an Inveon PET preclinical scanner. *Phys Med Biol* 2009;54:2885–99.
- [33] Visser EP, Disselhorst JA, Brom M, Laverman P, Gotthardt M, Oyen WJ, et al. Spatial resolution and sensitivity of the Inveon small-animal PET scanner. *J Nucl Med* 2009;50:139–47.
- [34] Maynard JW, Lucas WJ. Sucrose and glucose uptake into beta vulgaris leaf tissues: a case for general (apoplastic) retrieval systems. *Plant Physiol* 1982;70:1436–43.
- [35] Hendrix DL. Sugar uptake by cotton tissues leaf disc versus cultured roots. *Plant Physiol* 1984;74:16–20.
- [36] Conde C, Silva P, Agasse A, Tavares RM, Delrot S, Geros H. An Hg-sensitive channel mediates the diffusional component of glucose transport in olive cells. *Biochim Biophys Acta Biomembr* 2007;1768:2801–11.
- [37] Minchin P. Mechanistic modelling of carbon partitioning. *Frontis* 2007;22:113–22.
- [38] Thorpe MR, Ferrieri AP, Herth MM, Ferrieri RA. ^{11}C -imaging: methyl jasmonate moves in both phloem and xylem, promotes transport of jasmonate, and of photoassimilate even after proton transport is decoupled. *Planta* 2007;226:541–51.
- [39] Kobayashi T, Nishizawa NK. Iron uptake, translocation, and regulation in higher plants. *Annu Rev Plant Biol* 2012;63:131–52.
- [40] Schuler M, Rellán-Álvarez R, Fink-Straube C, Abadía J, Bauer P. Nicotianamine functions in the phloem-based transport of iron to sink organs, in pollen development and pollen tube growth in *Arabidopsis*. *Plant Cell* 2012;24:2380–400.
- [41] Rzhapishvskaya O, Ekstrand-Hammarström B, Popp M, Björn E, Bucht A, Sjöstedt A, et al. The antibacterial activity of Ga^{3+} is influenced by ligand complexation as well as the bacterial carbon source. *Antimicrob Agents Chemother* 2011;55:5568–80.
- [42] Ziegler H. Nature of transported substances. In: Zimmermann MH, Milburn JA, editors. *Transport in Plants I*. Berlin Heidelberg: Springer; 1975. p. 59–100.
- [43] Haritatos E, Medville R, Turgeon R. Minor vein structure and sugar transport in *Arabidopsis thaliana*. *Planta* 2000;211:105–11.
- [44] Schwachtje J, Baldwin IT. Why does herbivore attack reconfigure primary metabolism? *Plant Physiol* 2008;146:845–51.
- [45] Uchida H, Okamoto T, Ohmura T, Shimizu K, Satoh N, Koike T, et al. A compact planar positron imaging system. *Nucl Instrum Methods Phys Res A* 2004;516:564–74.
- [46] Alexoff DL, Dewey SL, Vaska P, Krishnamoorthy S, Ferrieri R, Schueller M, et al. PET imaging of thin objects: measuring the effects of positron range and partial-volume averaging in the leaf of *Nicotiana tabacum*. *Nucl Med Biol* 2011;38:191–200.

Supplementary Data:

Supplemental Figure 1. ^{18}F FDG uptake by *Arabidopsis thaliana* cell suspension. *Arabidopsis thaliana* cell culture was grown in JPL medium containing sucrose (1.5%). On the day of experiment, cells were suspended in 50 mL JPL medium containing equimolar concentration of Mannitol instead of sucrose. Control flasks contained only nutrient media. ^{18}F FDG solution (1.23 MBq) was added to each flask. Flasks for set-3 and set-4 were added with 100 μM glucose and 1 mM HgCl_2 respectively prior to ^{18}F FDG addition. Flasks were kept on rotary shaker at 60 rpm under normal laboratory light and temperature conditions. After 5 hours, the suspensions were filtered through 22 micron filter for cell pellet. Radioactivity accumulated in cell pellet was measured in counts per second (CPS) using a well counter (Isomed 2100, MED Nuklear-Medizintechnik Dresden GmbH, Dresden, Germany). Two biological replicates (each with three technical replicates) were performed for each set and average decay corrected CPS radioactivity for cell pellet was noted.

Supplemental Table 1. ^{18}F FDG uptake by *Arabidopsis thaliana* cell suspension.

Experimental Set	Average cell pellet radioactivity (CPS)
Set-1 control (only media)	22.6
Set-2 Expt (media+suspension+FDG)	23868.5
Set-3 Expt+glucose(media+suspension+glucose 100 μM +FDG)	8215.5
Set-4 Expt+ HgCl_2 (media+suspension+ HgCl_2 1mM+FDG)	604.6

Supplemental Figure 2 Radioactivity (Bq) observed in different plant parts plotted against time(s) in PET/CT imaging using ^{18}F FDG as a radiotracer. (A) represents radioactivity in the whole plant over time; (B) represents radioactivity in the ^{18}F FDG-supplied leaf over time; (C) represents radioactivity in roots over time; (D) represents radioactivity in the mature rosette leaf over time; (E) represents radioactivity in plant shoots over time.

[NOTE: The radioactivity (decay corrected value) measured in the whole plant and in the ^{18}F FDG-supplied leaf increased until 3 h after the start of the experiment and plateaued after this (graph A, B). This was observed because at the start of the experiment, ^{18}F FDG was concentrated in a small volume on the leaf. The flat shape of the leaf caused attenuation of only those positrons which emitted in the direction of surrounding leaf tissue. Rest of the

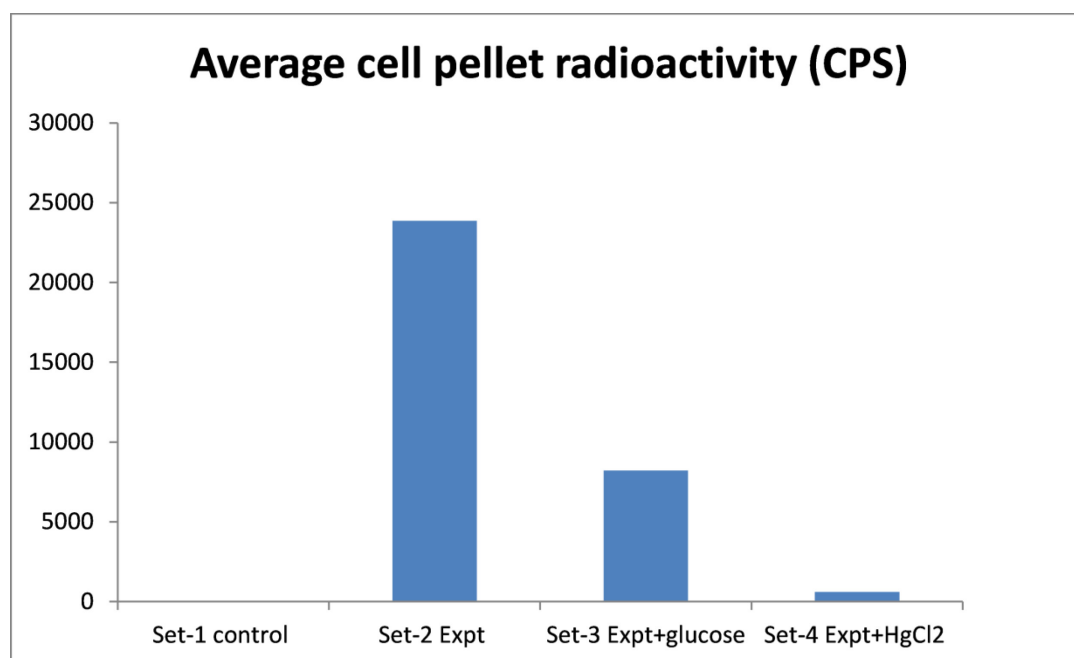
emitted positrons travelled long distances through the air before getting attenuated by nearby air molecules. This phenomenon caused the halo effect seen in PET/CT image (Figure 5). This also led to inaccurate calculation of region of interest (ROI) for ^{18}F FDG-supplied leaf and thus underestimated radioactivity contained in ^{18}F FDG-supplied leaf. However, during the course of experiment, the radiotracer spread throughout the leaf and other plant parts, getting surrounded by more leaf tissue. This improved the attenuation of emitted positrons over the course of experiment and resulted in corresponding signal increase. This effect was less pronounced in plant parts (such as root, mature rosette leaf and plant shoot) which had received the transported radiotracer in lower amounts. Here, radiotracer transported to these parts was always effectively attenuated by surrounding leaf tissue over the course of experiment. The radioactivity measurements in the regions of interest (roots, mature rosette leaves and plant shoots) which accumulate low amount of radioactivity, are not affected by the above-mentioned attenuation effect and thus could be regarded as readings depicting the correct trend of increase in radioactivity over time in these plant parts (graph C, D, E).]

Supplemental Figure 3 Radiotracer supplied through the cauline leaf and the subsequent translocation of radioactivity across the girdled region on the stem. (A) The stem of *A. thaliana* was girdled by passing hot air over the stem (girdled region shown by arrow). In ^{18}F FDG imaging, the ^{18}F FDG solution was supplied through a cauline leaf (1). After 4 hours, plant stem was cut and autoradiographed using an imaging plate (IP). (B) depicts the corresponding ^{18}F FDG autoradiogram. (C) In ^{68}Ga -citrate imaging, the stem of *A. thaliana* was girdled (girdled region shown by arrow) and ^{68}Ga -citrate solution was supplied through a cauline leaf (1). After 4 hours, the plant stem was cut and autoradiographed using an IP. (D) depicts the corresponding ^{68}Ga -citrate autoradiogram. In all autoradiograms, brightness marks the high radioactivity present in that area. All experiments were repeated at least three times and the representative data are shown.

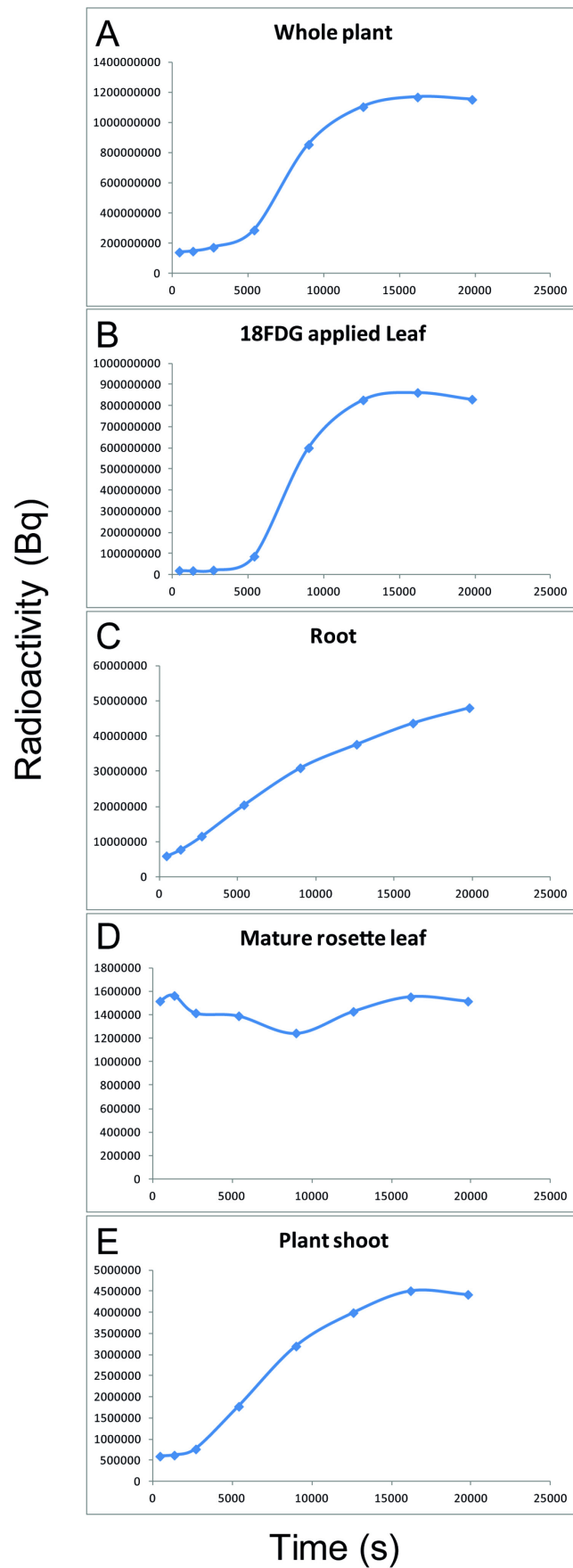
Supplemental Figure 4 Plant mounting on instrument bed for positron emission tomography/computed tomography (PET/CT) imaging. (A) shows plants placed on instrument beds. Only one of the above two plants was subjected to PET/CT imaging (B) shows plant assembly during *in vivo* imaging. Plant root was immersed in vials containing 2 mL aqueous solution and fixed vertically on a Styrofoam platform. Plant was placed inside thin plastic cylinders to minimize leaves movement due to air currents inside the scanner. The whole assembly was mounted on PET/CT bed as shown.

Supplemental video 1. (attached as **FDG PET-CT.mpeg**) PET/CT *in vivo* imaging of *A. thaliana*. The ^{18}F FDG was applied to one of the rosette leaves and radioactivity dynamics were monitored using PET/CT over 6 hours. The video depicts the series of 8 radioactivity snapshots at various viewing angles and time-points. The ^{18}F FDG-supplied leaf appears as a bright region due to the presence of high radioactivity. The brightness marks the high radioactivity present in that area. White, red, brown, yellow, green, blue colors represent diminishing concentrations of radioactivity.

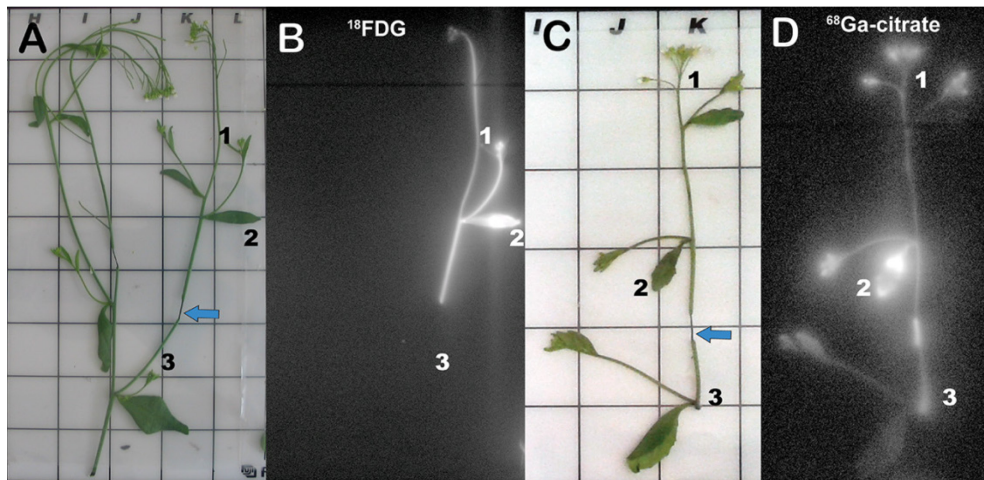
Supplemental Fig 1:



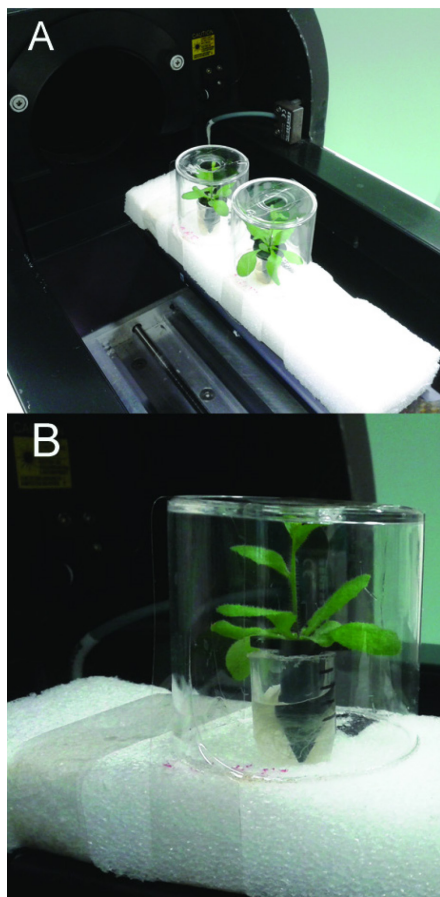
Supplemental Fig 2:



Supplemental Fig 3:



Supplemental Fig 4:



Supplemental Video 1: Submitted online as 'FDG PET-CT.mpeg' for PET/CT *in vivo* imaging of *A. thaliana*.

Chapter 2

Unravelling 2-deoxy-2-fluoro-D-glucose metabolism in *Arabidopsis thaliana*

Amol Fatangare[#], Christian Paetz, Bernd Schneider, Hans Peter Saluz, Aleš Svatoš^{*}

First author

** Corresponding author*

Title: Unravelling 2-deoxy-2-fluoro-D-glucose metabolism in *Arabidopsis thaliana*.

Amol Fatangare^{#1}, Christian Paetz², Hanspeter Saluz^{3,4}, Aleš Svatoš*¹

¹ Mass spectrometry/Proteomics research Group, Max Planck Institute for Chemical Ecology, Hans-Knöll-Straße 8, D-07745 Jena, Germany

² Biosynthesis/NMR research Group, Max Planck Institute for Chemical Ecology, Hans-Knöll-Straße 8, D-07745 Jena, Germany

³ Department of Cell and Molecular Biology, Leibniz Institute for Natural Product Research and Infection Biology – Hans Knöll Institute, Beutenbergstr. 11a, D-07745 Jena, Germany

⁴ Friedrich-Schiller-University Jena, D-07737 Jena, Germany

First author

* Corresponding author

Dr. Aleš Svatoš, Director, Mass spectrometry/Proteomics research Group, Max Planck Institute for Chemical Ecology, Hans-Knöll-Straße 8, D-07745 Jena, Germany. Tel: +493641 571700; Fax: +493641571701.

Abstract:

2-deoxy-2-fluoro-D-glucose (FDG) is fluorine labeled glucose analogue routinely used in clinical and animal radiotracer studies to trace glucose uptake but it has rarely been used in plants. Previous studies analyzed FDG translocation and distribution pattern in plants and proposed that FDG could be used as a tracer for photoassimilates in plants. Elucidating ¹⁸F-DG metabolism in plants is a crucial aspect for establishing its application as a radiotracer in plant imaging. However, FDG metabolism in plants is not fully characterized till yet. In this paper, we describe the metabolic fate of FDG in model plant species, *Arabidopsis thaliana*. We fed FDG to leaf tissue and analyzed leaf extract using MS and NMR. On the basis of exact mono-isotopic masses, MS/MS fragmentation, and NMR data; we identified 2-fluoro-gluconic acid, FDG-6-phosphate, 2-deoxy-2-fluoro-maltose, and uridine-di-phosphate-FDG as four major end products of FDG metabolism. Glycolysis and starch degradation seemed to be the important pathways for FDG metabolism. We showed that FDG metabolism in plants is considerably different than animal cells and goes beyond FDG-phosphate as previously presumed.

Keywords: 2-deoxy-2-fluoro-D-glucose, FDG, *Arabidopsis thaliana*, plant, Metabolism, radiotracer.

Introduction:

2-deoxy-2-[^{18}F]fluoro-D-glucose (^{18}FDG /FDG) is a radioactive glucose surrogate in which 2' C hydroxyl group of glucose is substituted by positron emitting ^{18}F Fluorine radio-isotope. ^{18}F Fluorine has a half-life ($t_{1/2}$) of 109.8 min [www.nndc.bnl.gov/chart/]. In ^{18}FDG , Fluorine has small atomic size and the C-F bond strength is comparable to that of C-OH bond. Small atomic radius of fluorine does not impose any structural constraints in the molecule. Therefore, resulting ^{18}FDG species is a structural analog of glucose which is able to conjugate with the target receptors or enzymes without any steric hindrances [Phelps ME, 2004]. ^{18}FDG uptake and distribution is found to be similar to that of glucose in the animal circulation system. It is commonly used in medical diagnostics and animal studies to trace uptake and the metabolism of glucose in metabolically active tissue such as brain tissue or cancer cells [Som et al, 1980; Alavi et al, 1982; Ung et al, 2007; Phelps ME, 2004].

^{18}FDG , owing to its longer half-life ($t_{1/2}=109.8$ min), is a suitable radiotracer for *in vivo* imaging studies spanning over several hours. In addition, the mean dispersion range of emitted positron is shortest of all thus allowing resolution in mm range in positron emission tomography (PET) [Sanchez-Crespo et al, 2004]. The application of ^{18}FDG as a radiotracer has been well established technique in animal system but it has rarely been used in the plant imaging experiments. Tsuji *et al* (2002) first reported ^{18}FDG uptake and distribution in tomato plants [Tsuji et al, 2002]. Later, Hattori *et al* (2008) described ^{18}FDG translocation in intact sorghum plants and suggested that it could be used as a tracer for photoassimilate translocation in plants [Hattori et al, 2008]. ^{18}FDG has also been used to study glycoside biosynthesis in plants as a measure of plant response to defense induction [Ferrieri et al, 2012]. Recently, ^{18}FDG has been employed as a radiotracer in plants to study amino-sugar-nitrogen (ASN esp. glucosamine) uptake [Li et al, 2014] or solute transport [Partelova et al, 2014]. We have previously shown that the radioactivity distribution pattern observed after ^{18}FDG feeding is significantly different than another radiotracer like ^{68}Ga -citrate (^{68}Ga -citrate) [Fatangare et al, 2014]. ^{18}FDG radioactivity distribution was also similar to photoassimilates [Fatangare et al, 2014]. There is growing evidence that ^{18}FDG could also be used as radiotracer in plant imaging studies to trace sugar dynamics. ^{18}FDG application in plant imaging necessitates successful ^{18}FDG tracer kinetics model which could be established after unraveling ^{18}FDG translocation and its metabolism in plants. Previous literature reported ^{18}FDG radioactivity translocation pattern in plants however did not provide the comprehensive picture of ^{18}FDG metabolism in plant cells.

FDG uptake and metabolism has been extensively studied in animal cells [McSheehy et al, 2000; Kaarstad et al, 2002; Southworth et al, 2003]. Being the glucose analogue, FDG is transported into the animal cells via the same transporters as glucose [Higashi et al, 1998; Brown et al, 1999; Yen et al, 2004; Avril N, 2004]. Upon intracellular uptake, FDG is phosphorylated to FDG-6-phosphate (FDG-6-P) by the action of hexokinase or glucokinase [Sols and Crane, 1954; Bessel et al, 1972; Smith T, 2001]. Further metabolism of FDG-6-P via the glycolytic pathway was found to be inhibited due to Fluorine substitution at 2' C position [Lampidis et al, 2006; Kurtoglu et al, 2007]. It was assumed that FDG-6-P underwent no further metabolism and simply accumulated inside the cell [Miller and Kiney, 1981; Reivich et al, 1985; Bessel and Thomas, 1973; Suolinna et al, 1986].

FDG metabolism in plant cells is not characterized till yet but rather presumed to be similar to animal cells [Hattori et al, 2008]. However, FDG metabolism in plants might be quite different than the FDG metabolism in animal cells. Plants photosynthesize sugars as photoassimilates. Photoassimilates flux is regulated through numerous sugar transporters towards specialized organelles like plastids, vacuoles or organs like fruits, tubers for storage or utilization. Because of the complexity of biochemical pathways in plants related to sugar metabolism, it is hard to envisage the metabolic fate of FDG in plant cells. Exploring FDG metabolism in plant leaf tissue is one of the critical aspects of ^{18}F FDG validation as radiotracer for *in vivo* imaging in plants. Thus, unraveling the FDG metabolism in plant cells is most logical step to follow after the ^{18}F FDG radiotracer imaging studies in plants.

In present work, we analyzed FDG metabolism in *Arabidopsis thaliana* (*A. thaliana*) leaf cells using 2-deoxy-2- ^{19}F fluoro-D-glucose (^{19}F FDG/FDG) which contains stable fluorine ^{19}F isotope. We fed ^{19}F FDG to *A. thaliana* rosette leaves and later analyzed leaf extracts using liquid chromatography coupled to mass spectrometry (LC-MS) and nuclear magnetic resonance spectroscopy (NMR) to elucidate major end product of ^{19}F FDG metabolism.

Materials and methods:

Reagent and chemicals:

¹⁹FDG was purchased from Sigma Aldrich (Sigma-Aldrich Chemie GmbH, Munich, Germany). All chemicals and solvent were of analytical grade.

Plant material and growth conditions:

Arabidopsis thaliana Col-0 plants were used for all the experiments. *A. thaliana* seeds were stratified for 3 days at 4° C and grown in soil. Vernalized seeds were placed in 10 cm round pots containing wet soil that consisted of 80% Fruhstorfer Nullerde™, 10% vermiculite, and 10% sand, fertilized with Triabon (1 g.L⁻¹) and Osmocote Exact Mini (1 g.L⁻¹) and treated with *Steinernema feltiae*. Plants were placed in a controlled environment growth chamber at 21° C temperature and 60% humidity under short-day conditions. Light of intensity 190 to 220 μmol.m⁻².S⁻¹ was provided for 12 hours followed by 12 hours of dark.

¹⁹FDG leaf application and extraction:

Six to seven week old *Arabidopsis thaliana* plants were used for all experiments. Four mature rosette leaves from plant were selected for ¹⁹FDG application. Leaf was gently scratched at 4 spots on abaxial surface of leaf lamina using micropipette tip. Five microliter of ¹⁹FDG (20 mg.mL⁻¹) solution was immediately applied on each scratched spot. Plants were kept under standard growth conditions. ¹⁹FDG applied leaves were cut from the rosette after 4 hour and extracted using slightly modified methanol/chloroform extraction procedure [Gromova and Roby, 2010]. Leaves were cut and ground in liquid nitrogen. Chloroform: methanol:water (1mL:2mL:1mL) was added to the 0.4 g of ground leaf sample. A mixture was sonicated in ultrasonic bath (Merck, Eurolab NV, Belgium) for 15 min at room temperature. After sonication, Sample was centrifuged at 4000g for 20 min at 4 °C. Supernatant was stored in glass vials at -80 °C until further analysis. Samples were analyzed by LC-MS on LTQ Orbitrap XL™ hybrid ion trap-orbitrap (LTQ-Orbitrap XL) mass spectrometer (Thermo Fisher Scientific GmbH, Bremen, Germany) or by direct infusion-MS on Q Exactive™ Plus hybrid quadrupole-orbitrap (Q-Exactive Plus) mass spectrometer (Thermo Fisher Scientific GmbH, Bremen, Germany).

¹⁹FDG leaf exudate analysis:

Leaf phloem exudate was collected as per following procedure [Tetyuk et al, 2013]. Mature rosette leaves were cut and their petioles were immediately placed in glass Petri dish

containing ethylenediaminetetraacetic acid dipotassium salt (K_2 -EDTA) (20 mM, pH 7) solution. Petioles were recut in K_2 -EDTA solution. After 30 minutes, leaves were transferred to plastic vials with petioles dipped in K_2 -EDTA solution. All leaves containing vials were placed inside a closed chamber constructed out of transparent plastic. Wet paper towels were placed at the base of the chamber to maintain high humidity. Ten leaves were gently scratched at 4 spots on abaxial surface of leaf lamina using micropipette tip. Five microliter of ^{19}F FDG (20 mg.mL⁻¹) solution was immediately applied on each scratched spot. After 60 min, K_2 -EDTA solution was removed from the plastic vials with the help of syringe needle. One mL of distilled water was added and subsequently removed from the plastic vial in order to wash the K_2 -EDTA solution from the petioles. Phloem exudate from the leaf petioles were collected in 1 mL of distilled water for 6 hours. Phloem exudate samples were concentrated using the rotary vacuum evaporator (Genevac HT-4X centrifugal vacuum evaporator, Genevac Ltd, UK). Dried samples were resuspended in 0.1 mL of water and stored at -80 °C until further analysis. Samples were analyzed by direct infusion MS on Q-Exactive Plus mass spectrometer.

LCMS and LCMSⁿ measurements:

LC-MS data were acquired using Dionex UltiMate 3000 UHPLC system coupled to LTQ-Orbitrap XL mass spectrometer. Extraction samples were separated on Supelco apHera Amino column (Supelco Analytical, Bellefonte, Pennsylvania, USA) (15 cm×4.6 mm, particle size- 5 μ m) at room temperature. The mobile phase consisted of water (A) and acetonitrile (B). Elution gradient was set as follows: 20% A (0 min), 20% A (0.5 min), 45% A (13 min), 45% A (18 min), 20% A (18.10 min) and 20% A (20 min). The mobile phase flow rate was 1 mL.min⁻¹ and one-quarter of the flow was directed towards MS using flow splitter. Sample injection volume was 5 μ L. Electrospray ionization (ESI) source was used for ionization of LC eluate in negative ion mode. Capillary temperature was 280°C, and sheath and auxiliary gas flow rates were 40 and 12 arb (arbitrary units), respectively. The sweep gas flow rate was set at 0 arb and source voltage at 4 kV. The capillary voltage and tube lens were set at -41 V and -198 V, respectively. During LCMS measurements, Fourier transform mass spectrometry (FTMS) analyzer resolution was set at 100,000 with full width at half maximum (FWHM) definition and samples were analyzed in full scan mass range of m/z 100–800 with the acquisition of profile-type mass spectra.

Extraction samples were also separated on ACQUITY UPLC BEH Amide Column (Waters Corporation, Milford, Massachusetts, USA) (15 cm×2.1 mm, particle size- 1.7 μm) at room temperature. The mobile phase consisted of water (A) and acetonitrile (B). Elution gradient was set as follows: 20% A (0 min), 20% A (5 min), 50% A (13 min), 50% A (18 min), 20% A (18.10 min) and 20% A (20 min). The mobile phase flow rate was 0.3 mL.min⁻¹ and the injected volume was set at 10 μL . Electrospray ionization (ESI) source was used for ionization of LC eluate in negative ion mode. Capillary temperature was 275°C, and sheath and auxiliary gas flow rates were 35 and 7 arb (arbitrary units), respectively. The sweep gas flow rate was set at 0 arb and source voltage at 5 kV. The capillary voltage and tube lens were set at -35 V and -110 V, respectively. During LCMS measurements, FTMS resolution was set at 30,000 with FWHM definition and samples were analyzed in full scan mass range of m/z 100–800 with the acquisition of profile-type mass spectra.

During LCMSⁿ measurements on LTQ-Orbitrap XL mass spectrometer, LC peak retention time (RT) window was given to acquire MS/MS spectra of few selected ions in that RT window. Ions were isolated with isolation window of 1.6 Da. All other parameters were identical to that of LCMS. MS/MS spectra were acquired at a FT resolution of 15,000 or more at increasing collision energies until fragmentation occurred. The raw data was processed and compared using Thermo Xcalibur version 3.0.63 (Thermo Fisher Scientific GmbH, Bremen, Germany). The mass accuracy error threshold was fixed at 5 ppm. We also did direct infusion to perform MS/MS analysis of some of the selected ions on Q-Exactive Plus mass spectrometer as it was more sensitive. For those ions, we report MS/MS data acquired on Q-Exactive Plus mass spectrometer due to its superior quality.

¹⁹FDG metabolite's bulk extraction for NMR:

Six to seven week old *Arabidopsis thaliana* plants (n=6) were used. Three to five mature rosette leaves from plant were selected for ¹⁹FDG application. Each leaf was gently scratched at 6 to 8 spots on abaxial surface of leaf lamina using micropipette tip. Five microliter of ¹⁹FDG (20 mg.mL⁻¹) solution was immediately applied on each scratched spot. On average, 30 μL of ¹⁹FDG solution was applied on each leaf. Plants were kept under standard growth conditions. ¹⁹FDG applied leaves were cut from the rosette after 4 hour and extracted cumulatively using methanol/chloroform extraction procedure as described previously. Supernatant was stored in glass vials at -80 °C until further processing. Supernatant was further subjected to partial purification procedure by F-SPE or LC separation.

Partial purification of polar ^{19}F metabolites using F-SPE:

SiliaPrep Fluorochrom silica gel SPE cartridge (SiliCycle Inc., Quebec City, Quebec, Canada) (3 mL, 500 mg) was equilibrated with distilled water. ^{19}F FDG applied leaf extract sample was concentrated and loaded onto the cartridge bed. Compounds were eluted from the cartridge with distilled water in sequential fractions of 500 μL . Fractions were vacuum dried, dissolved in 600 μL of D_2O and analyzed for the presence of ^{19}F metabolites using ^{19}F -NMR spectroscopy.

LC separation and fractionation of m/z 343.1051:

Extraction samples were firstly separated on apHera Amino column (15 cm \times 4.6 mm, particle size- 5 μm) at room temperature. The mobile phase consisted of water (A) and acetonitrile (B). Elution gradient was set as follows: 20% A (0 min), 20% A (4 min), 80% A (13 min), 80% A (18.50 min), 20% A (19 min) and 20% A (25 min). The mobile phase flow rate was 1 mL.min $^{-1}$ and one-quarter of the flow was directed towards MS for the detection of m/z 343.1051. Same ESI-MS parameters were used as described previously for ACQUITY UPLC BEH Amide Column. Sample injection volume was 4 μL . Retention time for m/z 343.1051 was found to be 5.90 min. We collected LC eluent in the retention time window of 4.75-6.75 minutes for fractionation of m/z 343.1051. Collected fraction was vacuum dried using the rotary vacuum evaporator. Dried fraction was resuspended in water and further subjected to LC fractionation using YMC-Pack Polyamine-II column (YMC co., Kyoto, Japan) (25 cm \times 4.6 mm, particle size- 5 μm) at room temperature. The mobile phase consisted of water (A) and acetonitrile (B). Elution gradient was set as follows: 20% A (0 min), 20% A (6.50 min), 55% A (18 min), 55% A (24 min), 20% A (24.10 min) and 20% A (30 min). The mobile phase flow rate was 1 mL.min $^{-1}$ and one-quarter of the flow was directed towards MS for the detection of m/z 343.1051. Same ESI-MS parameters were used as described previously for ACQUITY UPLC BEH Amide Column. Sample injection volume was 2 μL . Retention time for m/z 343.1051 was found to be 13.50 min. We collected the LC eluate in the retention time window of 13.00-14.00 minutes for fractionation of m/z 343.1051. Collected fraction was vacuum dried using the rotary vacuum evaporator. Dried fraction was resuspended in D_2O and further subjected to NMR analysis for structure elucidation.

NMR analysis:

For NMR structure elucidation, ^1H - and ^{13}C - chemical shift data were acquired on a Bruker Avance AV500 (Bruker BioSpin GmbH, Rheinstetten, Germany) equipped with a 5 mm TCI

cryoprobe. Data acquisition was controlled by Bruker Topspin ver.2.1., and pulse programs as implemented were used (^1H -, ^{13}C -, ^1H - ^1H -dqfCOSY, ^1H - ^{13}C -HSQC and ^1H - ^{13}C -HMBC). Selective TOCSY experiments were accomplished using a pulse sequence as suggested in Thrippleton et al (2003). For probing entire sugar spin systems, the mixing time was set to 200 ms and $^3J_{\text{HH}}$ correlations were probed by adjusting the mixing time to appropriate values (20-35 ms). For selective irradiation a Gaussian inversion pulse tailored to the respective signal width was used. Selective NOESY experiments were carried out using a Q3 Gaussian pulse cascade and a mixing time of 1.5 s. The fractions examined were dissolved in D_2O and ^1H -chemical shift data were referenced to the residual solvent peak at 4.70 ppm. ^{13}C -chemical shift data were left uncorrected. Carrier frequencies were carefully adjusted to 500.130 MHz for ^1H -NMR measurements and 125.758 MHz for ^{13}C -NMR measurements, respectively. For ^{19}F - and ^{31}P -NMR measurements, all 1D and 2D experiments were carried out on a Bruker Avance AV400 spectrometer using a 5 mm BBFO probe. Standard pulse programs as implemented in Bruker TopSpin ver.2.1 were used. All experiments were recorded at 25°C (298K). Prior to measurements, the carrier frequency was tuned to 376.498 MHz for ^{19}F -, 161.976 MHz for ^{31}P - and 400.130 MHz for ^1H -NMR experiments, respectively. ^{19}F -NMR spectra were recorded with inverse gated ^1H -decoupling using a spectral resolution of 256k data points. The interpulse delay was set to 1 s. 1024 scans were applied. Data were processed with a resolution of 128k and linear back prediction using 32 coefficients, the exponential line broadening was set to 5 Hz. Chemical shifts were referenced to an external standard of neat C_6F_6 at -164.9 ppm. ^{31}P -NMR spectra were recorded with power-gated ^1H -decoupling and a spectral resolution of 32k data points. The interpulse delay was set to 1s. Data processing was accomplished with 32k data points and an exponential line broadening of 3 Hz. Chemical shifts were referenced to an external standard of diluted H_3PO_4 in D_2O at 0 ppm. ^1H - ^{31}P HMBC-NMR spectra were recorded with 4k data points in F2 and 128 data points in F1, respectively. 256 scans were applied. For processing, data were zero-filled to a 2k x 1k matrix.

Results:

MS analysis:

We compared the LCMS and direct infusion MS spectra manually. We looked for characteristics parent ions which gave rise to fragment ions with HF or ¹⁹FDG neutral losses upon fragmentation. Table 1 lists those ions, their retention time and corresponding MS/MS fragments.

Table 1: List of parent ions which gave rise to fragment ions with HF or ¹⁹FDG neutral losses upon fragmentation, their monoisotopic mass, retention time and MS/MS fragmentation.

LC Column	Retention Time (min)	<i>m/z</i>	MS/MS Fragments
Supelco apHera Amino column	3.54	181.0513	163.0493, <u>161.0450</u> , 143.0344, 125.0237, 119.0341, 113.0235, 101.0234, 83.0127, 71.0126, 59.0126
Supelco apHera Amino column	5.32	343.1051	<u>323.0990</u> , 305.0876, 245.0670, <u>179.0564</u>
ACQUITY UPLC BEH Amide column	3.80 - 5.00 (broad and shifting peak)	197.0464	179.0359, <u>177.0401</u> , 170.0721, 161.0088, 151.0608, 142.9981, 126.9044, 101.0035, 87.0077, 61.9872, 59.0127
ACQUITY UPLC BEH Amide column	4.00 - 5.60 (broad and shifting peak)	261.0180	243.0073, <u>241.0116</u> , 223.0010, 204.9903, 199.0009, 145.0278, 138.9797, 96.9686, 78.9579
ACQUITY UPLC BEH Amide column	8.90 - 10.00 (broad and shifting peak)	567.0434	<u>384.9843</u> , 322.9735, 302.9677, <u>305.0179</u> , 272.9571, <u>261.0181</u> , 158.9248, 78.9579

Ion at m/z : 181:

Retention time for ^{19}F standard was found to be 3.54 min on Supelco ApHera Amino column. Measured m/z 181.0513 value matched with calculated monoisotopic mass of $\text{C}_6\text{H}_{10}\text{O}_5^{19}\text{F}^-$ (± 5 ppm). m/z 181.0513 retention time matched with ^{19}F standard. Upon fragmentation, m/z 181.0513 gave rise to secondary ions m/z 163.0493 and 161.0450. The first fragment can be rationalized by H_2O neutral loss (18.0020) and second by HF neutral loss (20.0063). We putatively identified this ^{19}F - metabolite as 2-deoxy-2-fluoro-D-glucose (^{19}F FDG/FDG) on the basis of its exact mono-isotopic mass (± 5 ppm mass error) and MS/MS fragmentation analysis. (supplementary Fig. 5A)

Ion at m/z : 343:

Retention time for m/z 343.1051 was found to be 5.32 min on Supelco ApHera Amino column. Measured m/z 343.1051 matched with calculated monoisotopic mass of $\text{C}_{12}\text{H}_{20}\text{O}_{10}^{19}\text{F}^-$ (± 5 ppm). Upon fragmentation, m/z 343.1051 gave rise to secondary ions m/z 323.0990 and 179.0564. The first fragment can be rationalized by HF neutral loss (20.0061), whereas the other fragment ion was identified as deprotonated glucose ($\text{C}_6\text{H}_{11}\text{O}_6^-$) which could be rationalized by $\text{C}_4\text{H}_9\text{O}_4^{19}\text{F}$ neutral loss. We putatively identified this ^{19}F - metabolite as 2-deoxy-2-fluoro-maltose (F-maltose) on the basis of its exact mono-isotopic mass (± 5 ppm mass error) and MS/MS fragmentation analysis. (supplementary Fig. 5D)

Ion at m/z : 197:

Retention time for m/z 197.0464 was varying in the range of 3.80 to 5.00 min on ACQUITY UPLC BEH Amide column. Measured m/z 197.0464 matched with calculated monoisotopic mass of $\text{C}_6\text{H}_{10}\text{O}_6^{19}\text{F}^-$ (± 5 ppm). Upon fragmentation, m/z 197.0464 gave rise to secondary ions m/z 179.0359 and 177.0401. The first fragment can be rationalized by H_2O neutral loss (18.0105) and second by HF neutral loss (20.0063). We putatively identified this ^{19}F - metabolite as 2-deoxy-2-fluoro-gluconic acid (F-gluconic acid) on the basis of its exact mono-isotopic mass (± 5 ppm mass error) and MS/MS fragmentation analysis. (supplementary Fig. 5B)

Ion at m/z : 261:

Retention time for m/z 261.0180 was varying in the range of 4.00 to 5.60 min on ACQUITY UPLC BEH Amide column. Measured m/z 261.0180 matched with calculated monoisotopic mass of $\text{C}_6\text{H}_{11}\text{O}_8\text{P}^{19}\text{F}^-$ (± 5 ppm). Upon fragmentation, m/z 261.0180 gave rise to secondary

ions m/z 243.0073 and 241.0116. The first fragment can be rationalized by H_2O neutral loss (18.0107) and second by HF neutral loss (20.0064). We putatively identified this ^{19}F -metabolite FDG-6-phosphate (FDG-6-P) on the basis of its exact mono-isotopic mass (± 5 ppm mass error) and MS/MS fragmentation analysis. (supplementary Fig. 5C)

Ion at m/z : 567:

Retention time for m/z 567.0434 was varying in the range of 8.90 to 10.00 min on ACQUITY UPLC BEH Amide column. Measured m/z 567.0434 matched with calculated monoisotopic mass of $C_{15}H_{22}O_{16}N_2P_2^{19}F^-$ (± 5 ppm). Upon fragmentation, m/z 567.0434 gave rise to secondary ions m/z 384.9843. This fragment can be rationalized by $C_6H_{11}O_5^{19}F$ neutral loss (182.0591). We also saw secondary ions of m/z 305.0179 and 261.0181 which matched with calculated monoisotopic mass of $C_9H_{10}O_8N_2P^-$ (± 5 ppm) and $C_6H_{11}O_8P^{19}F^-$ (± 5 ppm) respectively. We putatively identified this ^{19}F -metabolite as uridine-di-phosphate-FDG (UDP-FDG) on the basis of its exact mono-isotopic mass (± 5 ppm mass error) and MS/MS fragmentation analysis. (supplementary Fig. 5E)

To characterize some of the above ^{19}F -metabolites, we partially purified polar ^{19}F metabolites using F-SPE cartridge and subjected the fractions for NMR analysis. We have also purified ^{19}F -metabolite (m/z 343.1051) from ^{19}FDG applied leaf extract using two-step LC fractionation using Supelco ApHera Amino column and YMC-Pack Polyamine-II column (25 cm \times 4.6 mm, particle size- 5 μm). We collected the ^{19}F -metabolite (m/z 343.1051) fraction and subjected it to further NMR analysis for structure elucidation.

LCMS and direct infusion MS results confirmed the presence of above 5 different ^{19}F containing metabolites. In total, we putatively identified above ^{19}F containing metabolites as FDG (m/z 181.0513), F-gluconic acid (m/z 197.0464), FDG-6-P (m/z 261.0180), F-maltose (m/z 343.1051), and UDP-FDG (m/z 567.0434) on the basis of known literature information, their exact mono-isotopic mass (± 5 ppm mass error) and MS/MS fragmentation analysis. Characterization of purified compounds using NMR confirmed identification of ^{19}FDG -6-P (m/z 261.0180), and ^{19}F -maltose (m/z 343.1051) as major end products of ^{19}FDG metabolism in *A. thaliana* leaf cells.

NMR analysis:

FDG-6-P (2-deoxy-2-fluoroglucose-6-phosphate):

A phosphorylated derivative of FDG (m/z 261.0180) was putatively assigned by high resolution MS data, however, the exact structure and the site of phosphorylation remained unclear. A semi-purified fraction containing the phosphorylated FDG derivative was thus subjected to extensive NMR analysis. ^{19}F -NMR spectroscopy revealed FDG-6-P as the most abundant metabolite in the extract, showing two signals at δ_{F} -197.75 (α -FDG-6-P) and δ_{F} -197.55 (β -FDG-6-P) (Fig. 2). The assignment is based on the fact that chemical shift values for α -isomers appear generally shifted towards deeper field compared to the corresponding β -isomers (Southworth et al, 2003). It has to be noted that the determined chemical shifts are not in accordance with the literature, which might be caused by the impurities present in the samples. Structure elucidation was therefore based on ^1H - ^1H and ^1H - ^{13}C correlation experiments. Characteristic correlations in the ^1H - ^1H dqfCOSY spectrum (supplementary Fig. 6) revealed the signals of position 1 at δ_{H} 5.29 (d , $^3J_{\text{HH}}=3.8$) ($\text{H-1}\alpha$) and δ_{H} 4.76 (dd , $^3J_{\text{HH}}=7.8/3J_{\text{HF}}=2.0$) ($\text{H-1}\beta$), respectively. According to the corresponding signals in the ^1H - ^{13}C HSQC spectrum, the ^{13}C chemical shifts were assigned to δ_{C} 89.6 (d , $^2J_{\text{CF}}=21.2$) ($\text{C-1}\alpha$) and δ_{C} 93.5 (d , $^2J_{\text{CF}}=23.6$) ($\text{C-1}\beta$). Since the ^1H - and ^{13}C -NMR spectra were recorded without decoupling of heteroatoms, the extracted coupling patterns furthermore reveal that the site of phosphorylation is not at position 1, thus the presence of FDG-1-P could therefore be excluded.

For further structure elucidation, selective TOCSY experiments were performed (supplementary Fig. 7). From irradiation of $\text{H-1}_{\alpha/\beta}$ all remaining partners of the spin systems could be extracted. The resulting spectra served as projections for ^1H - ^1H dqfCOSY, ^1H - ^{13}C HSQC and ^1H - ^{13}C HMBC spectra. The signal $\text{H-2}\alpha$ of FDG-6-P appeared at δ_{H} 4.28 (ddd , $^3J_{\text{HH}}=3.8/9.5$, $^2J_{\text{HF}}=49.4$) and $\text{H-2}\beta$ appeared at δ_{H} 3.97 (ddd , $^3J_{\text{HH}}=7.8/9.0$, $^2J_{\text{HF}}=51.2$), both signals showed an additional splitting due to the coupling to the fluorine substituent through two bonds. The corresponding ^{13}C chemical shifts also showed a splitting because of coupling through one bond to the fluorine substituent. The signal $\text{C-2}\alpha$ resonated at δ_{C} 90.1 (d , $^1J_{\text{CF}}=185.8$), while $\text{C-2}\beta$ resonates at δ_{C} 92.7 (d , $^1J_{\text{CF}}=183.3$) (Fig. 3A). From crosspeaks in the ^1H - ^1H dqfCOSY and ^1H - ^{13}C HMBC spectra the chemical shifts of the positions $\text{H-3}_{\alpha/\beta}$ and $\text{C-3}_{\alpha/\beta}$ could be extracted (Fig. 3B). $\text{H-3}\alpha$ resonates at δ_{H} 3.82 (ddd , $^3J_{\text{HH}}=9.5/9.5$, $^3J_{\text{HF}}=13.0$) and the corresponding carbon signal $\text{C-3}\alpha$ appears at δ_{C} 70.8 (d , $^2J_{\text{CF}}=16.4$). $\text{H-3}\alpha$ is overlapped with $\text{H-5}\alpha$, but considering the signal geometry in the ^1H - ^{13}C HSQC spectrum, the multiplicity could be estimated. $\text{H-3}\beta$ appears as well resolved signal at δ_{H} 3.65 (ddd ,

$^3J_{HH}=9.0/9.0$, $^3J_{HF}=15.0$) and the corresponding C-3 $_{\beta}$ resonates at δ_C 73.6 (*d*, $^2J_{CF}=17.6$). H-4 $_{\alpha}$ resonates at δ_H 3.41 (*dd*, $^3J_{HH}=9.5/9.5$) and the attached C-4 $_{\alpha}$ appears at δ_C 68.5 (*d*, $^3J_{CF}=8.0$). H-4 $_{\beta}$ resonates at δ_H 3.42 (*ddd*, $^3J_{HH}=9.5/9.5$ and the corresponding C-4 $_{\beta}$ appears at δ_C 68.6 (*d*, $^3J_{CF}=7.8$). The proton signals of position 5 $_{\alpha/\beta}$ show considerable broadening and overlap, therefore only the chemical shift value can be extracted. The chemical shift of C-5 $_{\alpha/\beta}$ was extracted from the 1H - ^{13}C HMBC spectrum (Fig. 3B). H-5 $_{\alpha}$ resonates at δ_H 3.80 (*m*) with a corresponding carbon signal C-5 $_{\alpha}$ at δ_C 70.2 (*d*, $^3J_{CP}=6.2$). The signal for H-5 $_{\beta}$ appears at δ_H 3.46 (*m*) with a corresponding carbon signal C-5 $_{\beta}$ at δ_C 74.8 (*d*, $^3J_{CP}=6.0$). The chemical shifts of H-6 $_{\alpha/\beta}$ are very similar. The signal of the methylene group at position 6 appears at δ_H 3.91 (*bs*) for the α -sugar and at δ_H 3.87 (*m*) and δ_H 3.97 (*m*), respectively, for the β -sugar. The corresponding carbon resonance for C-6 $_{\alpha/\beta}$ appears at δ_C 63.5 as broad singlet signal with a half width of 9 Hz. The splitting of the ^{13}C -NMR signal of C-5 $_{\alpha/\beta}$ as well as the broadening for C-6 $_{\alpha/\beta}$ is caused by phosphorylation at position 6 $_{\alpha/\beta}$ which was further corroborated by a 1H - ^{31}P -HMBC experiment (supplementary Fig. 8). The chemical shift of the phosphate residue was determined from a ^{31}P -NMR experiment to be δ_P 0.83 (*bs*). The structures including determined chemical shifts and coupling constants are summarized in supplementary Fig. 9.

F-maltose (4-*O*-(α -D-glucopyranosyl)-2-deoxy-2-fluoro-D-glucopyranose):

A fluorinated disaccharide (*m/z* 343.1051) was identified by high resolution MS. NMR studies revealed this compound to be 4-*O*-(α -D-glucopyranosyl)-2-deoxy-2-fluoro-D-glucopyranose. Data extracted are in agreement with published results in Tantanarat et al (2012) [Tantanarat et al, 2012].

The ^{19}F -NMR spectrum of the semi-purified fraction showed two signals at δ_F -198.26 (β -F-maltose) and δ_F -198.50 (α -F-maltose), revealing this compound to be the second most abundant metabolite formed in *A. thaliana* after FDG administration. A 1H - 1H dqfCOSY spectrum showed characteristic crosspeaks (supplementary Fig. 10). The 3J -coupling partners of H-1 $_{\alpha/\beta}$ show the large characteristic split caused by the $^2J_{HF}$ coupling. Similar to α/β -FDG-6-P, two signals at δ_H 5.31 (*d*, $^3J_{HH}=3.8$, H-1 $_{\alpha}$) and δ_H 4.78 (*dd*, $^3J_{HH}=7.8/3J_{HF}=2.2$, H-1 $_{\beta}$), respectively, represent the anomeric position 1 of the parent FDG structure. A signal overlapping with H-1 $_{\alpha}$ was assigned to H-1'. Again, selective TOCSY spectra have been employed to reduce signal overlap from impurities (supplementary Fig. 11). The resulting spectra were used as projections for 2D experiments (1H - 1H dqfCOSY, 1H - ^{13}C HSQC and 1H - ^{13}C HMBC). Characteristic signals and coupling constants are shown in a section of the

¹H-¹³C HSQC spectrum (Fig. 4A). Structure elucidation was based on information gathered from ¹H-¹³C-HMBC and a series of selective ¹H-¹H COSY and selective ¹H-¹H NOESY spectra (Fig. 4B). The structures with chemical shifts are summarized in (supplementary Fig. 12A and 12B).

Discussion:

FDG metabolism in *A. thaliana*:

¹⁸FDG is widely accepted as a radiotracer for glucose in animal studies. Being glucose analogue, FDG is transported into the animal cells via the same transporters as glucose [Higashi et al, 1998; Brown et al, 1999; Yen et al, 2004; Avril N, 2004]. It was assumed till recently that upon intracellular uptake, FDG metabolism is just restricted to enzymatic phosphorylation, producing FDG-6-phosphate (FDG-6-P) by the action of hexokinase or glucokinase [Miller and Kiney, 1981; Reivich et al, 1985; Bessel and Thomas, 1973; Suolinna et al, 1986]. The phosphorylation reaction also introduces the negative charge on the radiotracer preventing its efflux across cell membrane. This leads to increased accumulation of FDG-6-P inside the cell. The assumption that FDG flux is only directed towards FDG-6-P and thus leads to intracellular radioisotope accumulation forms the basis of ¹⁸FDG application as a glucose radiotracer. However, numerous studies have demonstrated that FDG metabolism in animal tissue goes beyond FDG-6-P [Kanazawa et al, 1996; McSheehy *et al.*, 2000; Kaarstad *et al.*, 2002; Southworth *et al.*, 2003]. These studies listed 2-deoxy-2-fluoro-D-mannose (FDM), 2-deoxy-2-fluoro-D-mannose-6-phosphate (FDM-6-P), 2-deoxy-2-fluoro-D-glucose-1-phosphate (FDG-1-P), 2-deoxy-2-fluoro-D-glucose-1,6-biphosphate (FDG-1,6-biP), 2-deoxy-2-fluoro-D-mannose-1-phosphate (FDM-1-P), 6-phospho-2-deoxy-2-fluoro-D-gluconolactone (6-PFDGL), 6-phospho-2-deoxy-2-fluoro-D-gluconate (FDG-6-PG), nucleotide-di-phosphate bound FDG (NDP-FDG) *etc.* as metabolic end products of FDG in animal cells [Kanazawa et al, 1996; McSheehy et al, 2000; Bender et al, 2001; Kaarstad et al, 2002; Southworth et al, 2003]. Important thing to notice here is that these reported metabolites are either situated down the FDG-6-P in glycolytic pathway or arise from it. Thus, net radioactivity accumulated in that tissue still reflects the rate of phosphorylation of FDG and does not challenge the basis of current hypothesis (Kaarstad *et al.*, 2002) that net FDG uptake by the cell (i.e. total radioactivity acquired by the cell) represents net sugar flux going into glycolysis pathway.

Among all the studies related to FDG imaging in plants, only few have looked at the metabolism of FDG in plant cells. Thus, FDG metabolism in plants is yet poorly understood topic. Ferrieri et al (2012) reported incorporation of FDG in anthocyanin glycoside biosynthesis as a measure of plant defense induction. In this paper, Ferrieri et al (2012) also raised a possibility of another F-metabolite whose identity was not discovered. Our present work elucidated FDG metabolism in *Arabidopsis thaliana* leaf cells. We have putatively identified the presence of 4 different ^{19}F containing metabolites viz. F-gluconic acid, FDG-6-P, F-maltose, and UDP-FDG on the basis of known literature information from animal studies, exact mono-isotopic mass for these compounds and MS/MS fragmentation analysis. We have partially purified and characterized of two of the compounds (FDG-6-P and F-maltose) using NMR. We also looked for ^{19}F -compounds which were previously reported in literature for FDG metabolism in animal tissue. To our surprise, we have not detected 2-fluoro-2-deoxy-6-phospho-D-gluconolactone (FD-6-PGL), 2-fluoro-2-deoxy-6-phospho-D-gluconate (FD-PG1) or FDG-1,6-biphosphate (FDG-1,6-biP) [Bender et al, 2001, Kaarstad et al, 2002; Southworth et al, 2003] like compounds which were previously reported in various animal studies. We also could not detect the ions for ^{19}F -containing major anthocyanin glycosides (m/z 1344) in our LCMS or direct infusion data. This may happen because we acquired and analyzed negative mode MS data whereas anthocyanin glycoside ions may only appear in positive mode MS data.

In our previous paper, we have shown that *A. thaliana* plants take up ^{18}F FDG from the pricked leaf spot and radioactivity was differentially distributed to various plants parts [Fatangare et al, 2014]. *A. thaliana* plant suspension cells are able to take up FDG from external nutrient and glucose acts as a competitive inhibitor of FDG uptake [Fatangare et al, 2014; supplementary Fig. 1]. We also found that FDG uptake by *A. thaliana* suspension cells is severely inhibited by addition of 1 mM HgCl_2 in the media [Fatangare et al, 2014; supplementary Fig. 1 and 2]. FDG uptake time course also follows exponential curve [supplementary Fig.1] similar to glucose uptake rate in glucose starved *Olea europaea* (olive) cells [Oliveira et al, 2002; Conde et al, 2007]. This glucose uptake process in olive cells is shown to be mediated by glucose repressible, H^+ -dependent active saturable transport system which is sensitive to HgCl_2 [Oliveira et al, 2002; Conde et al, 2007]. However, when high external glucose concentrations are present, glucose uptake occurs through low-affinity, high capacity, protein mediated facilitated transport process which is also sensitive to HgCl_2 [Conde et al, 2007]. On this basis, we hypothesize that FDG is being taken up into the cells

via glucose repressible, H^+ -dependent active saturable transport system at low external FDG concentrations and low-affinity, facilitated-diffusion process at high external FDG concentrations.

The H^+ -dependent monosaccharide transporters of olive cells exhibited broad specificity, being able to accept D-glucose, D-fructose, D-galactose, D-xylose, 2-deoxy-D-glucose, and 3-O-methyl-D-glucose [Oliveira et al, 2000]. Similarly, numerous monosaccharide transporters (MST) with broad specificity, transporting a range of hexoses and pentoses, have been reported in literature to transport monosaccharides across the plasma membrane [Büttner et al, 2000; Büttner and Sauer, 2000; Büttner M, 2007]. We think that FDG, being a glucose analogue, is transported through one or more of the MST family transporters which are sensitive to $HgCl_2$ [Fatangare et al, 2014]. Due to broad specificity and highly redundant functional nature of these monosaccharide transporters, it's hard to comment upon which will be the key transporters facilitating FDG uptake in *A. thaliana* leaf cells.

After uptake, FDG is being metabolized to $^{19}FDG-6-P$. This is the first enzymatic conversion in glycolytic pathway catalyzed by hexokinase. Hexokinase is known to accept FDG as a substrate [Machado de Domenech and Sols, 1980; Muzi et al, 2001]. Hexokinase mediated conversion of FDG into FDG-6-P will add negative charge on influxed FDG and leading to its trapping inside the cell. This will maintain the downhill concentration gradient which favours the facilitated transport of FDG into the cell [Printz et al, 1993]. This may explain the favorable uptake of external FDG into the cell resulting in high localized accumulation [Fatangare et al, 2014]. Upon uptake, FDG was transformed into various metabolites other than FDG-6-P. In future work, we will try to elucidate underlying pathways involved in biosynthesis of these metabolites.

Formation of F-gluconic acid requires spontaneous or enzymatic oxidation of FDG. Buriova et al (2001) showed formation of F-gluconic acid upon oxidation of FDG [Buriova et al, 2001]. We also checked possibility of spontaneous oxidation of free FDG into F-gluconic acid during the solvent extraction process. Results showed that there is no formation of F-gluconic acid from the externally added free FDG in the final extracts. This removes the possibility that F-gluconic acid originated as an artefact of spontaneous oxidation process during the solvent extraction procedure. In such case, enzymatic dehydrogenation and hydration seems to be plausible way to explain formation of F-gluconic acid. Glucose oxidase (enzyme: 1.1.3.4) or Glucose dehydrogenase (EC 1.1.5.9) could convert glucose to glucono-

lactone which upon enzymatic hydration by gluconolactonase (EC 3.1.1.17) can transform into gluconic acid [www.brenda-enzymes.org/enzyme.php?ecno=3.1.1.17]. However, none of the above enzymes have been reported in *Arabidopsis*. Other plausible enzymatic path leading to F-gluconic acid biosynthesis exists but goes through three intermediates like FDG-6-P; 2-deoxy-2-fluoro-D-glucono-1,5-lactone-6-P; 2-deoxy-2-fluoro-D-gluconate-6-P. However, we could not detect these intermediates. At the current moment, we could not comment upon the mechanism of biosynthesis of F-gluconic acid which may be either spontaneous or enzymatic oxidation.

We have observed F-disaccharide as one of the end products of FDG metabolism in plant leaf tissue. Upon NMR analysis, we found out it to be F-maltose. Cytosolic component of transitory starch breakdown pathway seems to be most the plausible mechanisms leading to F-maltose biosynthesis *in vivo*. Maltose metabolism in *Arabidopsis* depends upon a disproportionating enzyme and alpha-glucan phosphorylase [Lu et al, 2006]. In *Arabidopsis*, cytosolic maltose is mainly metabolized via glucosyltransfer reaction catalyzed by cytosolic glucosyltransferase disproportionating enzyme 2 (DPE2) (EC 2.4.1.25) which transfers one of the glucosyl units of maltose as free glucose and transfers the other to glycogen [Lu and Sharkey, 2004; Chia et al, 2004] or highly branched, soluble heteroglycan [Lu et al, 2006]. Reversibly, DPE2 is able to catalyze the transfer of a segment of a (1-4)-alpha-D-glucan to a new position in an acceptor, which may be glucose, a (1-4)-alpha-D-glucan [Kaper et al, 2004; Lin and Preiss, 1988; Lu and Sharkey, 2004; Lu et al, 2006; Steichen et al, 2008] or FDG [Tantanarat et al, 2012]. FDG could be converted into the F-maltose *in vitro* using DPE2-mediated trans-glycosylation reaction with glycogen acting as a glucosyl donor [Tantanarat et al, 2012]. We hypothesize that similar DPE2-mediated trans-glycosylation reaction mechanism must have been involved in biosynthesis of F-maltose.

Previous studies have demonstrated nucleotide bound forms of FDG [Schmidt et al, 1978; Kanazawa et al, 1996; Southworth et al, 2003]. Schmidt et al, (1978) have demonstrated the formation of UDP and GDP derivatives of FDG in yeast and chick embryo cells. NDP-FDG and NDP-FDM were shown to be end products of FDG metabolism in animal tissue [Kanazawa et al, 1996; Southworth et al, 2003]. However, assignment of nucleotide species (NDP moiety) was a source of ambiguity in these reports. In our study, we were able to detect only m/z 567.0434 which corresponds to UDP-FDG. Thus, we could conclusively point out UDP-FDG as a nucleotide bound form of FDG. Biosynthesis of UDP-FDG has already been

described by Kanazawa et al (1997). We think that similar mechanism exists for the UDP-FDG biosynthesis in plant tissue. The possible UDP-FDG biosynthetic pathway has been shown in Fig. 1. This assumption presupposes presence of FDG-1-P as one of the intermediates formed in the process of UDP-FDG biosynthesis. In our studies, we could not detect FDG-1-P as one of the intermediates. We think that FDG-1-P might be present but in low abundance. We might not have been able to detect FDG-1-P as a separate compound because of low chromatographic separation between FDG-6-P and FDG-1-P. Also, we were not able to differentiate between FDG-1-P and FDG-6-P in MS as they will have same m/z value or show similar MS/MS fragmentation. UDP-FDG acts as a glucosyl moiety donor in various biosynthetic pathways such as starch, anthocyanin or flavonoid biosynthesis etc. Considering UDP-FDG role in diverse pathways, it's hard to imagine the multitude of FDG conjugated compounds it leads to. We think that UDP-FDG may have been involved in biosynthesis of fluorinated anthocyanin [Ferrieri et al, 2012].

Deciphering “Why FDG metabolism is directed towards formation of above mentioned end products” is still unanswered. We think, FDG, upon intracellular uptake, will be considered as energy source by the cell and will be fluxed into glycolytic pathway leading to synthesis of FDG-6-P. However, all taken-up FDG could not be metabolized into FDG-6-P as building-up concentration of FDG-6-P inside the cell slow down this bio-transformation through feedback inhibition of hexokinase. FDG-6-P will actually become a catabolic block brining glycolysis to halt. This has already been shown in hypoxic animal tissue [Datema et al, 1980; Kurtoglu et al, 2007]. This may lead to rest of the free FDG pushed into F-maltose or F-gluconic acid biosynthetic pathways [Fig. 1]. FDG-6-P may be further transformed into FDG-1-P and finally to UDP-FDG as depicted in Fig. 1. Formation of various fluorine-metabolites in plants can be a way of plants to cope up with high intracellular concentration of FDG which is known glycolytic inhibitor. Thus, biosynthesis of various F-metabolites could also be viewed as utilization of FDG as energy source and a corrective-protective mechanism in the plant cells to counteract its consequences.

In our experiment, we observed signs of tissue death/damage at FDG application site (supplementary Fig. 3). FDG, at high local concentrations, may cause cytotoxicity in plant cells. It has been shown that FDG interferes with glycolysis thus resulting in cytotoxicity in hypoxic tumor cells which solely rely on glycolysis for deriving their energy [Lampidis et al, 2006; Maher et al, 2004, Kurtoglu et al, 2007]. In contrast, the aerobically growing cells,

with functional mitochondria, survive glycolytic inhibition by using carbon sources other than glucose (fats and proteins) to generate ATP via oxidative phosphorylation [McKeehan, 1982; Mazurek et al, 1997; Reitzer 1979; Kurtoglu et al, 2007]. Plant cells might experience the similar glycolytic inhibition when fed with FDG. However, for well aerated leaf tissue, FDG should not result in cytotoxicity. FDG also hampers the *N*-linked glycosylation by inhibiting the incorporation of mannose and glucose into lipid-linked oligosaccharides [Datema et al, 1980; Kurtoglu et al, 2007a; Kurtoglu et al, 2007b]. Inhibition of glycolysis and *N*-linked glycosylation might explain the observed signs of tissue death/damage at FDG application site. However, this could be only confirmed with ¹⁹FDG cytotoxicity studies in plant tissue

It has been reported that FDG-6-P reversibly epimerizes to 2-Fluoro-2-deoxy mannose-6-phosphate (FDM-6-P) under the action of phosphoglucose isomerase [Kanazawa et al., 1986; Kojima et al., 1988; Pouremad and Wyrwicz, 1991; O'Connell and London, 1995]. 2-deoxy-2-fluoro-D-mannose (FDM) metabolites such as FDM-1-P, FDM-1,6-biP and nucleotide diphosphate-FDM (NDP-FDM) have been reported in animal tissue [Kanazawa et al, 1996; Southworth et al, 2003]. However, in our study, we only focused upon abundant FDG metabolites but we could not deny presence of corresponding FDM-metabolites. In this paper, we have not reported the amount of various FDG metabolites or time kinetics of their biosynthesis. We have rather noted F-gluconic acid, FDG-6-P, F-maltose and UDP-FDG as 4 major end products of FDG metabolism in *A. thaliana* leaf tissue. We hope that this work will pave way for discovery of further FDG metabolic end products and FDG kinetics in plant tissue.

Acknowledgements:

We thank A. Weber and the greenhouse team of MPI-Chemical Ecology for growing the *A. thaliana* plants; Emily Wheeler for editorial assistance. We thank Dr. Stefan Meldau, Dr. Abigail Ferrieri and Dr. Jerrit Weißflog for their guidance and fruitful discussions. We are also grateful to the Hans Knöll Institute for permission to use the radio-laboratory and PET/CT facility; the Max Planck Society for a stipend to Amol Fatangare and for financial support.

References:

- [1] Alavi A, Reivich M, Jones S, Greenberg J, and Wolf A. Functional imaging of the brain with positron emission tomography. *Nuclear medicine annual* 1982; 1982.
- [2] Avril N. GLUT1 expression in tissue and (18) F-FDG uptake. *Journal of nuclear medicine: official publication, Society of Nuclear Medicine* 2004;45:930.
- [3] Bender D, Munk O, Feng H, and Keiding S. Metabolites of (18) F-FDG and 3-O-(11) C-methylglucose in pig liver. *Journal of nuclear medicine: official publication, Society of Nuclear Medicine* 2001;42:1673.
- [4] Bessell E, Foster A, and Westwood J. The use of deoxyfluoro-D-glucopyranoses and related compounds in a study of yeast hexokinase specificity. *Biochemical Journal* 1972;128:199.
- [5] Bessell E and Thomas P. The effect of substitution at C-2 of D-glucose 6-phosphate on the rate of dehydrogenation by glucose 6-phosphate dehydrogenase (from yeast and from rat liver). *The Biochemical journal* 1973;131:83.
- [6] Brown RS, Leung JY, Kison PV, Zasadny KR, Flint A, and Wahl RL. Glucose transporters and FDG uptake in untreated primary human non-small cell lung cancer. *Journal of Nuclear Medicine* 1999;40:556-65.
- [7] Buriova E, Medová M, Macášek F, and Brúder P. Separation and detection of oxidation products of fluorodeoxyglucose and glucose by high-performance liquid chromatography–electrospray ionisation mass spectrometry. *Journal of Chromatography A* 2004;1034:133-7.
- [8] Büttner M. The monosaccharide transporter (-like) gene family in Arabidopsis. *FEBS letters* 2007;581:2318.
- [9] Büttner M and Sauer N. Monosaccharide transporters in plants: structure, function and physiology. *Biochimica et Biophysica Acta (BBA)-Biomembranes* 2000;1465:263-74.
- [10] Büttner M, Truernit E, Baier K, Scholz-Starke J, Sontheim M, Lauterbach C, et al. AtSTP3, a green leaf-specific, low affinity monosaccharide-H⁺ symporter of Arabidopsis thaliana. *Plant, Cell & Environment* 2000;23:175-84.
- [11] Chia T, Thorneycroft D, Chapple A, Messerli G, Chen J, Zeeman SC, et al. A cytosolic glucosyltransferase is required for conversion of starch to sucrose in Arabidopsis leaves at night. *The Plant Journal* 2004;37:853-63.
- [12] Conde C, Silva P, Agasse A, Tavares RM, Delrot S, and Gerós H. An Hg-sensitive channel mediates the diffusional component of glucose transport in olive cells. *Biochimica et Biophysica Acta (BBA)-Biomembranes* 2007;1768:2801-11.

- [13] Datema R, Schwarz R, and Jankowski A. Fluoroglucose-inhibition of protein glycosylation in vivo. Inhibition of mannose and glucose incorporation into lipid-linked oligosaccharides. *European journal of biochemistry/FEBS* 1980;109:331.
- [14] Fatangare A, Gebhardt P, Saluz H, and Svatoš A. Comparing 2-^[18F]fluoro-2-deoxy-D-glucose and [⁶⁸Ga]gallium-citrate translocation in *Arabidopsis thaliana*. *Nuclear medicine and biology* 2014;41:737-43.
- [15] Ferrieri A, Appel H, Ferrieri R, and Schultz J. Novel application of 2-[(18) F] fluoro-2-deoxy-D-glucose to study plant defenses. *Nuclear medicine and biology* 2012;39:1152.
- [16] Gromova M and Roby C. Toward *Arabidopsis thaliana* hydrophilic metabolome: assessment of extraction methods and quantitative ¹H NMR. *Physiologia plantarum* 2010;140:111-27.
- [17] Hattori E, Uchida H, Harada N, Ohta M, Tsukada H, Hara Y, et al. Incorporation and translocation of 2-deoxy-2-[¹⁸F] fluoro-D-glucose in *Sorghum bicolor* (L.) Moench monitored using a planar positron imaging system. *Planta* 2008;227:1181-6.
- [18] Higashi T, Tamaki N, Torizuka T, Nakamoto Y, Sakahara H, Kimura T, et al. FDG uptake, GLUT-1 glucose transporter and cellularity in human pancreatic tumors. *Journal of nuclear medicine: official publication, Society of Nuclear Medicine* 1998;39:1727.
- [19] Kaarstad K, Bender D, Bentzen L, Munk OL, and Keiding S. Metabolic fate of ¹⁸F-FDG in mice bearing either SCCVII squamous cell carcinoma or C3H mammary carcinoma. *Journal of Nuclear Medicine* 2002;43:940-7.
- [20] Kanazawa Y, Momozono Y, Ishikawa M, Yamada T, Yamane H, Haradahira T, et al. Metabolic pathway of 2-deoxy-2-fluoro-D-glucose studied by F-19 NMR. *Life sciences* 1986;39:737-42.
- [21] Kanazawa Y, Yamane H, Shinohara S, Kuribayashi S, Momozono Y, Yamato Y, et al. 2-Deoxy-2-fluoro-D-glucose as a functional probe for NMR: the unique metabolism beyond its 6-phosphate. *Journal of neurochemistry* 1996;66:2113.
- [22] Kaper T, van der Maarel M, Euverink G, and Dijkhuizen L. Exploring and exploiting starch-modifying amylomaltases from thermophiles. *Biochemical Society Transactions* 2004;32:279-82.
- [23] Kojima M, Kuribayashi S, Kanazawa Y, Haradahira T, Maehara Y, and Endo H. Metabolic pathway of 2-deoxy-2-fluoro-D-glucose and 2-deoxy-2-fluoro-D-mannose in mice bearing sarcoma 180 studied by fluorin-19 nuclear magnetic resonance. *Chemical & pharmaceutical bulletin* 1988;36:1194.

- [24] Kurtoglu M, Gao N, Shang J, Maher JC, Lehrman MA, Wangpaichitr M, et al. Under normoxia, 2-deoxy-D-glucose elicits cell death in select tumor types not by inhibition of glycolysis but by interfering with N-linked glycosylation. *Molecular cancer therapeutics* 2007;6:3049-58.
- [25] Kurtoglu M, Maher JC, and Lampidis TJ. Differential toxic mechanisms of 2-deoxy-D-glucose versus 2-fluorodeoxy-D-glucose in hypoxic and normoxic tumor cells. *Antioxidants & redox signaling* 2007;9:1383-90.
- [26] Lampidis TJ, Kurtoglu M, Maher JC, Liu H, Krishan A, Sheft V, et al. Efficacy of 2-halogen substituted D-glucose analogs in blocking glycolysis and killing “hypoxic tumor cells”. *Cancer chemotherapy and pharmacology* 2006;58:725-34.
- [27] Lin T-P and Preiss J. Characterization of D-enzyme (4- α -glucanotransferase) in *Arabidopsis* leaf. *Plant physiology* 1988;86:260-5.
- [28] Lu Y and Sharkey TD. The role of amylomaltase in maltose metabolism in the cytosol of photosynthetic cells. *Planta* 2004;218:466-73.
- [29] Lu Y, Steichen JM, Yao J, and Sharkey TD. The role of cytosolic α -glucan phosphorylase in maltose metabolism and the comparison of amylomaltase in *Arabidopsis* and *Escherichia coli*. *Plant physiology* 2006;142:878-89.
- [30] Machado de Domenech EE and Sols A. Specificity of hexokinases towards some uncommon substrates and inhibitors. *FEBS letters* 1980;119:174-6.
- [31] Maher JC, Krishan A, and Lampidis TJ. Greater cell cycle inhibition and cytotoxicity induced by 2-deoxy-D-glucose in tumor cells treated under hypoxic vs aerobic conditions. *Cancer chemotherapy and pharmacology* 2004;53:116-22.
- [32] Mazurek S, Boschek C, and Eigenbrodt E. The role of phosphometabolites in cell proliferation, energy metabolism, and tumor therapy. *Journal of bioenergetics and biomembranes* 1997;29:315-30.
- [33] McKeehan WL. Glycolysis, glutaminolysis and cell proliferation. *Cell biology international reports* 1982;6:635-50.
- [34] McSheehy PM, Leach MO, Judson IR, and Griffiths JR. Metabolites of 2'-fluoro-2'-deoxy-D-glucose detected by ^{19}F magnetic resonance spectroscopy in vivo predict response of murine RIF-1 tumors to 5-fluorouracil. *Cancer research* 2000;60:2122-7.
- [35] Miller A and Kiney C. Metabolism of [^{14}C] fluorodeoxyglucose by rat brain in vivo. *Life sciences* 1981;28:2071.

- [36] Muzi M, Freeman SD, Burrows RC, Wiseman RW, Link JM, Krohn KA, et al. Kinetic characterization of hexokinase isoenzymes from glioma cells: implications for FDG imaging of human brain tumors. *Nuclear medicine and biology* 2001;28:107-16.
- [37] O'Connell T and London R. Identification of 2-fluoro-2-deoxy-D-glucose metabolites by ¹⁹F (1H) hetero-RELAY. *Journal of magnetic resonance. Series B* 1995;109:264.
- [38] Oliveira J, Tavares RM, and Gerós H. Utilization and transport of glucose in *Olea europaea* cell suspensions. *Plant and cell physiology* 2002;43:1510-7.
- [39] Partelová D, Uhrovčík J, Lesný J, Horník M, Rajec P, Kováč P, et al. Application of positron emission tomography and 2-[¹⁸F] fluoro-2-deoxy-D-glucose for visualization and quantification of solute transport in plant tissues. *Chemical Papers* 2014;68:1463-73.
- [40] Partelová D, Uhrovčík J, Lesný J, Horník M, Rajec P, Kováč P, et al. Application of positron emission tomography and 2-[¹⁸F] fluoro-2-deoxy-D-glucose for visualization and quantification of solute transport in plant tissues. *Chemical Papers* 2014;68:1463-73.
- [41] Phelps ME. PET: molecular imaging and its biological applications: Springer, 2004.
- [42] Pouremad R and Wyrwicz AM. Cerebral metabolism of fluorodeoxyglucose measured with ¹⁹F NMR spectroscopy. *NMR in biomedicine* 1991;4:161-6.
- [43] Printz RL, Magnuson MA, and Granner DK. Mammalian glucokinase. *Annual review of nutrition* 1993;13:463-96.
- [44] Reitzer LJ, Wice BM, and Kennell D. Evidence that glutamine, not sugar, is the major energy source for cultured HeLa cells. *Journal of Biological Chemistry* 1979;254:2669-76.
- [45] Reivich M, Alavi A, Wolf A, Fowler J, Russell J, Arnett C, et al. Glucose metabolic rate kinetic model parameter determination in humans: the lumped constants and rate constants for [¹⁸F] fluorodeoxyglucose and [¹¹C] deoxyglucose. *Journal of Cerebral Blood Flow & Metabolism* 1985;5:179-92.
- [46] Sanchez-Crespo A, Andreo P, and Larsson SA. Positron flight in human tissues and its influence on PET image spatial resolution. *European journal of nuclear medicine and molecular imaging* 2004;31:44-51.
- [47] Schmidt M, Biely P, Krátký Z, and Schwarz R. Metabolism of 2-deoxy-2-fluoro-D-[³H] glucose and 2-deoxy-2-fluoro-D-[³H] mannose in yeast and chick-embryo cells. *European journal of biochemistry/FEBS* 1978;87:55.
- [48] Smith T. The rate-limiting step for tumor [¹⁸F]fluoro-2-deoxy-D-glucose (FDG) incorporation. *Nuclear medicine and biology* 2001;28:1-4.
- [49] Sols A and Crane RK. Substrate specificity of brain hexokinase. *Journal of Biological Chemistry* 1954;210:581-95.

- [50] Som P, Atkins H, Bandoypadhyay D, Fowler J, MacGregor R, Matsui K, et al. A fluorinated glucose analog, 2-fluoro-2-deoxy-D-glucose (F-18): nontoxic tracer for rapid tumor detection. *J Nucl Med* 1980;21:670-5.
- [51] Southworth R, Parry CR, Parkes HG, Medina RA, and Garlick PB. Tissue-specific differences in 2-fluoro-2-deoxyglucose metabolism beyond FDG-6-P: a ^{19}F NMR spectroscopy study in the rat. *NMR in Biomedicine* 2003;16:494-502.
- [52] Steichen JM, Petty RV, and Sharkey TD. Domain characterization of a 4- α -glucanotransferase essential for maltose metabolism in photosynthetic leaves. *Journal of Biological Chemistry* 2008;283:20797-804.
- [53] Suolinna E, Haaparanta M, Paul R, Härkönen P, Solin O, and Sipilä H. Metabolism of 2-[^{18}F] fluoro-2-deoxyglucose in tumor-bearing rats: chromatographic and enzymatic studies. *International journal of radiation applications and instrumentation. Part B, Nuclear medicine and biology* 1986;13:577.
- [54] Tantanarat K, Rejzek M, O'Neill E, Ruzanski C, Hill L, Fairhurst SA, et al. An expedient enzymatic route to isomeric 2-, 3-and 6-monodeoxy-monofluoro-maltose derivatives. *Carbohydrate research* 2012;358:12-8.
- [55] Tetyuk O, Benning U, and Hoffmann-Benning S. Collection and Analysis of Arabidopsis Phloem Exudates Using the EDTA-facilitated Method. *Journal of visualized experiments: JoVE* 2013.
- [56] Thrippleton MJ and Keeler J. Elimination of Zero-Quantum Interference in Two-Dimensional NMR Spectra. *Angewandte Chemie* 2003;115:4068-71.
- [57] Tsuji A UH, Yamashita T, Matsushashi S, Ito T, Mizuniwa C, Ishioka NS, Watanabe S, Sekine T. Uptake of ^{18}F FDG and $^{13}\text{NO}_3^-$ in tomato plants. In: *TIARA Annu Rep* 2001. Japan: Japan Atomic Energy Research Institute, 2002;035:103-4.
- [58] Ung YC, Maziak DE, Vanderveen JA, Smith CA, Gulenchyn K, Lacchetti C, et al. ^{18}F Fluorodeoxyglucose positron emission tomography in the diagnosis and staging of lung cancer: a systematic review. *Journal of the National Cancer Institute* 2007;99:1753-67.
- [59] Yen T-C, See L-C, Lai C-H, Yah-Huei CW, Ng K-K, Ma S-Y, et al. ^{18}F -FDG uptake in squamous cell carcinoma of the cervix is correlated with glucose transporter 1 expression. *Journal of Nuclear Medicine* 2004;45:22-9.

Figures:

Figure 1: Schematics of the potential routes of FDG metabolism in plant cell. FDG, 2-deoxy-2-fluoro-D-glucose; FDG-6-P, FDG-6-phosphate; FDG-1-P, FDG-1-phosphate; UDP, Uridine-di-phosphate; F-maltose, 2-deoxy-2-fluoro-maltose; Glu, glucose; *DPE2*, Arabidopsis Disproportionating enzyme 2.

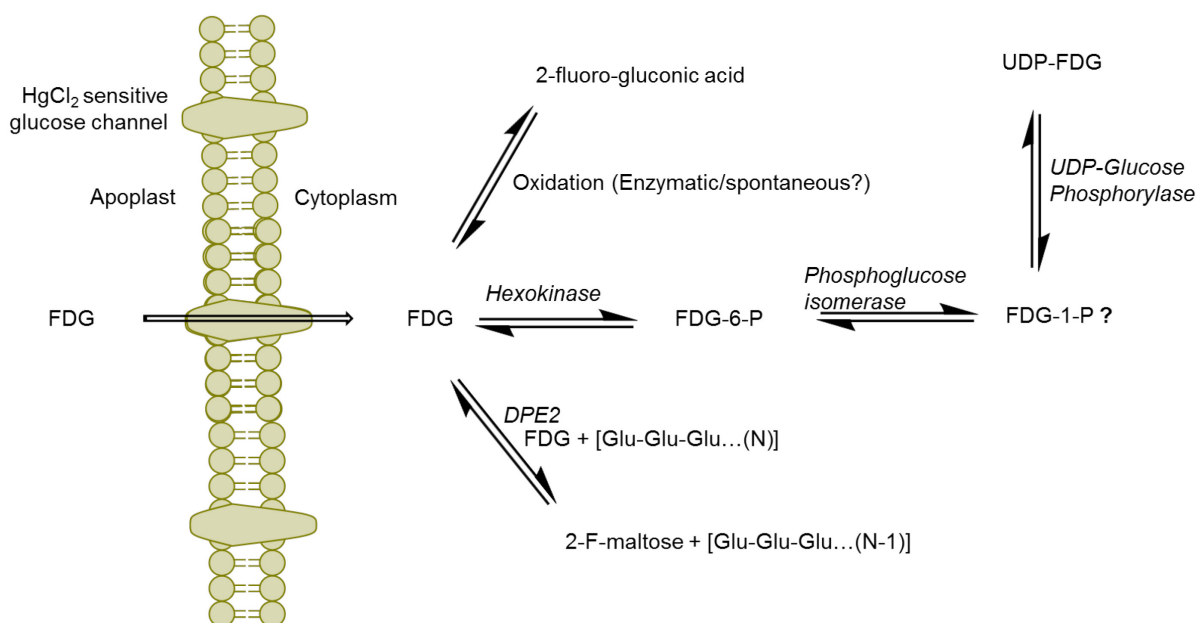


Figure 2: ^1H -decoupled ^{19}F -NMR spectra of fractions containing fluorinated metabolites including chemical shifts. Signals are referenced to C_6F_6 at δ_{F} -164.9. **(A)** Raw extract of *A. thaliana* after FDG administration before separation. The two most intense signals belong to α -FDG (δ_{F} -197.63) and β -FDG (δ_{F} -197.52) **(B)** Fraction containing the fluorinated compound α/β -FDG-6-P (m/z 261.0180). The α -isomer shows a chemical shift of δ_{F} -197.75, the β -isomer resonates at δ_{F} -197.55. **(C)** Fraction containing the fluorinated compound α/β -F-maltose (m/z 343.1051). The compound shows signals that appear most deep-field shifted among the identified metabolites (α : δ_{F} -198.50, β : δ_{F} -198.26) **(D)** Fraction assumed to contain a fluorinated derivative of gluconic acid (m/z 197.0464). The signals indicated likely represent impurities from compounds α/β -FDG-6-P and α/β -F-Maltose.

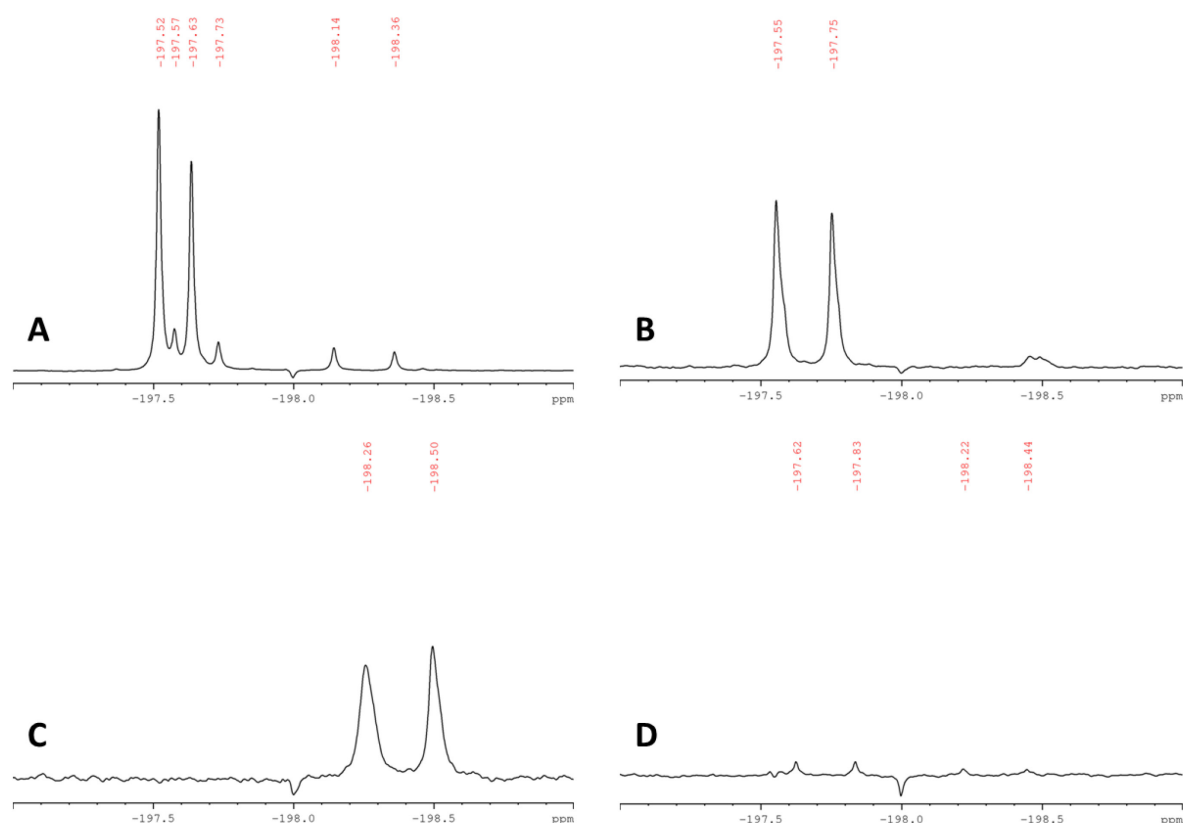


Figure 3: Assignment of FDG-6-P. (A) ^1H - ^{13}C HSQC spectrum FDG-6-P. The red F_2 -projection represents the selective TOCSY spectrum of β -FDG-6-P, the black F_2 -trace belongs to α -FDG-6-P. The F_1 -projection shows the ^{13}C -NMR spectrum. Coupling constants were extracted from ^1H - and ^{13}C -NMR spectra, respectively. (B) 2D-NMR key correlations used for the assignment of FDG-6-P (α -FDG-6-P and β -FDG-6-P forms, respectively). Blue arrows represent ^1H - ^{13}C HMBC correlations from $\text{H}-1_{\alpha/\beta}$. Red arrows indicate ^1H - ^1H COSY key correlations.

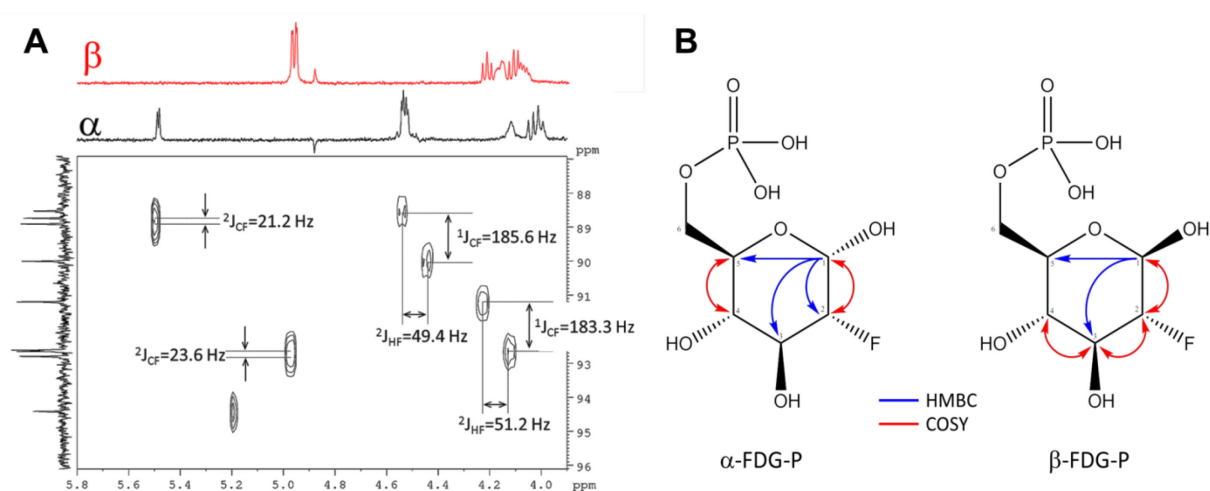
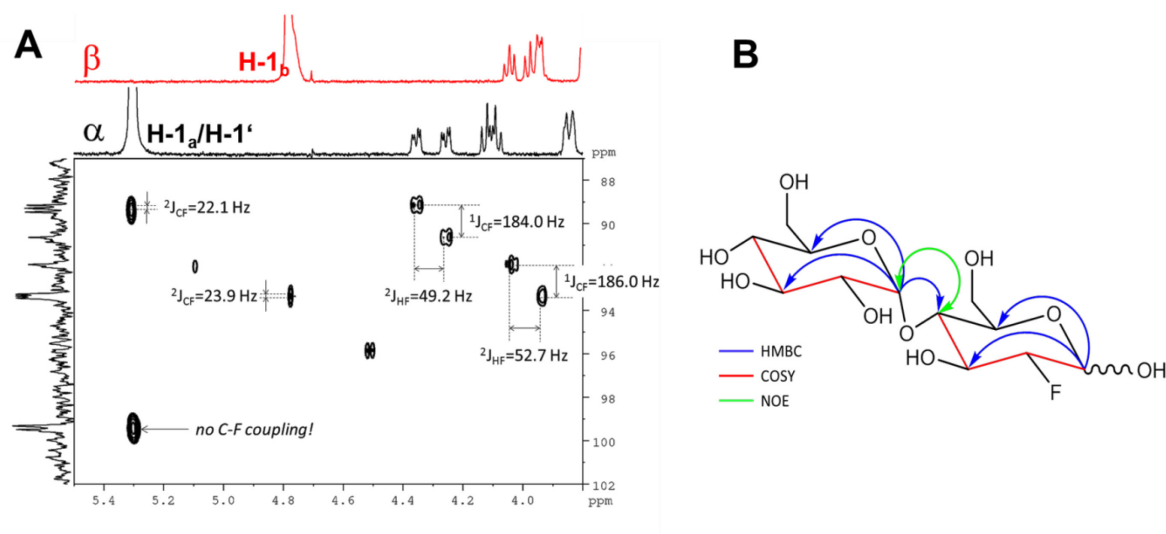


Figure 4: Assignment of fluorinated disaccharide. **(A)** Detail of the ^1H - ^{13}C HSQC spectrum from the fraction containing the fluorinated disaccharide m/z 343.1051. Characteristic C-F and H-F couplings are given. Two different shifts (δ_c 99.3/99.5) for C-1' appear depending from the configuration of the FDG part. The F2-Projection shows the selective TOCSY spectra for the α/β -FDG part. **(B)** Key correlations used for the structure elucidation of the fluorinated disaccharide m/z 343.1051. Blue arrows indicate ^1H - ^{13}C HMBC correlations from the position 1 of the respective sugar units. The red parts of the structure indicate for neighboring positions probed by selective COSY experiments. The green double tipped arrow shows the NOE evidence for the $\alpha(1\rightarrow4)$ junction between the two sugar units.



Supplementary data

Supplementary Figure 1. ^{18}F FDG uptake by *Arabidopsis thaliana* cell suspension.

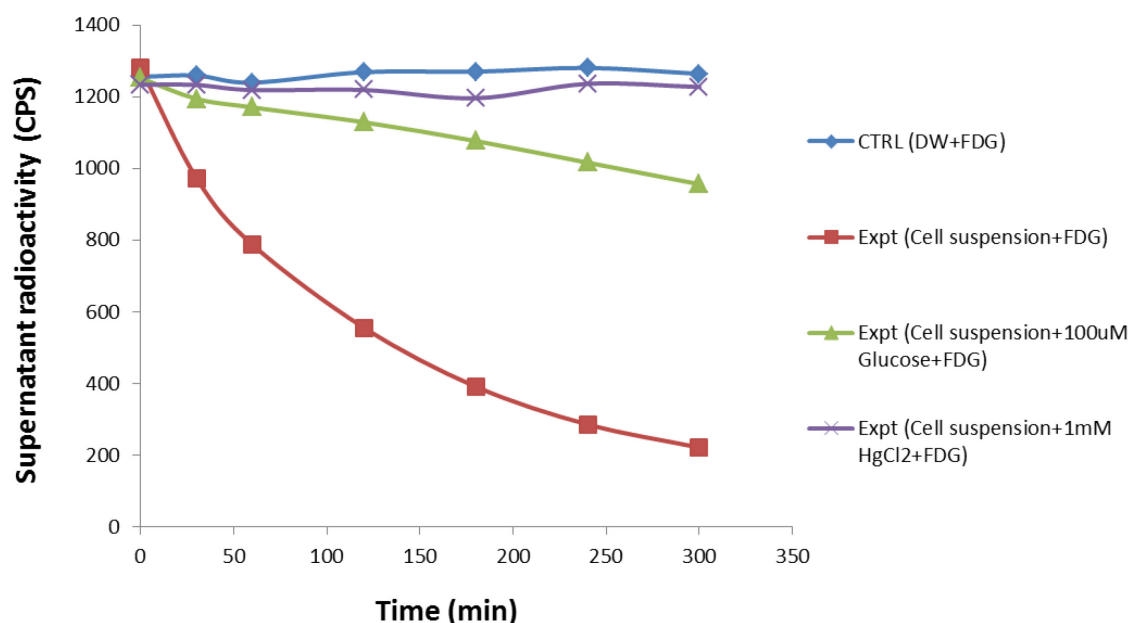
Arabidopsis thaliana cell culture was grown in JPL medium containing sucrose (1.5%). On the day of experiment, cells were suspended in 50 mL JPL medium containing equimolar concentration of mannitol instead of sucrose. Control flasks contained only nutrient media. ^{18}F FDG solution (1.23 MBq) was added to each flask. Flasks for set-3 and set-4 were added with 100 μM glucose and 1 mM HgCl_2 respectively prior to ^{18}F FDG addition. Flasks were kept on rotary shaker at 60 rpm under normal laboratory light and temperature conditions. 0.5 mL supernatant was collected at sequential time points (30 min, 1 hr, 2 hr, 3 hr, 4 hr, 5 hr time-points) and filtered through 22 μm filter for removing cell pellet. Radioactivity remained in the supernatant was measured measured in counts per second (CPS) using a well counter (Isomed 2100, MED Nuklear-Medizintechnik Dresden GmbH, Dresden, Germany). Two biological replicates (each with three technical replicates) were performed for each set and average decay corrected CPS radioactivity for cell pellet was noted.

NOTE: Cell suspension was not completely homogeneous. Small clumps of cells were visible. Thus, cell pellet in 0.5 mL sampling volume could not be extrapolated for total cell pellet activity. Supernatant radioactivity, however, forms a good indicator for FDG concentration remained in the in the flask at time point. Therefore, only supernatant radioactivity but not cell pellet radioactivity was measured.

Supplementary Table for Fig. 1. ^{18}F FDG uptake by *Arabidopsis thaliana* cell suspension.

Flask/time	CTRL (DW+FDG)	Expt (Cell suspension+FDG)	Expt (Cell suspension+100uM Glucose+FDG)	Expt (Cell suspension+1mM HgCl ₂ +FDG)
0	1255.8	1279.9	1252.3	1233.7
30	1259.1	973.2	1194.2	1232.9
60	1239.4	787.7	1170.4	1218.6
120	1268.8	555.3	1128.7	1218.9
180	1269.9	390.9	1076.6	1195.9
240	1280.5	285.6	1016.2	1236.2
300	1264.0	221.2	955.9	1227.2

Supplementary Figure 1:



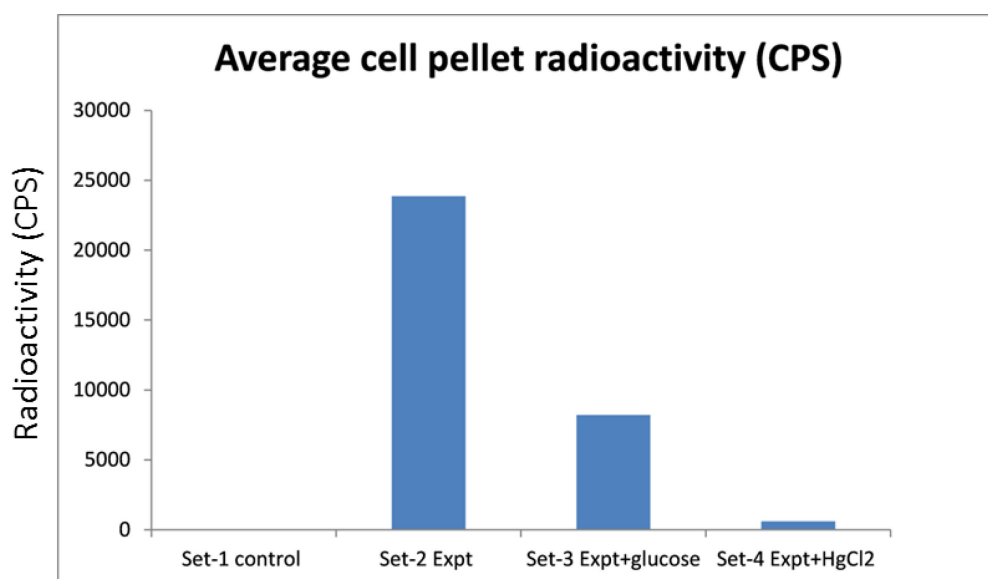
Supplementary Figure 2. [Taken from Fatangare et al, 2014]

Arabidopsis thaliana cell culture was grown in JPL medium containing sucrose (1.5%). On the day of experiment, cells were suspended in 50 mL JPL medium containing equimolar concentration of mannitol instead of sucrose. Control flasks contained only nutrient media. ¹⁸FDG solution (1.23 MBq) was added to each flask. Flasks for set-3 and set-4 were added with 100 μ M glucose and 1 mM HgCl₂ respectively prior to ¹⁸FDG addition. Flasks were kept on rotary shaker at 60 rpm under normal laboratory light and temperature conditions. After 5 hours, the suspensions were filtered through 22 micron filter for cell pellet. Radioactivity accumulated in cell pellet was measured in counts per second (CPS) using a well counter (Isomed 2100, MED Nuklear-Medizintechnik Dresden GmbH, Dresden, Germany). Two biological replicates (each with three technical replicates) were performed for each set and average decay corrected CPS radioactivity for cell pellet was noted.

Supplementary Table for Fig. 2. ¹⁸FDG uptake by *Arabidopsis thaliana* cell suspension.

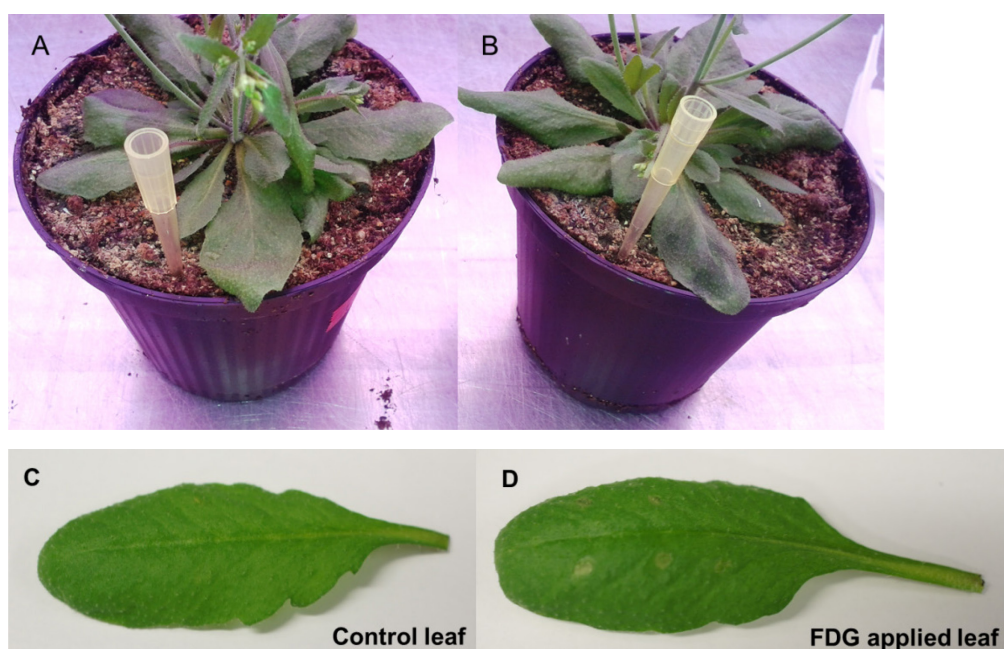
Experimental Set	Average cell pellet radioactivity (CPS)
Set-1 control (only media)	22.6
Set-2 Expt (media+suspension+FDG)	23868.5
Set-3 Expt+glucose(media+suspension+glucose 100 μ M+FDG)	8215.5
Set-4 Expt+HgCl ₂ (media+suspension+HgCl ₂ 1mM+FDG)	604.6

Supplementary Figure 2:



Supplementary Figure 3:

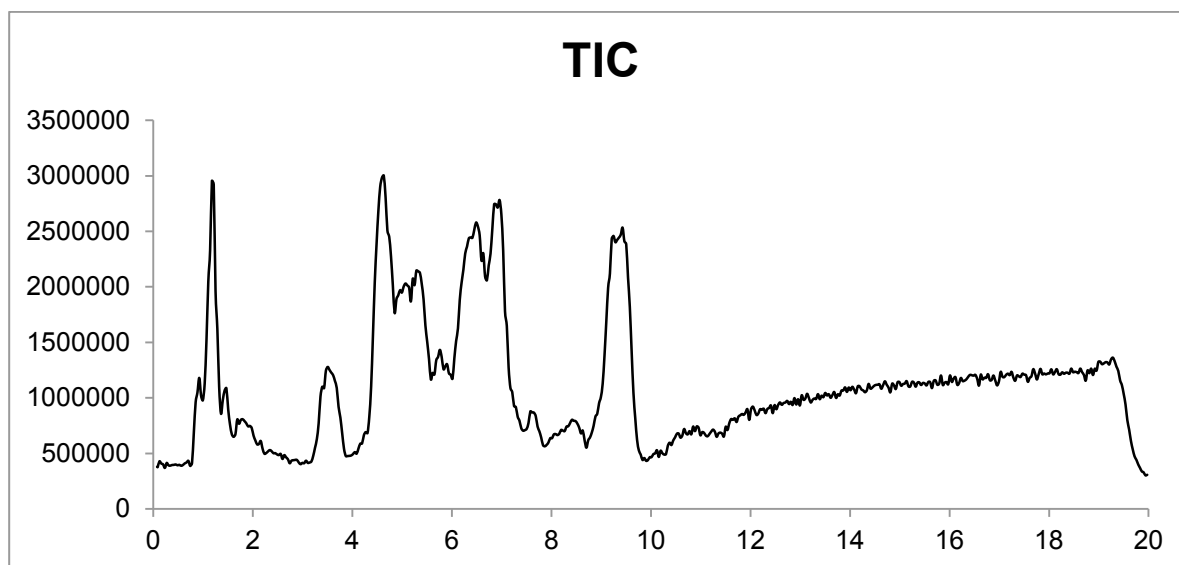
Leaf tissue death/damage caused by FDG application. (A) Mature leaf of the control plant was applied with 50 μL of DW using syringe infiltration. Leaf has been marked with plastic tip on the left. Control leaf showed no signs of darkening and wilting after 30 min. (B) Mature leaf of the experimental plant was applied with 50 μL of FDG (40 $\text{mg}\cdot\text{mL}^{-1}$) using syringe infiltration. Leaf has been marked with plastic tip on the left. FDG applied leaf showed signs of darkening and wilting after 30 min. (C) Mature leaf were pricked and 20 μL of DW was applied locally. (D) Mature leaf was pricked and 20 μL of FDG (20 $\text{mg}\cdot\text{mL}^{-1}$) was applied locally. Local tissue damage is clearly visible in FDG applied leaf.



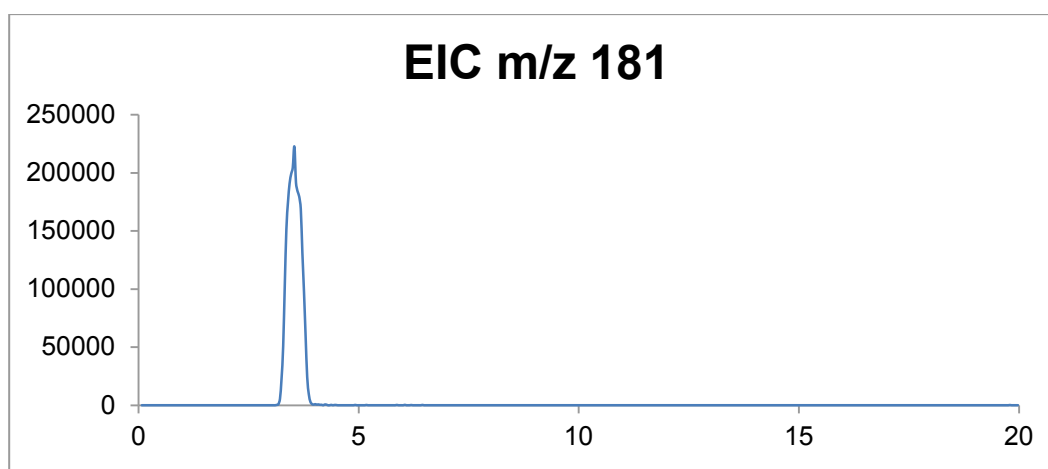
Supplementary figure 4.

TIC and EIC for F-metabolites (depicted in Absolute Ion intensity vs RT in minutes)

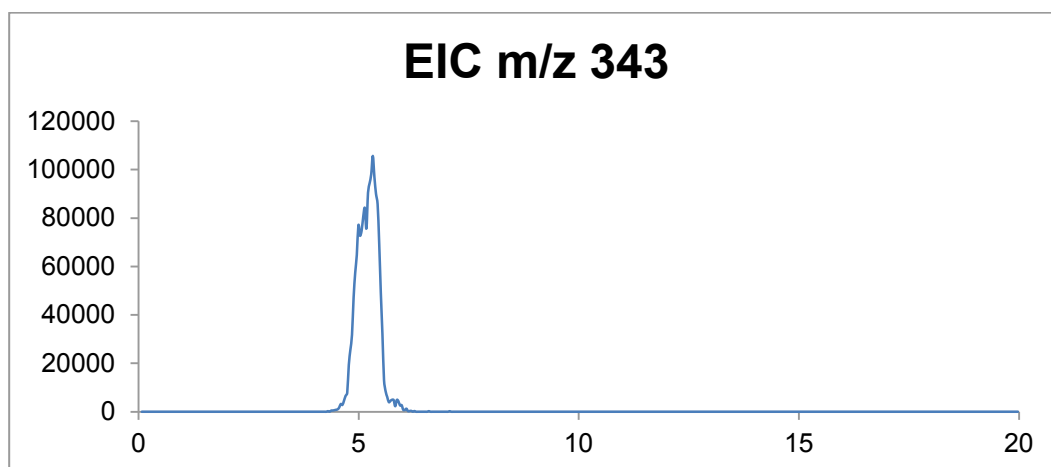
(A) Total ion chromatogram (TIC) on Supelco apHera Amino column



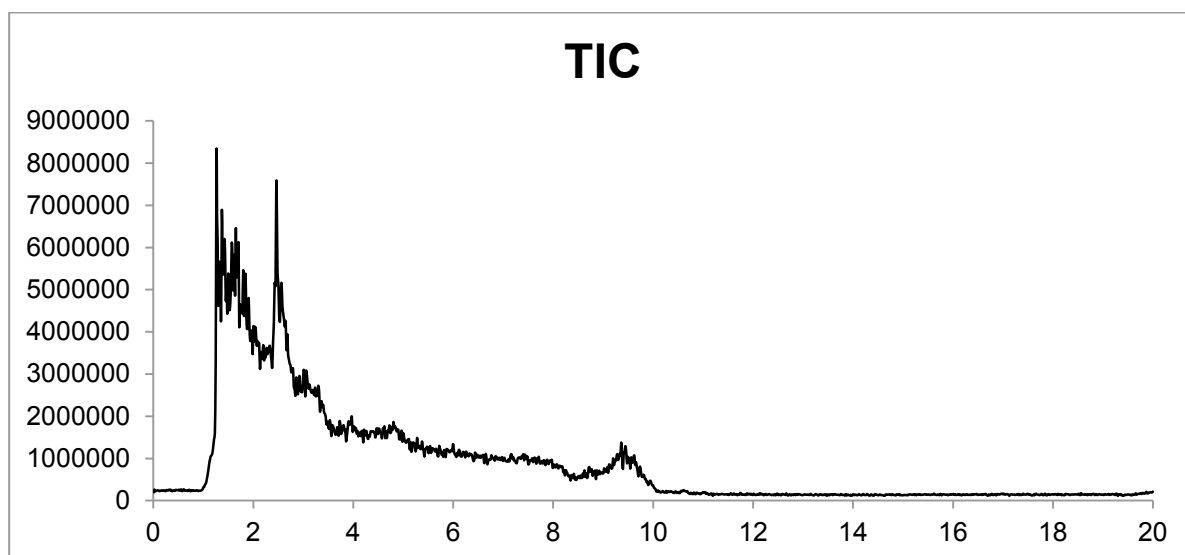
(B) Extracted ion chromatogram (EIC) for m/z : 181 (RT: 3.5) on Supelco apHera Amino column



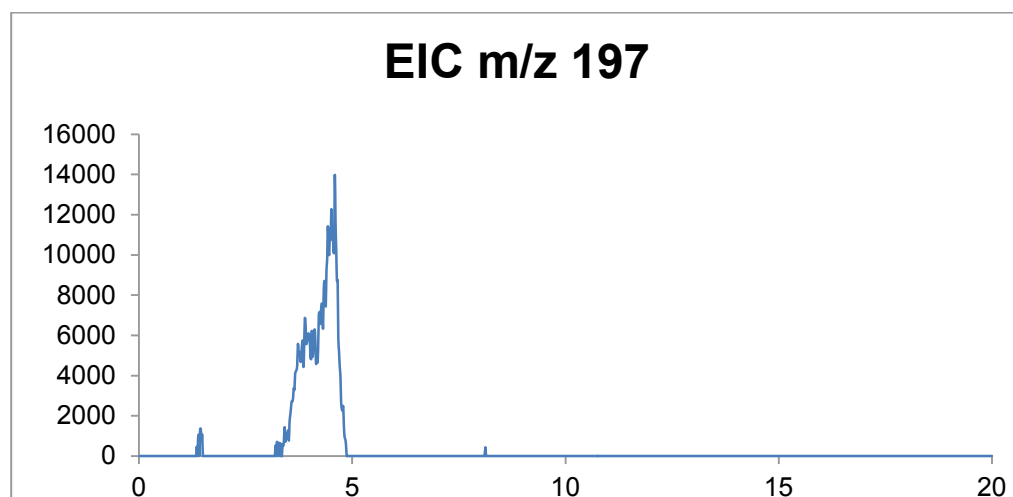
(C) Extracted ion chromatogram (EIC) for m/z : 343 (RT: 5.3) on Supelco apHera Amino column



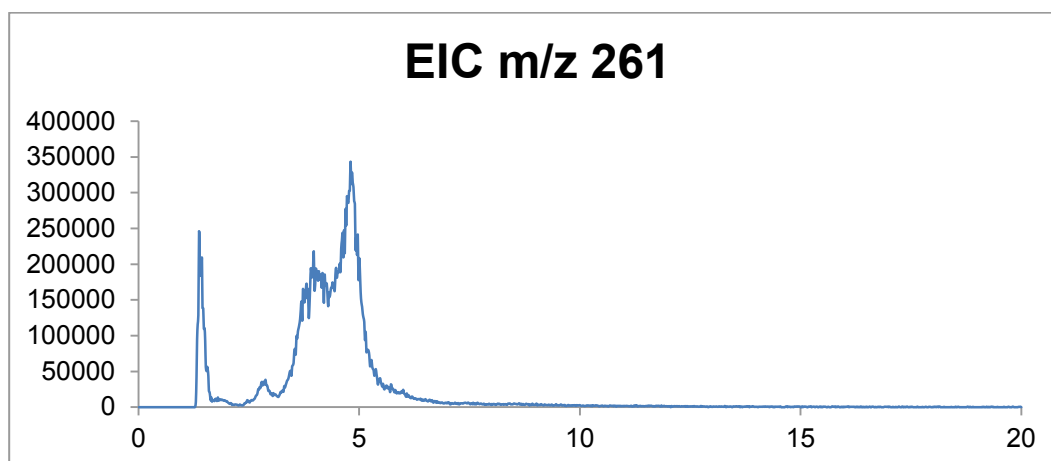
(D) Total ion chromatogram (TIC) on ACQUITY UPLC BEH Amide column:



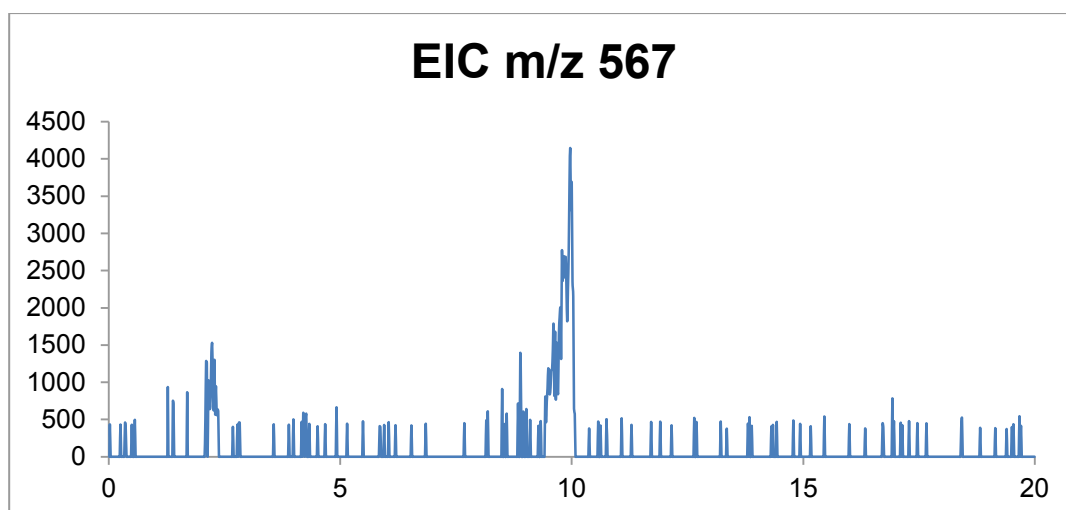
(F) Extracted ion chromatogram (EIC) for m/z : 197 (RT: 3.8-5.0 broad peak) on ACQUITY UPLC BEH Amide column



(G) Extracted ion chromatogram (EIC) for m/z : 261 (RT: 4.0-5.6 broad peak) on ACQUITY UPLC BEH Amide column



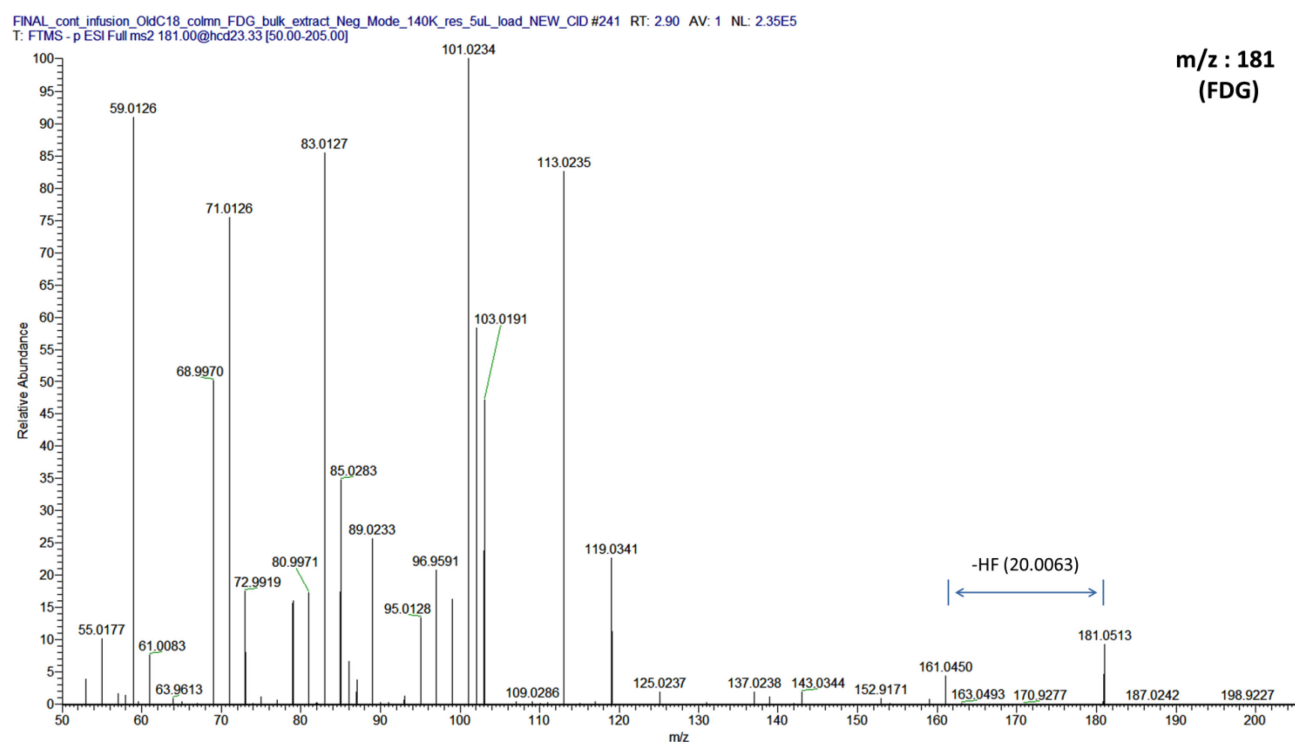
(H) Extracted ion chromatogram (EIC) for m/z : 567 (RT: 8.9-10.0 broad peak) on ACQUITY UPLC BEH Amide column



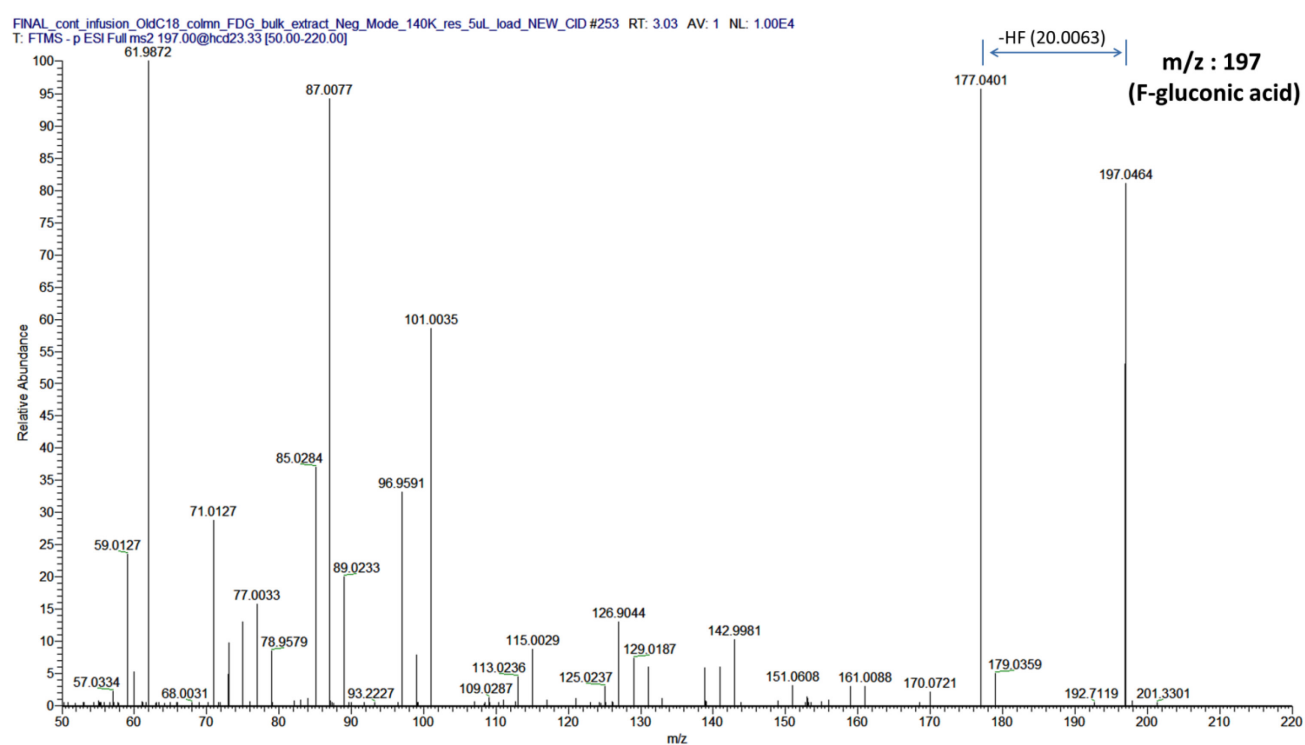
Supplementary figure 5.

MS/MS spectra for F-metabolites ions (depicted in relative ion intensity vs m/z)

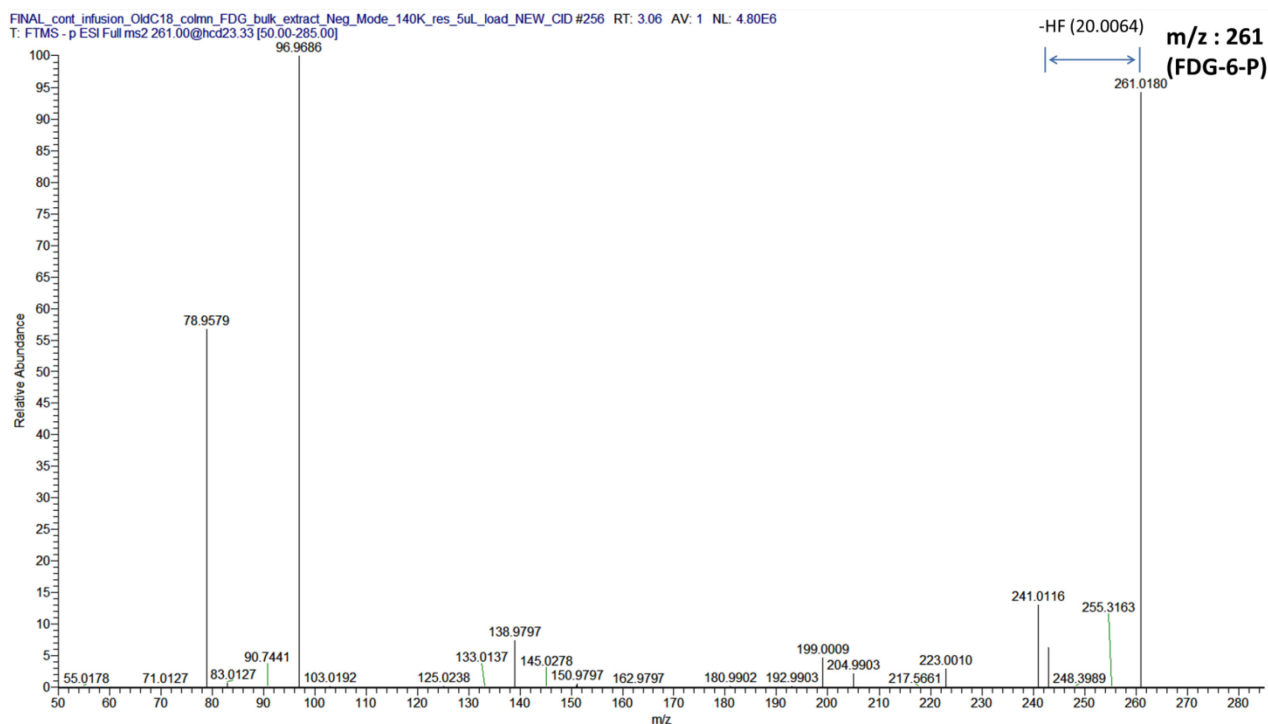
(A) m/z : 181 (FDG)



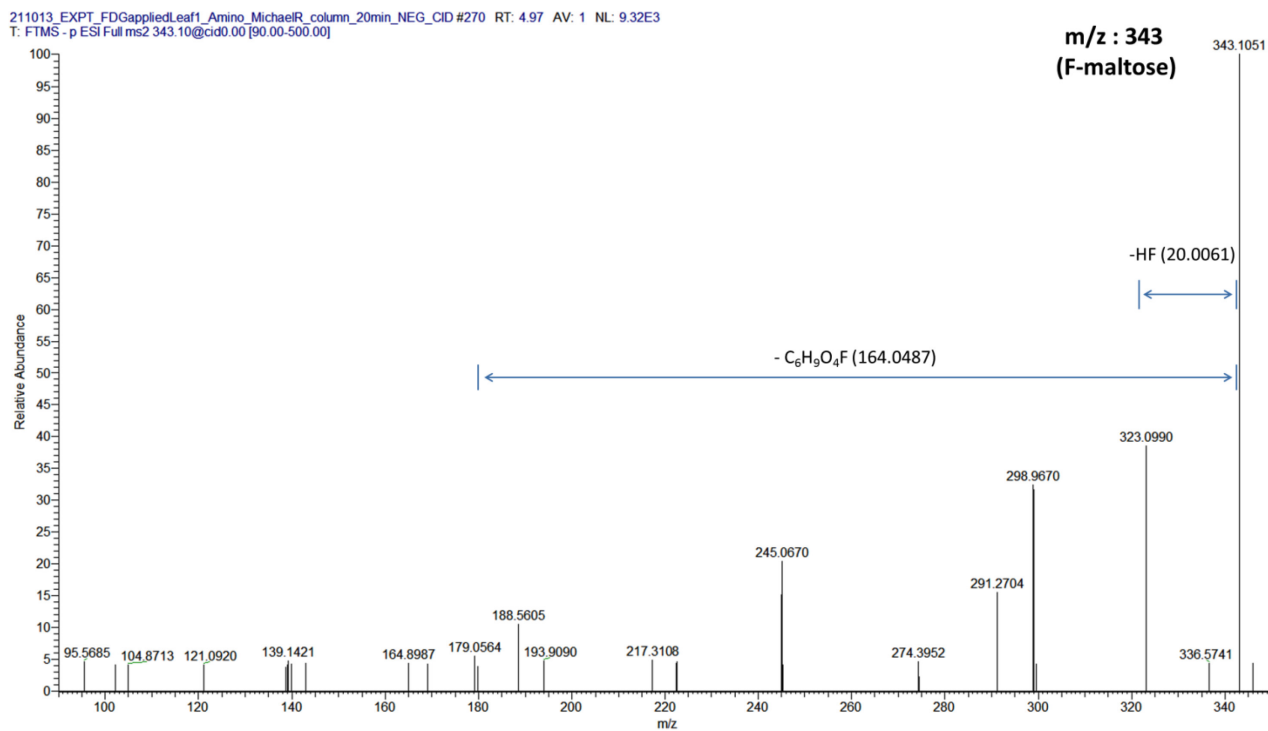
(B) m/z : 197 (F-gluconic acid)



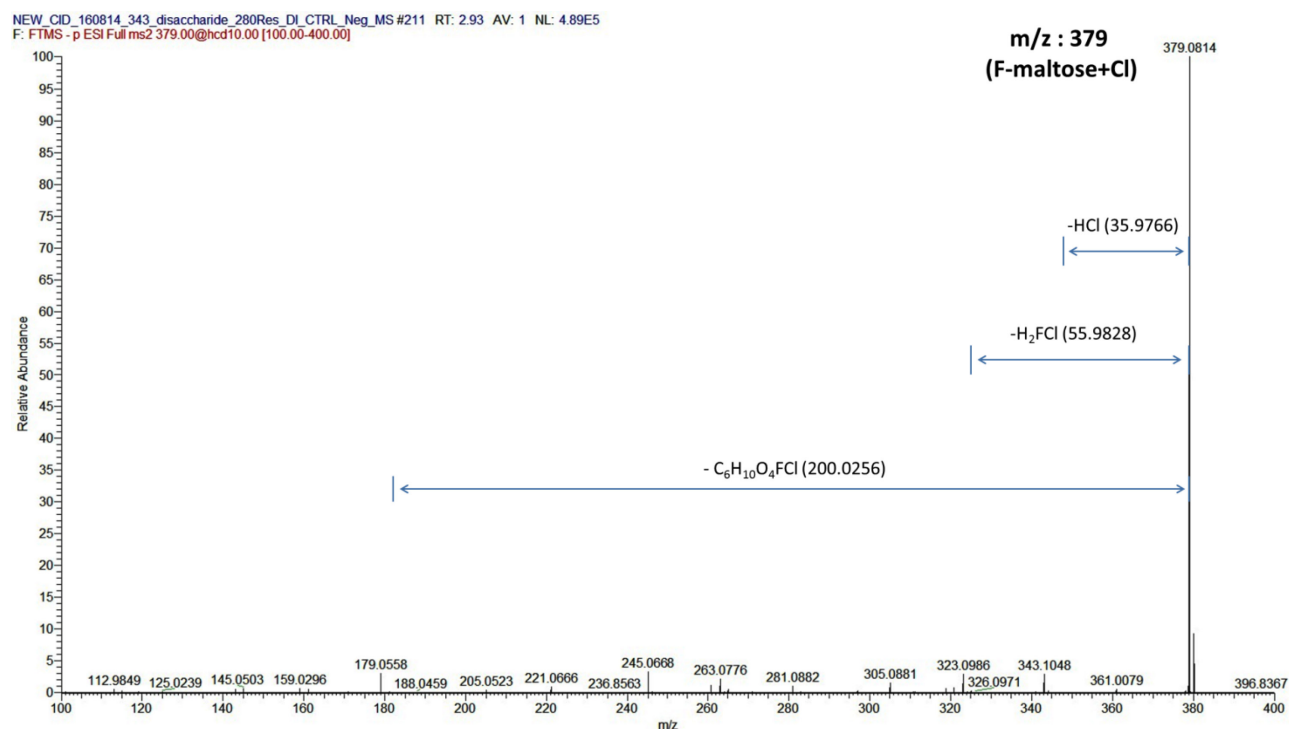
(C) m/z : 261 (FDG-6-P)



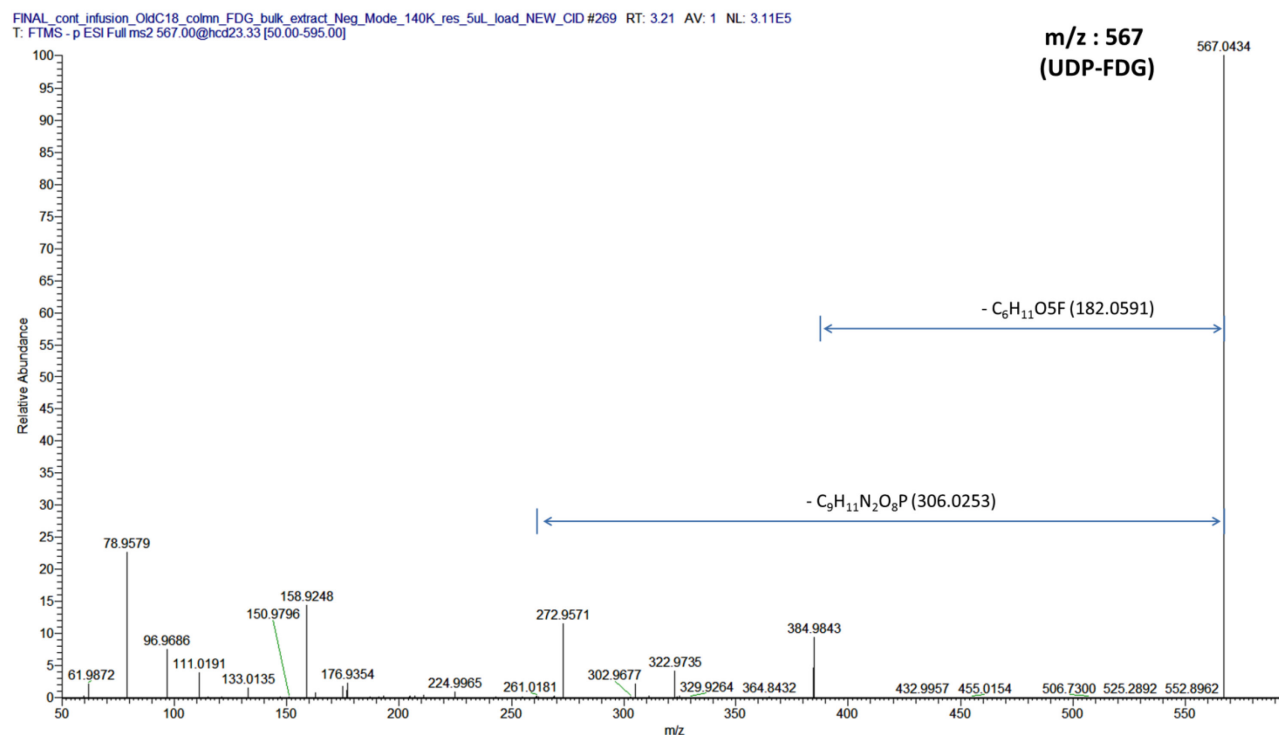
(D) m/z : 343 (F-maltose)



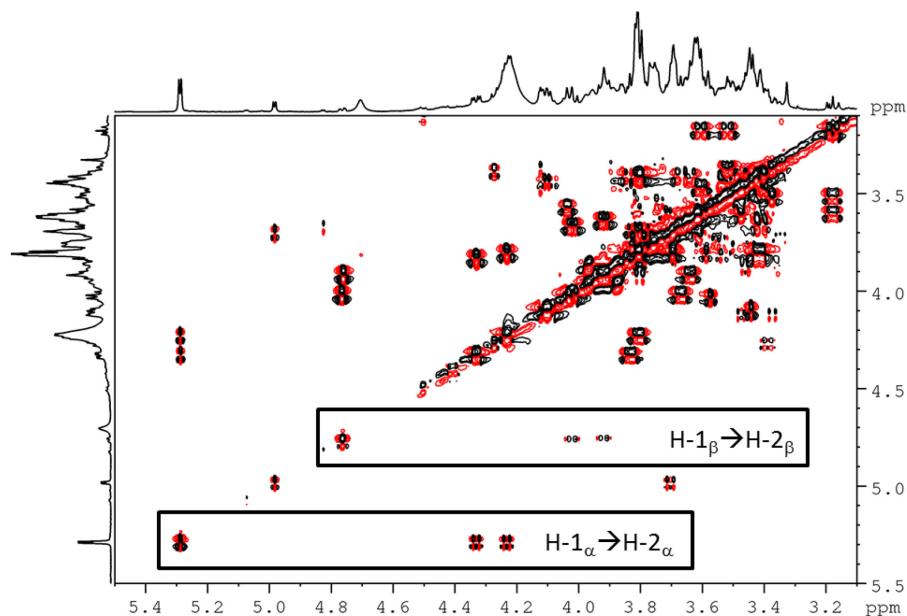
(E) m/z : 379 (F-maltose + Cl adduct)



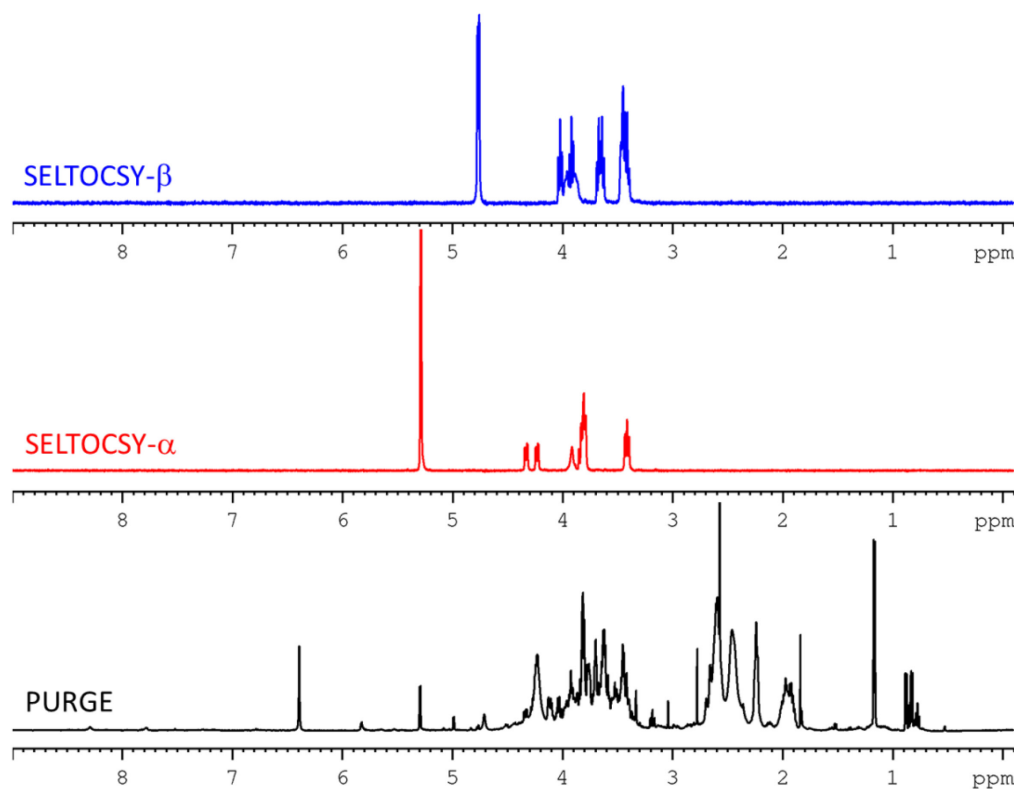
(F) m/z : 567 (UDP-FDG)



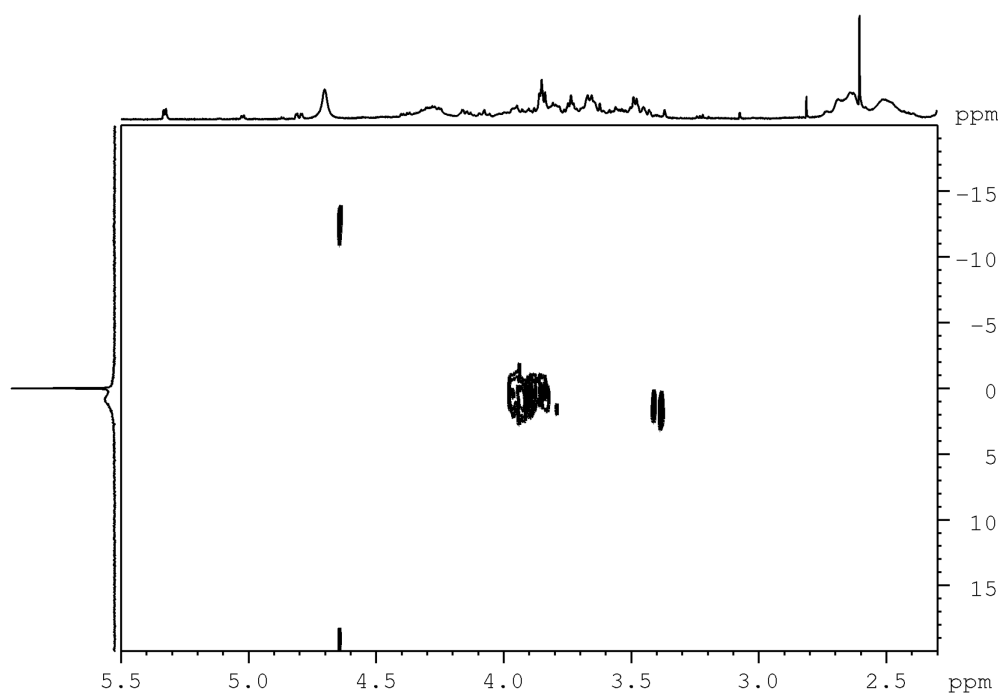
Supplementary Figure 6: ^1H - ^1H dqfCOSY spectrum of the semi-purified fraction of the fluorinated compound m/z 261.0180 (FDG-6-P). Key correlations of $\text{H-1}_{\alpha/\beta} \rightarrow \text{H-2}_{\alpha/\beta}$ are indicated. The projections show the water-suppressed ^1H -NMR spectrum.



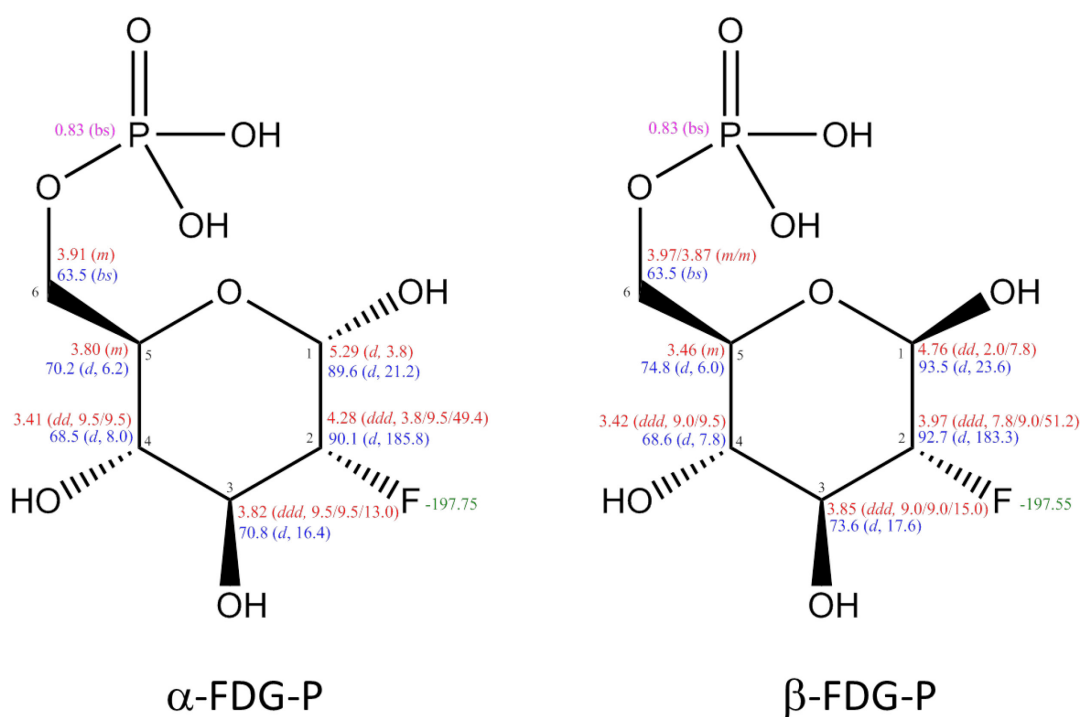
Supplementary Figure 7: Comparison of the presaturated ^1H -NMR spectrum (PURGE, black curve) and the selective TOCSY spectra (SELTOCSY- α/β , red/blue curve) of FDG-6-P.



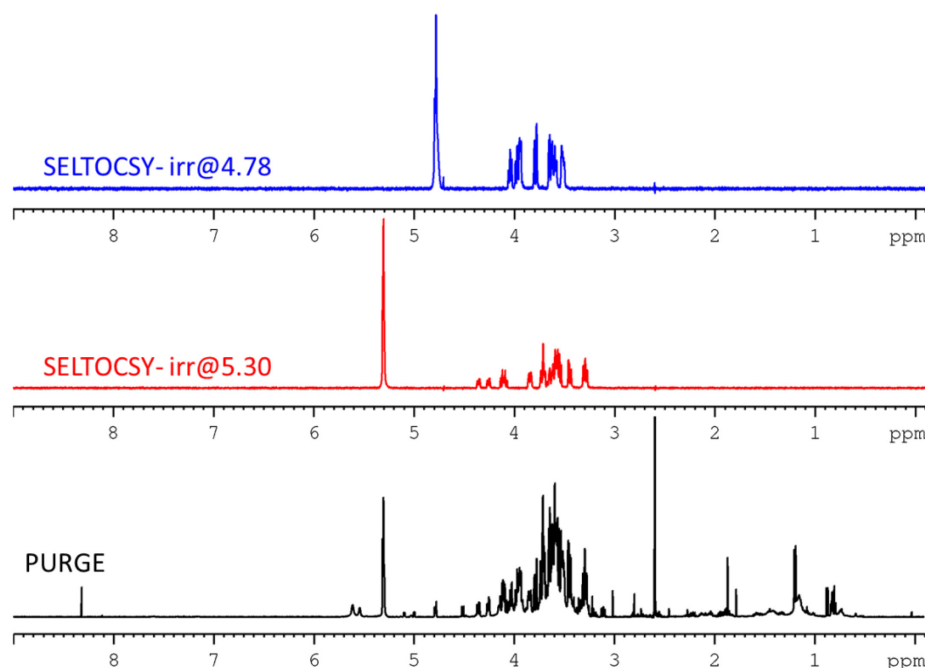
Supplementary Figure 8: ^1H - ^{31}P -HMBC spectrum of FDG-6-P. A presaturated ^1H -spectrum serves as F2-projection. The projection in F1 is a ^{31}P -NMR spectrum.



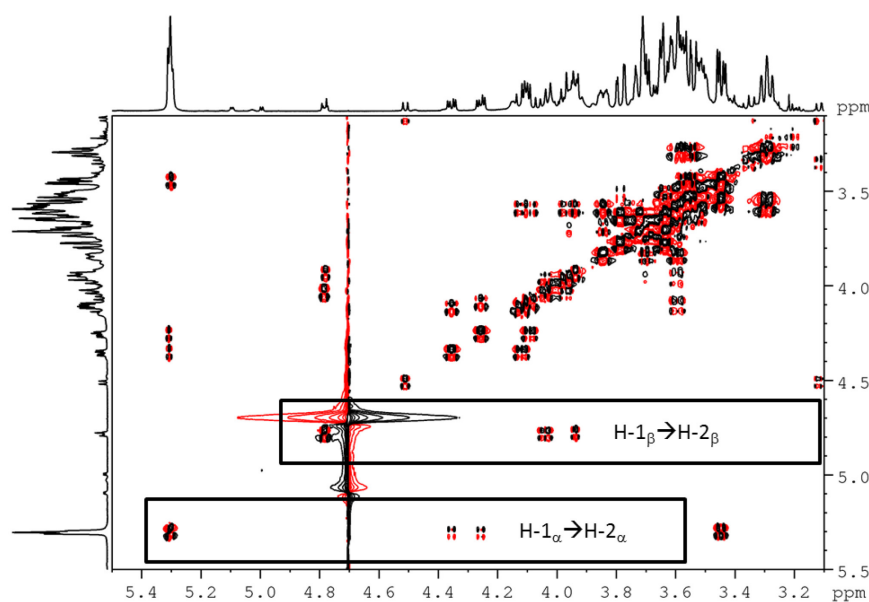
Supplementary Figure 9: Structures of α/β -FDG-6-P including chemical shifts, signal multiplicities and coupling constants (^1H chemical shifts in red, ^{13}C chemical shifts in blue, ^{19}F chemical shifts in green and ^{31}P chemical shifts in magenta. Coupling constants are given in Hz).



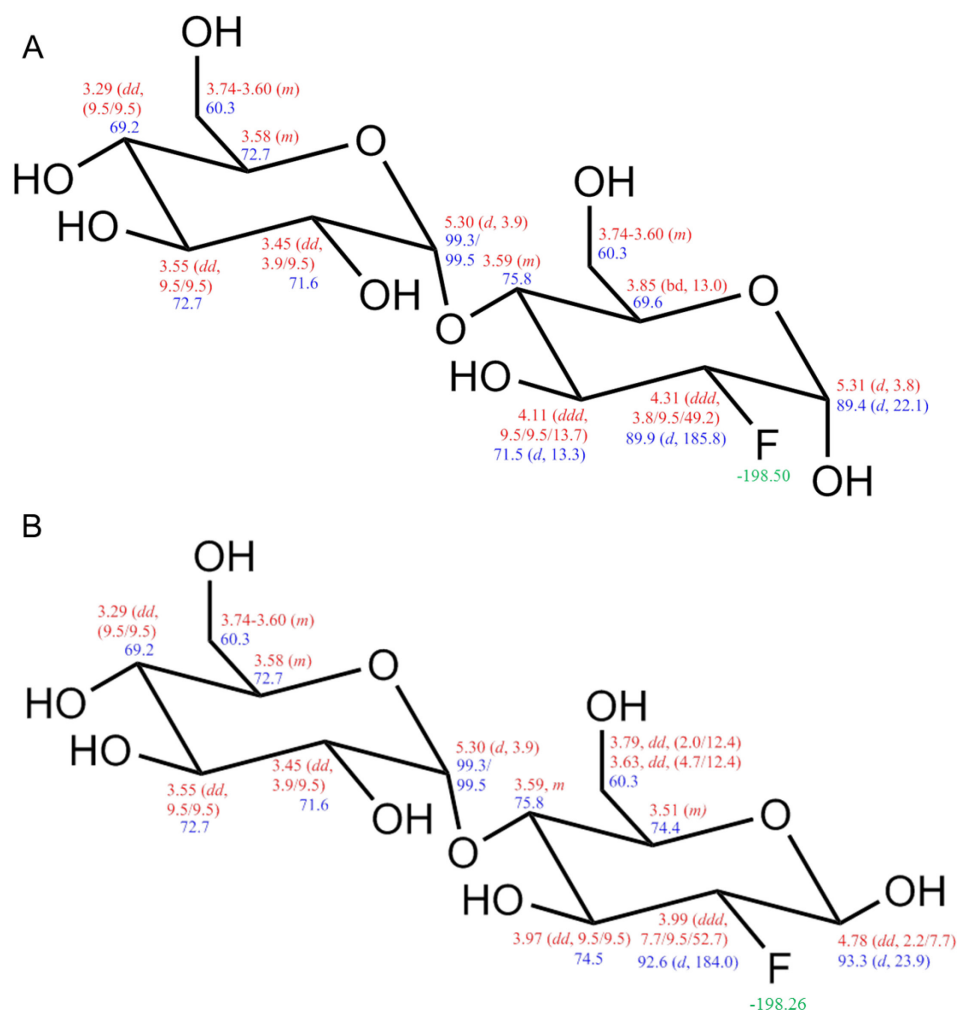
Supplementary Figure 10: Presaturated ^1H -NMR spectrum (using PURGE water suppression) of the fraction containing the fluorinated disaccharide m/z 343.1051 (black trace). The red trace shows a selective ^1H - ^1H TOCSY spectrum derived from irradiating overlapping signals ($\text{H-1}_\alpha/\text{H-1}'$) around δ_{H} 5.30. The blue trace shows a selective ^1H - ^1H TOCSY spectrum acquired after irradiating H-1_β at δ_{H} 4.78.



Supplementary Figure 11: ^1H - ^1H dqfCOSY spectrum of the semi-purified fraction of the fluorinated disaccharide (m/z 343.1051). Key correlations of $\text{H-1}_{\alpha/\beta} \rightarrow \text{H-2}_{\alpha/\beta}$ are indicated. Note the irregular shape of the signal for H-2_β . The projections show the water-suppressed ^1H -NMR spectrum.



Supplementary Figure 12: F-maltose. (A) Structure of α -F-maltose including chemical shifts, signal multiplicities and coupling constants (^1H chemical shifts in red, ^{13}C chemical shifts in blue, ^{19}F chemical shifts in green. Coupling constants are given in Hz). (B) Structure of β -F-maltose including chemical shifts, signal multiplicities and coupling constants (^1H chemical shifts in red, ^{13}C chemical shifts in blue, ^{19}F chemical shifts in green. Coupling constants are given in Hz).



Chapter 3

Using 2-deoxy-2-[^{18}F]fluoro-D-glucose to study carbon allocation in plants after herbivore attack

Stefan Meldau^{#*}, Melkamu Woldemariam[#], **Amol Fatangare**, Aleš Svatoš, Ivan Galis

First author

** Corresponding author*

Title

Using 2-deoxy-2-[¹⁸F]fluoro-D-glucose ([¹⁸F]FDG) to study carbon allocation in plants after herbivore attack

Short title

Carbon partitioning after simulated herbivory

Authors

Stefan Meldau^{1,2,3,*,#}, Melkamu G. Woldemariam^{1,4, #}, Amol Fatangare⁵, Ales Svatos⁵ and Ivan Galis^{1,6}

Affiliations

¹ Department of Molecular Ecology, Max-Planck-Institute for Chemical Ecology, Hans-Knöll-Str.8, 07745 Jena

² German Centre for integrative Biodiversity Research (iDiv), Deutscher Platz 5, 04107 Leipzig

³present address: KWS SAAT AG, Molecular Physiology, R&D, RD-ME-MP, Grimsehlstrasse 31, D-37555 Einbeck

⁴present address: Boyce Thompson Institute for Plant Research, 533 Tower Road, Ithaca, 14853 New York

⁵ Mass Spectrometry Research Group, Max-Planck-Institute for Chemical Ecology, Hans-Knöll-Str.8, 07745 Jena, Germany

⁶ Present address: Okayama University, Institute of Plant Science and Resources, Chuo 2-20-1, 710-0046 Kurashiki, Japan

*Corresponding author, email: stefan.meldau@kws.com

#These authors contributed equally

Abstract

Background

Although leaf herbivory-induced changes in allocation of recently assimilated carbon between the shoot and below-ground tissues have been described in several species, it is still unclear which part of the root system is affected by resource allocation changes and which signalling pathways are involved. We investigated carbon partitioning in root tissues following wounding and simulated leaf herbivory in young *Nicotiana attenuata* plants.

Results

Using 2-deoxy-2-[^{18}F]fluoro-D-glucose ([^{18}F]FDG), which was incorporated into disaccharides *in planta*, we found that simulated herbivory, but not wounding alone, reduced carbon partitioning specifically to the root tips. In jasmonate (JA) signalling deficient *COI1* plants, the wound-induced allocation of [^{18}F]FDG to the roots was decreased, while more [^{18}F]FDG was transported to young leaves, demonstrating an important role of the JA pathway in regulating the wound-induced carbon partitioning between shoots and roots.

Conclusions

Our data highlight the use of [^{18}F]FDG to study stress-induced carbon allocation responses in plants and indicate an important role of the JA pathway in regulating wound-induced shoot to root signaling.

Keywords

2-deoxy-2-[^{18}F]fluoro-D-glucose ([^{18}F]FDG), herbivory, jasmonate signalling, *Nicotiana attenuata*, Fatty acid-amino acid conjugates

64

65 **Background**

66 Plants face a dilemma when stressed by wounding or herbivore attack - to
67 invest resources into defence reactions or into growth processes. Research on how
68 plants solve this dilemma is important for understanding the evolution of resistance
69 and tolerance strategies of plants, and helps to facilitate the development of crop
70 improvement strategies. The production of defensive metabolites is tightly linked to
71 the wound- and herbivory-induced activation of defence hormones, including
72 jasmonic acid (JA) and its isoleucine conjugate JA-Ile [1]. Activation of JA-dependent
73 resistance pathways is often accompanied by changes in the levels of primary
74 metabolites, such as sugars, amino acids and organic acids, which serve as
75 substrates and precursors or provide energy required for defence metabolite
76 biosynthesis [2-7]. Although the wound- and herbivory-induced signalling or
77 treatment with JA increase a plant's response to herbivore attack [8], activation of the
78 JA pathway can limit the availability of resources required for plant growth and fitness
79 [9-12].

80 Biotic and abiotic stress can increase sink strength of certain plant tissues; a
81 common response in many plant species, including carrot [13], tomato [14], hybrid
82 poplar trees [2, 15, 16] and pea [17]. However, the opposite response also occurs,
83 such as the flow of carbon away from stressed tissues, often to storage organs, such
84 as roots [7, 18-20]. But the direction of resource re-allocation can change with
85 environmental conditions and plant ontogeny. For example, in *Arabidopsis thaliana*,
86 2-deoxy-2-[¹⁸F]fluoro-D-glucose ([¹⁸F]FDG), a radioactive tracer that is used to study
87 carbohydrate allocation, is transported mainly to the root system in vegetative plants
88 but is directed to above-ground tissues when plants enter the reproductive stage [21].

89 One of the best plant model systems to study responses upon herbivore
90 attack is *Nicotiana attenuata*, an annual plant that grows in the post-fire environment
91 in the Great Basin Desert (Utah, USA). The interaction between *N. attenuata* and its
92 Lepidopteran herbivore *Manduca sexta* has been intensively studied. During *M. sexta*
93 attack, fatty acid-amino acid conjugates (FACs) present in the herbivores' oral
94 secretions (OS) are rapidly recognized by *N. attenuata*; FACs amplify and modify
95 wound-induced responses in *N. attenuata*, including the biosynthesis of JA and JA-Ile
96 [22, 23]. The Biosynthesis of JA-Ile and its consequent perception through SCF^{COI1}
97 results in transcriptional reprogramming that leads to the accumulation of various

anti-herbivore secondary metabolites [10, 24-26]. JA-mediated herbivory-induced responses are associated with large fitness costs in *N. attenuata* [11], demonstrating the trade-off between plant growth and defence. However, it is not known whether, in *N. attenuata*, the JA pathway orchestrates the resource allocation changes that follow herbivore attack.

Schwachtje and colleagues found that simulated herbivory increases partitioning of recently assimilated carbon to roots of *N. Attenuata* plants; a response that has been linked to a process termed as “herbivory-induced resource sequestration” [7, 19, 20, 27-31]. The role of the extra carbon in the below-ground parts remains unknown: it could be utilized for growth of the roots, be stored within the root system, or help in the synthesis of defence compounds such as nicotine. However, it was shown recently that herbivory reduces sugar levels and starch in the roots of *N. attenuata* [32]. This depletion of carbon resources correlates well with reduced growth of the primary root after wounding and simulated herbivory [33, 34] and with a diminished ability to regrow and tolerate herbivore attack [32]. Until now, it has been unclear in which parts of the *N. attenuata* root system these changes in carbon allocation are manifested.

We used the short-lived isotope ^{18}F in simulated herbivory experiments with leaf-application of the sugar analogue [^{18}F]FDG to analyse carbon allocation at a fine spatial scale in the root system. In addition, we analysed the role of the JA pathway in herbivore-induced [^{18}F]FDG distribution by using transgenic plants silenced in the expression of COI1. Our results demonstrate that [^{18}F]FDG partitioning to root tips is strongly reduced after leaf herbivory. Plants silenced in COI1 expression reveal a distinct role of JA perception in [^{18}F]FDG distribution after wounding.

Materials and Methods

Plant cultivation

Transgenic irCOI1 *N. attenuata* plants were described elsewhere [25]. These lines are transformed with inverted-repeat constructs, allowing reduced transcript levels of the gene involved in JA perception (irCOI1). For [^{18}F]FDG experiments, cultivation of *N. attenuata* plants was described elsewhere [35], with the following modifications: 14 d old seedlings were transferred from Petri dish to sand (0.7-1.2 mm grain size, Raiffeisen GmbH, Germany) and fertilized with 0.15 gL⁻¹ Ferty B1 (Planta Düngemittel GmbH, Regenstauf, Germany); 0.25 gL⁻¹ Ca₂(NO₃). A small lid

was placed over the plants to avoid drought stress. After three days, the lid was moved to allow some air exchange, and after five more days the lid was removed completely. Twelve days later, the plants were transferred to hydroponic solution (for 1L: 0.1929 g Ca₂SO₄; 0.1232 g Mg₂SO₄, 0.0479 g K₂HPO₄, 0.0306 g KH₂PO₄ and 0.5 mL micronutrient solution (for 1L: 2.533 g H₃BO₃; 1.634 g MnSO₄, 0.151 g Na₂MoO₄, 0.08 g CuSO₄, 0.02 g CoCl₂, 0.5 mL Fe-DTPA (for 1 L: 2.78 g FeSO₄, 3.93 g Titriplex (Merck KGaA, Darmstadt, Germany))). Plants were grown in growth chambers under 16 h light (133 $\mu\text{mol m}^{-2} \text{s}^{-1}$) at 22 °C and 65 % humidity.

TLC plate analysis

We used one WOS-treated plant to analyze if [¹⁸F]FDG can be metabolized by *N. attenuata* plants. We applied 5 μL of [¹⁸F]FDG to a single punctured wound of a source-sink transition leaf of a 4.5 weeks old WT plant. Another younger leaf was treated with WOS. After 8 h, the plant was disassembled and leaf and root tissues (50 mg) were extracted with MeOH. 15 μL of the extract was applied to a 0.2 mm HPTLC silica gel 60 F254 plate (Merck) and chromatography was done using acetonitrile–water (17:3, v/v), containing 0.05 % of 2-aminoethyl diphenylborinate. After chromatography, the plate was sprayed with detection reagent (4 g of diphenylamine and 4 mL of aniline dissolved in 160 mL of acetone, 20 mL of conc. H₃PO₄ added and filled to 200 mL with acetone) and heated up to 120 °C for two minutes until bands were clearly visible. The plate was then transferred to an imaging cassette, covered with a positron imaging plate and scanned after 1 h exposure (FLA 3000 system, Fujifilm, Tokyo, Japan).

[¹⁹F]FDG experiments

Three mature rosette leaves from each plant were selected for [¹⁹F]FDG application. Leaves were wounded on leaf lamina on either side of the midrib using micropipette tip. Five μL of [¹⁹F]FDG (20 mg mL⁻¹, Sigma Aldrich, St. Louis, MO, USA) solution was immediately applied on each wounded region. After 30 min, 5 μL of water was applied on the same region to aid [¹⁹F]FDG uptake. Four hours after treatments, the leaves were harvested and extracted using slightly modified methanol/chloroform extraction procedure [36]. In brief, leaves were ground in liquid nitrogen. Methanol (1.5 mL) containing ¹³C labeled glucose (10 $\mu\text{g mL}^{-1}$, Sigma Aldrich, St. Louis, MO, USA) and chloroform (0.75 mL) were added to the tissue

sample. The mixture was sonicated in ultrasonic bath (Merck, Eurolab NV, Belgium) for 15 min at room temperature. After sonication, water (0.5 mL) and chloroform (0.5 mL) was added to the sample. Sample was centrifuged at 4000g for 15 min at 4 °C. Supernatant was concentrated using the rotating vacuum dryer (Concentrator 5301, Eppendorf Vertrieb, Germany). Dried supernatant sample was resuspended in 0.1 mL of water and stored at -80 °C until further LC-MS analysis.

LCMS and LCMSⁿ measurements

LC-MS data were acquired using Dionex UltiMate 3000 UHPLC system coupled to Thermo-Fisher LTQ-Orbitrap XL hybrid mass spectrometer (both Thermo Fisher Scientific, Bremen, Germany). The extracts were separated on Supelco apHera NH2 column (15 cm×4.6 mm, particle size- 5 µm) at room temperature. The mobile phase consisted of water (A) and acetonitrile (B). Elution gradient was set as follows: 20 % A (0 min), 20 % A (0.5 min), 45 % A (13 min), 45 % A (18 min) and 20 % A (20 min). The mobile phase flow rate was 1 mL min⁻¹ and the injected volume was set at 2 µL. Electrospray ionization (ESI) source was used for ionization of LC eluate in negative ion mode. Capillary temperature was 280°C, and sheath and auxiliary gas flow rates were 50 and 10 arb (arbitrary units), respectively. The sweep gas flow rate was set at 5 arb and source voltage at 4 kV. The capillary voltage and tube lens were set at -47 V and -120 V, respectively. During LCMS measurements, FTMS resolution was set to 100,000 and samples were analyzed in full scan mass range of m/z 100–800 with the acquisition of profile-type mass spectra. During LCMSⁿ measurements, LC peak retention time (RT) window was given to acquire MS/MS spectra of few selected ions in that RT window. All other parameters were identical to that of LCMS. MS/MS spectrums were acquired at a FT resolution of 15,000 at collision energies of 5, 10, 20 and 30 respectively and with isolation window of 1.6 Da. The raw data was processed and compared using Xcalibur version 2.0.7 (Thermo Fisher Scientific, Bremen, Germany). The mass accuracy error threshold was fixed at 5 ppm.

[¹⁸F]FDG experiments

Using size-matched, early rosette-stage plants (rosettes of approximately 5 cm radius), 1 µL of [¹⁸F]FDG solution (1.5-2 MBq µL⁻¹; in H₂O, FCON, Holzhausen a.d. Haide, Germany) was applied to puncture wounds made on both sides of the

midrib of the third oldest leaf (Fig. 5A). Four hours after the application of [^{18}F]FDG, 5 μL of water was applied to the wounds to aid uptake of remaining FDG on the leaf surface. Treatments were applied immediately after tracer application (see Fig. 5A) to the leaf next younger to the load leaf. This leaf was either left untreated (CON), or was puncture-wounded in two places, with application of 1 μL water (WW) or 1:5 diluted *M. sexta* oral secretions (WOS). For FAC treatments, leaves of three week old plants were punctured with a needle and applied with [^{18}F]FDG. Another leaf was wounded and treated with 1 μL of water (WW) or 1 μL of the fatty acid-amino acid conjugate N-linolenoyl-glutamate (WFAC), at a concentration similar to *M. sexta* OS [37]. Eight hours after these treatments, all leaves (except the leaf that was labelled with ^{18}F), shoot-root junction and roots were carefully separated, transferred to an imaging cassette, covered with a positron imaging plate and scanned after 1 h exposure (FLA 3000 system, Fujifilm, Tokyo, Japan). For radioactivity measurements, plant parts were transferred to plastic tubes and radioactivity was measured with a well counter (Isomed 2100, Nuklear Medizintechnik Dresden GmbH, Dresden, Germany).

Results and Discussion

It has been suggested that [^{18}F]FDG, a radioactive glucose analogue, could be used as a tracer for photoassimilates distribution in plant studies [38]. Although, [^{18}F]FDG uptake and metabolism has been extensively studied in animal cells [39-41], its metabolism in plant tissues is not well characterized. First, we first performed thin layer chromatography (TLC) experiments to analyze whether [^{18}F]FDG is metabolized in *N. attenuata* plants, as has been shown in *A. thaliana* [21]. The detection of multiple radioactive bands in local and systemic leaf and root tissues suggest that [^{18}F]FDG is taken up, transported and metabolized by the plant (Fig. 1). To further characterize the metabolism of FDG in plants, we supplied the stable-isotope-labelled [^{19}F]FDG to plant leaves and analysed [^{19}F]FDG metabolites via liquid chromatography-mass spectrometry (LC-MS). In all extracts from [^{19}F]FDG-labelled leaves, we found a peak eluting at retention time of 5.4 min with m/z 343.1042 and with calculated monoisotopic mass of $\text{C}_{12}\text{H}_{20}\text{O}_{10}^{19}\text{F}^-$ (± 4 ppm, Fig. 2). Upon fragmentation, m/z 343.1042 gave rise to secondary ions m/z 323.0975 and 179.0554. The first fragment can be rationalized by neutral loss of HF (20.0061), whereas the other fragment ion was identified as deprotonated glucose ($\text{C}_6\text{H}_{11}\text{O}_6^-$).

Retention time of the new compound was found to be between [^{19}F]FDG and sucrose retention times. Taken together, our data show the *in planta* incorporation of [^{19}F]FDG into different metabolites, including disaccharides, presumably [^{19}F] sucrose.

Since FDG is a metabolically active compound in *N. attenuata*, we measured effects of simulated herbivory treatments on the distribution of the radioactivity after exogenous administration of [^{18}F]FDG. When we analysed the distribution of ^{18}F in wild-type plants, root tips of control and WW-treated plants accumulated high concentrations of ^{18}F -radioactivity relative to the root axes; however, the accumulation of ^{18}F in root tips was highly reduced after simulated herbivory (WOS) (Fig. 2 A, B; Fig.3B). There was also a reduction in ^{18}F at root tips after leaves were treated with FACs, the active elicitors in the oral secretions of *M. sexta* (Fig. 2C). In above-ground tissues, radioactivity accumulated mostly in young leaves and in the shoot-root junction (data not shown), but there were no apparent effects of WW or WOS.

Because root responses after simulated herbivory, such as sugar levels, root growth inhibition and plant re-growth, has been shown in *N. attenuata* to partially depend on JA-perception through NaCOI1 [32, 34], we tested the hypothesis that the distribution of [^{18}F]FDG or its metabolites depend on JA-signalling. In addition to imaging tracer distribution, we also quantified tissue radioactivity by gamma counting in this experiment (see Fig. 3A for experimental outline). In contrast to the strong WOS-treatment effect apparent in the autoradiographs for ^{18}F -accumulation in root tips, ^{18}F -content of the entire root system showed no significant differences (nor did leaf tissues, Fig. 3C). Apparently, the treatments induced a highly localized response at root tips, which was not detectable when the entire root system was analysed. In plants silenced in NaCOI1 expression (irNaCOI1,[25]), autoradiography showed that the fraction of ^{18}F in their root tips was markedly reduced after WW treatment and also, to some extent, after WOS (Fig. 3B). Further, the radioactivity distribution (Fig. 3C) showed a significant effect of the WW treatment, and not for WOS. After WW, NaCOI1 plants showed a change in distribution in favour of the young leaves, at the expense of the roots. These responses contrast with those in WT plants, where none of the treatments significantly affected whole organ ^{18}F distribution. Taken together, these data demonstrate that simulated herbivory altered the accumulation of

[¹⁸F]FDG or its metabolites specifically in root tips, and that JA perception is important for resource allocations to roots of wounded plants.

Two reports in *N. attenuata* show that leaf herbivory specifically induces changes in carbon allocation to roots [7, 32]. While Schwachtje et al. [7] found that simulated herbivory increases allocation of recently assimilated ¹¹CO₂ to roots, they did not find increases in root carbohydrate pools. In contrast, Machado et al [32] recently demonstrated that leaf herbivory in *N. attenuata* reduced root carbohydrate pools and negatively influenced plant tolerance responses measured as plant re-growth [32]. In addition, while JA signalling did not affect carbon allocation to roots in the Schwachtje et al [7] study, Machado and colleagues found that sugar and starch levels did not change in COI1-silenced plants. Our results support the notion that *N. attenuata* does not “bunker” carbon resources in root after leaves are attacked but rather that allocation within the root is altered. In vegetative *A. thaliana* plants, wounding and MeJA application to leaves did not result in increased allocation of [¹⁸F]FDG or its metabolites to the root system [21], which suggests that different plant species at similar ontogenic stages may not only have different responses of root growth [42], but also have different resource allocation strategies when responding to herbivory. In agreement with this, Diezel and colleagues reported a strong effect of ontogeny on the response of *N. attenuata* plants to herbivory [43]. Our results may differ from those of Schwachtje et al. [7] because their plants were at a late-rosette stage of development, while plants that we used were around 10 days younger. Using plants at different developmental stages may help to test this hypothesis.

Changes in carbon allocation patterns within the root system

In the images taken after labelling the plants with [¹⁸F]FDG, it was clear that the radioactive tracer was not evenly distributed within the root system, and that the distribution changed after the experimental treatments (Figs. 2, 3). We observed a decrease in [¹⁸F]FDG or its metabolites to the secondary root tips in response to wounding and simulated herbivory. Root tips harbour apical meristems and are the region of both cell proliferation and cell expansion [44]. Whether the reduced carbon allocation signatures at the roots tips correlate with lower expansion and meristematic activity and contribute to root growth reduction after herbivory requires further analysis. In fact, graminaceous plants exposed to galactose in the rooting medium show similar reactions: allocation of recent photosynthates to the roots

increases dramatically, but at the same time decreases into the root tips, associated with cell wall tightening and reduced elongation rate [45]. The conclusion was that solute import and growth inhibition were spatially separated within the root, which might also explain our results for *N. attenuata*. Kim *et al.* [46] reported decreases in disaccharide levels in sink tissues of early elongated *N. attenuata* plants within 1 h following simulated herbivory. In tomato, another Solanaceous plant, the concentrations of glucose, fructose and sucrose decreased 4 h after wounding and subsequent application of water or *M. sexta* regurgitant [19]. Future analyses of the spatial regulation of internal sugar pools in different root areas in *N. attenuata* are needed to determine how carbohydrate pools are regulated at a fine-scale in root systems.

Regulation of allocation processes after herbivory

The nature of the signals important for the regulation of resource allocations and growth responses in roots after leaf herbivory is under debate. The oxylipin pathway, including JA and JA-Ile, is the major signalling pathway that mediates defence responses upon wounding or herbivory [47]. Simulating leaf herbivory in seedlings of *N. attenuata* also leads to the accumulation of JA in roots, and *irNaCOI1* plants show somewhat higher root growth velocity than WT plants, suggesting that JA perception is, at least partially, involved in regulating this developmental response [34]. Our experiments with [¹⁸F]FDG also indicate that JA perception is involved in restricting wound-induced resource allocation processes (Fig. 5C). However, JA is not the only plant hormone that is altered after leaf herbivory; growth-related hormones also change during herbivory (reviewed in [47]). Auxin, which is mainly supplied through the shoot apex, can be generally considered as a reporter for the integrity of apical tissues, and herbivory could strongly influence the provision of auxin from the shoot to the root system [48]. Machado *et al* [32] showed transient changes in auxin levels upon leaf treatments with WOS and that external auxin applications change herbivory-induced carbohydrate and re-growth patterns. However, auxin itself is not likely to be the only messenger that induces systemic growth responses and resource allocations [49-51]. Cytokinins, whose biosynthesis and transport are inhibited by auxin [48, 52-54], may play profound roles in stress-induced growth responses [55] and regulate root growth and development, such as limiting the size of the root apical meristem and the rate of root growth [56, 57]. Future research will

reveal how auxin, cytokinins or other hormones (e.g. Absciscic acid), may change the carbon allocation and growth responses and how the JA pathway may interact with these responses.

List of abbreviations

JA = Jasmonic acid; WW = wounding and application of water, WOS = wounding and application of oral secretions, WFAC = wounding and application of fatty acid-amino acid conjugates; FDG = 2-deoxy-2-fluoro-D-glucose.

Competing interests

The authors declare that they have no conflict of interest.

Authors contributions

All authors designed experiments, performed experiments and analysed the data. SM drafted the manuscript. All authors edited the manuscript.

Acknowledgements

We thank Hans-Peter Saluz, Peter Gebhardt and Thomas Opfermann for providing technical assistance with [^{18}F]FDG and equipment at the Leibniz Institute for Natural Product Research and Infection Biology, Jena, Germany. The work of Stefan Meldau is funded by Advanced Grant No 293926 of the European Research Council to Ian Baldwin. Melkamu GW was funded by the German Academic Exchange Service (DAAD). This study is supported by the Max Planck Society.

Captions

Figure 1. [^{18}F]FDG and [^{19}F]FDG metabolism in *N. attenuata* leaves. (A) [^{18}F]FDG is metabolized in *Nicotiana attenuata*. One leaf (AP) of a 3.5 week old plant was punctured with a needle and applied with 5 μL [^{18}F]FDG solution. Another leaf was induced with wounding and treated with 1 μL of 1:5 diluted *Manduca sexta* oral secretions (IL). After 8 hours the plants were disassembled, tissues were extracted and qualitative sugar analysis was done by performing thin layer chromatography

(TLC, left picture). Autoradiograph was taken of the same TLC plate (right picture). Labeling: YL = youngest leaves, IL = induced leaf, RO = root, AP = apical part of the [^{18}F]FDG treated leaf, AU = apical bud of the plant, AB = basal part of the [^{18}F]FDG treated leaf, standards: S = sucrose, F = fructose, G = glucose, UDPG = Uridindiphosphat-Glucose, G6P = glucose-6-phosphate, F6P = Fructose-6-phosphate, FDG = [^{18}F]FDG. (B) Comparison of total (TIC) and extracted ion chromatograms ([^{19}F]FDG Disaccharide: m/z 343.10) of leaf extract (ctrl, i and iii) and [^{19}F]FDG applied leaf extract (ii and iv). (C) MS² of m/z: 343.10 (retention time: 5.50 min). (D) Comparison TIC of CTRL-leaf extract (i) with [^{19}F]FDG applied leaf extract (ii) for depicting [^{19}F]FDG and [^{19}F]-disaccharide chromatographic peaks.

Figure 2. [^{18}F]FDG distribution after simulated herbivory in *Nicotiana attenuata* plants. (A) Autoradiograph from plant parts of [^{18}F]FDG-treated wild type *N. attenuata* plants. Leaves of 3.5 week old plants were punctured with a needle and applied with [^{18}F]FDG. Another leaf kept untreated (CON) or was wounded and treated with 1 μL of water (WW) or 1 μL of 1:5 diluted *Manduca sexta* oral secretions (WOS). After 8 hours the plants were disassembled and an autoradiographic picture was taken. (B) Root pictures from (A) were magnified and assembled next to each other to demonstrate the reduced accumulations of radioactivity after WOS treatments. (C) Autoradiograph roots of [^{18}F]FDG-treated *N. attenuata* plants. Leaves of three week old plants were punctured with a needle and applied with [^{18}F]FDG. Another leaf was wounded and treated with 1 μL of water (WW) or 1 μL of the fatty acid-amino acid conjugate N-linolenoyl-glutamate (WFAC), one of the active elicitor in *M. sexta* oral secretions.

Figure 3. Radioactivity accumulation after [^{18}F]FDG labelling and simulated herbivory in *N. attenuata*. (A) Scheme of the experimental setup. Leaves of 3 week old plants were punctured with a needle and applied with FDG (red dots). Another leaf kept untreated (CON) or was wounded and treated with 1 μL of water (WW, blue dots) or 1 μL of 1:5 diluted *Manduca sexta* oral secretions (WOS, green dots). After 8 h the plants were disassembled and an autoradiographic picture was taken from a set of plants. Plant parts were then weighed and radioactivity was measured. Autoradiographs (B) and radioactivity measurements in (C) roots and (D) sink leaves

396 of [¹⁸F]FDG-labelled wild type (WT) and inverted repeat COI1 (irCOI1) plants. Red
397 arrows indicate changes at root tips (B). Letters indicate significant differences
398 between treatments (ANOVA, root: F_{2,12} = 5.16; P = 0.077; young leaves: F_{2,12} =
399 3.06; P = 0.0301), N ≥ 5 ± SE.

References

1. De Geyter N, Gholami A, Goormachtig S, Goossens A: **Transcriptional machineries in jasmonate-elicited plant secondary metabolism.** *Trends Plant Sci* 2012, **17**:349-359.
2. Arnold T, Appel H, Patel V, Stocum E, Kavalier A, Schultz J: **Carbohydrate translocation determines the phenolic content of *Populus* foliage: a test of the sink-source model of plant defense.** *New Phytol* 2004, **164**:157-164.
3. Bolton MD: **Primary Metabolism and Plant Defense-Fuel for the Fire.** *Mol Plant Microbe In* 2009, **22**:487-497.
4. Broeckling CD, Huhman DV, Farag MA, Smith JT, May GD, Mendes P, Dixon RA, Sumner LW: **Metabolic profiling of *Medicago truncatula* cell cultures reveals the effects of biotic and abiotic elicitors on metabolism.** *Journal of Experimental Botany* 2005, **56**:323-336.
5. Hanik N, Gomez S, Best M, Schueller M, Orians CM, Ferrieri RA: **Partitioning of new carbon as C-11 in *Nicotiana tabacum* reveals insight into methyl jasmonate induced changes in metabolism.** *Journal of Chemical Ecology* 2010, **36**:1058-1067.
6. Hanik N, Gomez S, Schueller M, Orians CM, Ferrieri RA: **Use of gaseous ¹³NH(3) administered to intact leaves of *Nicotiana tabacum* to study changes in nitrogen utilization during defence induction.** *Plant Cell Environ* 2010, **33**:2173-2179.
7. Schwachtje J, Minchin PE, Jahnke S, van Dongen JT, Schittko U, Baldwin IT: **SNF1-related kinases allow plants to tolerate herbivory by allocating carbon to roots.** *Proc Natl Acad Sci U S A* 2006, **103**:12935-12940.
8. Baldwin IT: **Jasmonate-induced responses are costly but benefit plants under attack in native populations.** *Proc Natl Acad Sci U S A* 1998, **95**:8113-8118.

9. Cipollini D: **Consequences of the overproduction of methyl jasmonate on seed production, tolerance to defoliation and competitive effect and response of *Arabidopsis thaliana*.** *New Phytol* 2007, **173**:146-153.
10. Halitschke R, Baldwin IT: **Antisense LOX expression increases herbivore performance by decreasing defense responses and inhibiting growth-related transcriptional reorganization in *Nicotiana attenuata*.** *Plant J* 2003, **36**:794-807.
11. Meldau S, Ullman-Zeunert L, Govind G, Bartram S, Baldwin IT: **MAPK-dependent JA and SA signalling in *Nicotiana attenuata* affects plant growth and fitness during competition with conspecifics.** *Bmc Plant Biology* 2012, **12**.
12. Redman AM, Cipollini DF, Schultz JC: **Fitness costs of jasmonic acid-induced defense in tomato, *Lycopersicon esculentum*.** *Oecologia* 2001, **126**:380-385.
13. Sturm A, Chrispeels MJ: **Cdna cloning of carrot extracellular beta-Fructosidase and its expression in response to wounding and bacterial-infection.** *Plant Cell* 1990, **2**:1107-1119.
14. Ohyama A, Nishimura S, Hirai M: **Cloning of cDNA for a cell wall-bound acid invertase from tomato (*Lycopersicon esculentum*) and expression of soluble and cell wall-bound invertases in plants and wounded leaves of *L. esculentum* and *L. peruvianum*.** *Genes Genet Syst* 1998, **73**:149-157.
15. Arnold TM, Schultz JC: **Induced sink strength as a prerequisite for induced tannin biosynthesis in developing leaves of *Populus*.** *Oecologia* 2002, **130**:585-593.
16. Philippe RN, Ralph SG, Mansfield SD, Bohlmann J: **Transcriptome profiles of hybrid poplar (*Populus trichocarpa x deltoides*) reveal rapid changes in undamaged, systemic sink leaves after simulated feeding by forest tent caterpillar (*Malacosoma disstria*).** *New Phytol* 2010, **188**:787-802.
17. Zhang L, Cohn NS, Mitchell JP: **Induction of a pea cell-wall invertase gene by wounding and its localized expression in phloem.** *Plant Physiology* 1996, **112**:1111-1117.
18. Babst BA, Ferrieri RA, Gray DW, Lerdau M, Schlyer DJ, Schueller M, Thorpe MR, Orians CM: **Jasmonic acid induces rapid changes in carbon transport and partitioning in *Populus*.** *New Phytol* 2005, **167**:63-72.
19. Gomez S, Steinbrenner AD, Osorio S, Schueller M, Ferrieri RA, Fernie AR, Orians CM: **From shoots to roots: transport and metabolic changes in tomato**

after simulated feeding by a specialist lepidopteran. *Entomol Exp Appl* 2012, **144**:101-111.

20.Holland JN, Cheng WX, Crossley DA: **Herbivore-induced changes in plant carbon allocation: Assessment of below-ground C fluxes using carbon-14.** *Oecologia* 1996, **107**:87-94.

21.Ferrieri AP, Appel H, Ferrieri RA, Schultz JC: **Novel application of 2-[F-18]fluoro-2-deoxy-D-glucose to study plant defenses.** *Nucl Med Biol* 2012, **39**:1152-1160.

22.Kallenbach M, Alagna F, Baldwin IT, Bonaventure G: ***Nicotiana attenuata* SIPK, WIPK, NPR1, and fatty acid-amino acid conjugates participate in the induction of jasmonic acid biosynthesis by affecting early enzymatic steps in the pathway.** *Plant Physiol* 2010, **152**:96-106.

23.Wu JQ, Hettenhausen C, Meldau S, Baldwin IT: **Herbivory rapidly activates MAPK signaling in attacked and unattacked leaf regions but not between leaves of *Nicotiana attenuata*.** *Plant Cell* 2007, **19**:1096-1122.

24.Wang L, Halitschke R, Kang JH, Berg A, Harnisch F, Baldwin IT: **Independently silencing two JAR family members impairs levels of trypsin proteinase inhibitors but not nicotine.** *Planta* 2007, **226**:159-167.

25.Paschold A, Halitschke R, Baldwin IT: **Co(i)-ordinating defenses: NaCOI1 mediates herbivore- induced resistance in *Nicotiana attenuata* and reveals the role of herbivore movement in avoiding defenses.** *Plant J* 2007, **51**:79-91.

26.Woldemariam MG, Dinh ST, Oh Y, Gaquerel E, Baldwin IT, Galis I: **NaMYC2 transcription factor regulates a subset of plant defense responses in *Nicotiana attenuata*.** *BMC Plant Biol* 2013, **13**.

27.Babst BA, Ferrieri RA, Thorpe MR, Orians CM: ***Lymantria dispar* herbivory induces rapid changes in carbon transport and partitioning in *Populus nigra*.** *Entomol Exp Appl* 2008, **128**:117-125.

28.Bazot S, Mikola J, Nguyen C, Robin C: **Defoliation-induced changes in carbon allocation and root soluble carbon concentration in field-grown *Lolium perenne* plants: do they affect carbon availability, microbes and animal trophic groups in soil?** *Funct Ecol* 2005, **19**:886-896.

29.Briske DD, Boutton TW, Wang Z: **Contribution of flexible allocation priorities to herbivory tolerance in C-4 perennial grasses: An evaluation with C-13 labeling.** *Oecologia* 1996, **105**:151-159.

30. Dyer MI, Acra MA, Wang GM, Coleman DC, Freckman DW, Mcnaughton SJ, Strain BR: **Source-sink carbon relations in 2 *Panicum coloratum* ecotypes in response to herbivory.** *Ecology* 1991, **72**:1472-1483.

31. Gomez S, Ferrieri RA, Schueller M, Orians CM: **Methyl jasmonate elicits rapid changes in carbon and nitrogen dynamics in tomato.** *New Phytol* 2010, **188**:835-844.

32. Machado RAR, Ferrieri AP, Robert CAM, Glauser G, Kallenbach M, Baldwin IT, Erb M: **Leaf-herbivore attack reduces carbon reserves and regrowth from the roots via jasmonate and auxin signaling.** *New Phytol* 2013, **200**:1234-1246.

33. Hummel GM, Naumann M, Schurr U, Walter A: **Root growth dynamics of *Nicotiana attenuata* seedlings are affected by simulated herbivore attack.** *Plant Cell Environ* 2007, **30**:1326-1336.

34. Hummel GM, Schurr U, Baldwin IT, Walter A: **Herbivore-induced jasmonic acid bursts in leaves of *Nicotiana attenuata* mediate short-term reductions in root growth.** *Plant Cell Environ* 2009, **32**:134-143.

35. Krugel T, Lim M, Gase K, Halitschke R, Baldwin IT: ***Agrobacterium*-mediated transformation of *Nicotiana attenuata*, a model ecological expression system.** *Chemoecology* 2002, **12**:177-183.

36. Gromova M, Roby C: **Toward *Arabidopsis thaliana* hydrophilic metabolome: assessment of extraction methods and quantitative ¹H NMR.** *Physiol Plantarum* 2010, **140**:111-127.

37. Hettenhausen C, Baldwin IT, Wu J: ***Nicotiana attenuata* MPK4 suppresses a novel jasmonic acid (JA) signaling-independent defense pathway against the specialist insect *Manduca sexta*, but is not required for the resistance to the generalist *Spodoptera littoralis*.** *New Phytologist* 2013, **199**:787-799.

38. Hattori E, Uchida H, Harada N, Ohta M, Tsukada H, Hara Y, Suzuki T: **Incorporation and translocation of 2-deoxy-2-[F-18]fluoro-D-glucose in *Sorghum bicolor* (L.) Moench monitored using a planar positron imaging system.** *Planta* 2008, **227**:1181-1186.

39. Kaarstad K, Bender D, Bentzen L, Munk OL, Keiding S: **Metabolic fate of F-18-FDG in mice bearing either SCCVII squamous cell carcinoma or C3H mammary carcinoma.** *J Nucl Med* 2002, **43**:940-947.

40. McSheehy PMJ, Leach MO, Judson IR, Griffiths JR: **Metabolites of 2 '-fluoro-2 '-deoxy-D-glucose detected by F-19 magnetic resonance spectroscopy**

in vivo predict response of murine RIF-1 tumors to 5-fluorouracil. *Cancer Res* 2000, **60**:2122-2127.

41. Southworth R, Parry CR, Parkes HG, Medina RA, Garlick PB: **Tissue-specific differences in 2-fluoro-2-deoxyglucose metabolism beyond FDG-6-P: a (19)F NMR spectroscopy study in the rat.** *Nmr Biomed* 2003, **16**:494-502.

42. Schmidt L, Hummel GM, Schöttner M, Schurr U, Walter A: **Jasmonic acid does not mediate root growth responses to wounding in *Arabidopsis thaliana*.** *Plant, Cell & Environment* 2009.

43. Diezel C, Allmann S, Baldwin IT: **Mechanisms of optimal defense patterns in *Nicotiana attenuata*: flowering attenuates herbivory-elicited ethylene and jasmonate signaling.** *J Integr Plant Biol* 2011, **53**:971-983.

44. Ivanov VB, Dubrovsky JG: **Longitudinal zonation pattern in plant roots: conflicts and solutions.** *Trends in Plant Science* 2013, **18**:237-243.

45. Pritchard J, Tomos AD, Farrar JE, Minchin PEH, Gould N, Paul MJ, MacRae EA, Ferrieri RA, Gray DW, Thorpe MR: **Turgor, solute import and growth in maize roots treated with galactose.** *Funct Plant Biol* 2004, **31**:1095-1103.

46. Kim SG, Yon F, Gaquerel E, Gulati J, Baldwin IT: **Tissue specific diurnal rhythms of metabolites and their regulation during herbivore attack in a native tobacco, *Nicotiana attenuata*.** *PLoS One* 2011, **6**.

47. Erb M, Meldau S, Howe GA: **Role of phytohormones in insect-specific plant reactions.** *Trends Plant Sci* 2012, **17**:250-259.

48. McSteen P, Leyser O: **Shoot branching.** *Annual Review of Plant Biology* 2005, **56**:353-374.

49. Booker J, Chatfield S, Leyser O: **Auxin acts in xylem-associated or medullary cells to mediate apical dominance.** *Plant Cell* 2003, **15**:495-507.

50. Hillman JR, Math VB, Medlow GC: **Apical dominance and levels of indole acetic-acid in *Phaseolus* lateral buds.** *Planta* 1977, **134**:191-193.

51. Morris DA: **Transport of exogenous auxin in 2-branched dwarf Pea-seedlings (*Pisum-sativum*-L) - Some implications for polarity and apical dominance.** *Planta* 1977, **136**:91-96.

52. Bangerth F: **Response of cytokinin concentration in the xylem exudate of Bean (*Phaseolus-vulgaris* L) plants to decapitation and auxin treatment, and relationship to apical dominance.** *Planta* 1994, **194**:439-442.

53. Eklof S, Astot C, Blackwell J, Moritz T, Olsson O, Sandberg G: **Auxin-cytokinin interactions in wild-type and transgenic tobacco.** *Plant and Cell Physiology* 1997, **38**:225-235.

54. Nordstrom A, Tarkowski P, Tarkowska D, Norbaek R, Astot C, Dolezal K, Sandberg G: **Auxin regulation of cytokinin biosynthesis in *Arabidopsis thaliana*: A factor of potential importance for auxin-cytokinin-regulated development.** *P Natl Acad Sci USA* 2004, **101**:8039-8044.

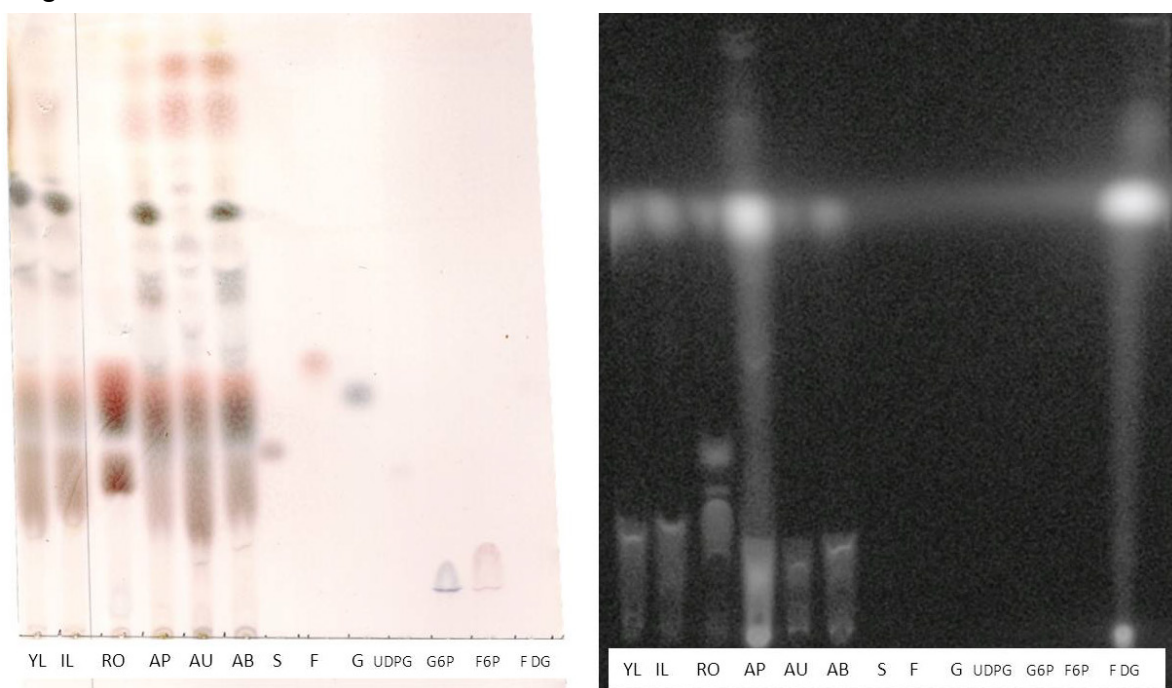
55. Argueso CT, Ferreira FJ, Kieber JJ: **Environmental perception avenues: the interaction of cytokinin and environmental response pathways.** *Plant Cell Environ* 2009, **32**:1147-1160.

56. Dello Loio R, Linhares FS, Sabatini S: **Emerging role of cytokinin as a regulator of cellular differentiation.** *Current Opinion in Plant Biology* 2008, **11**:23-27.

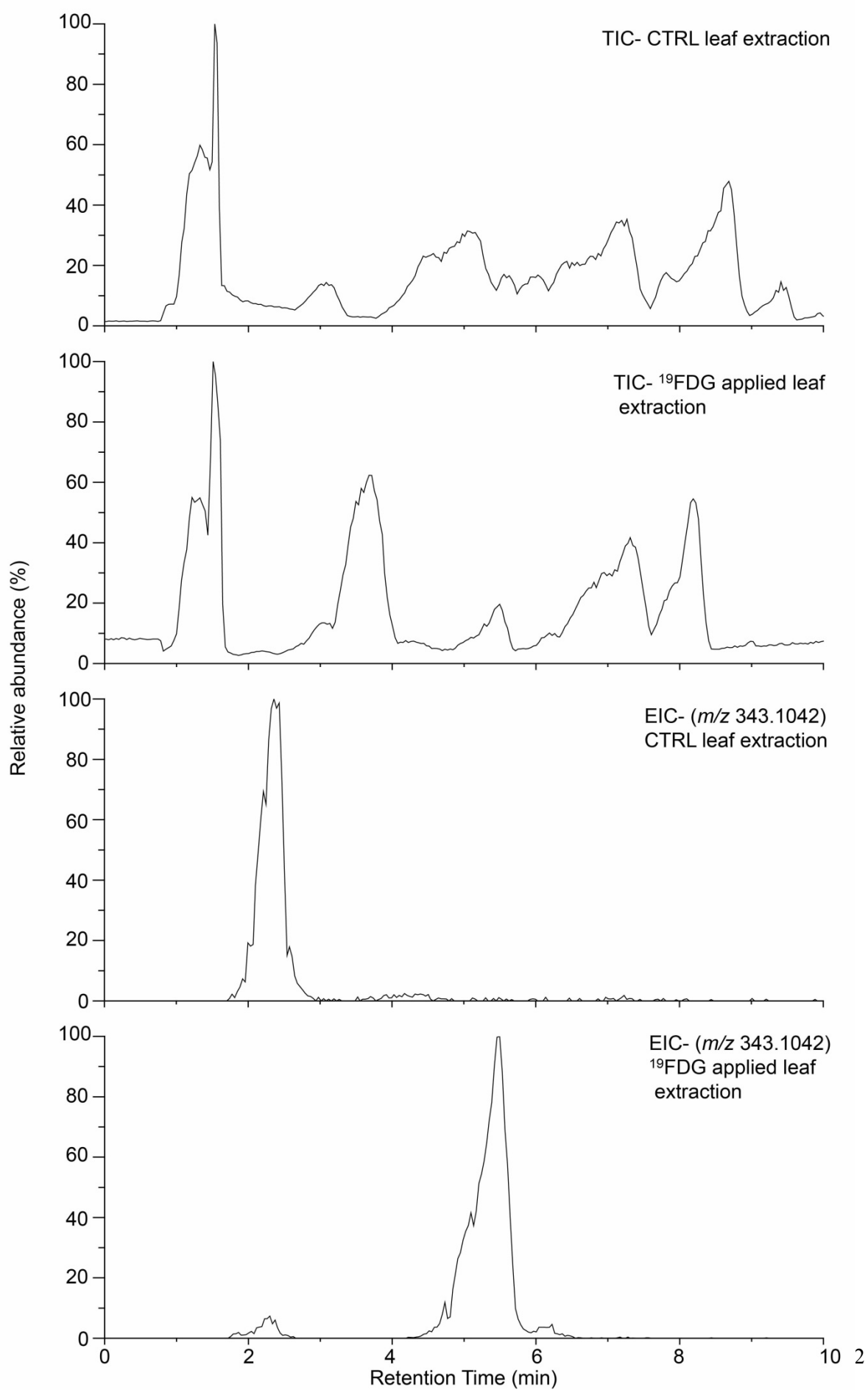
57. Werner T, Motyka V, Laucou V, Smets R, Van Onckelen H, Schmulling T: **Cytokinin-deficient transgenic *Arabidopsis* plants show multiple developmental alterations indicating opposite functions of cytokinins in the regulation of shoot and root meristem activity.** *Plant Cell* 2003, **15**:2532-2550.

Figures

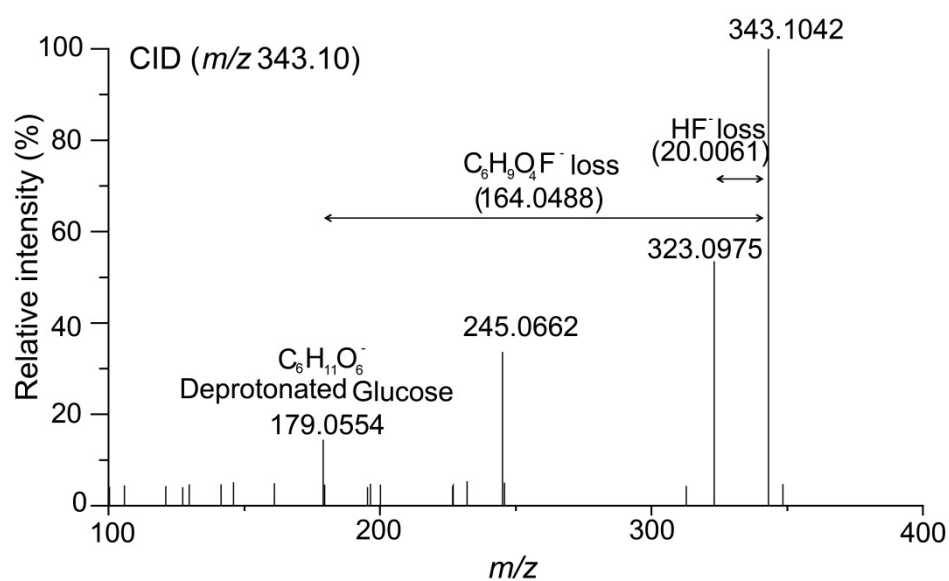
Figure :1 A



B (i, ii, iii, iv)



C



D

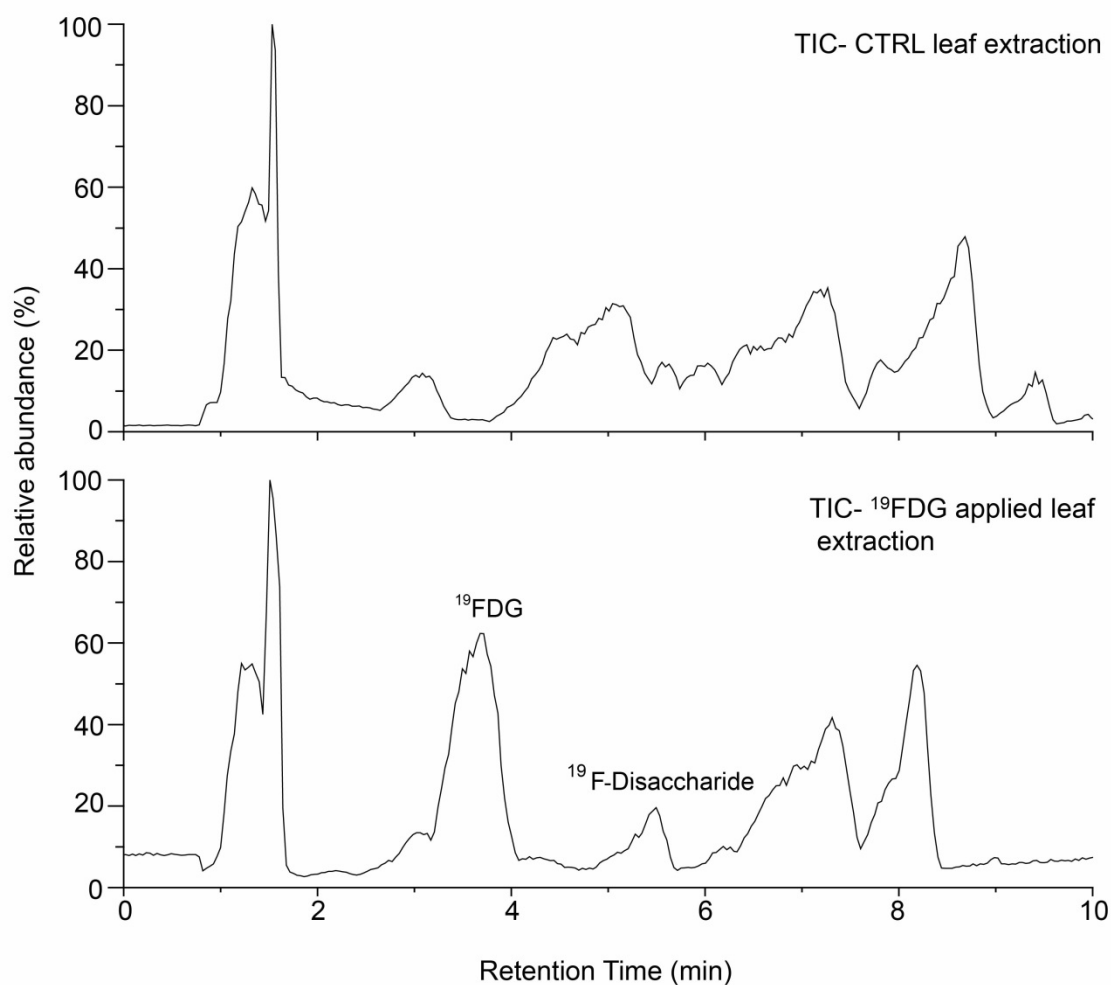


Figure :2

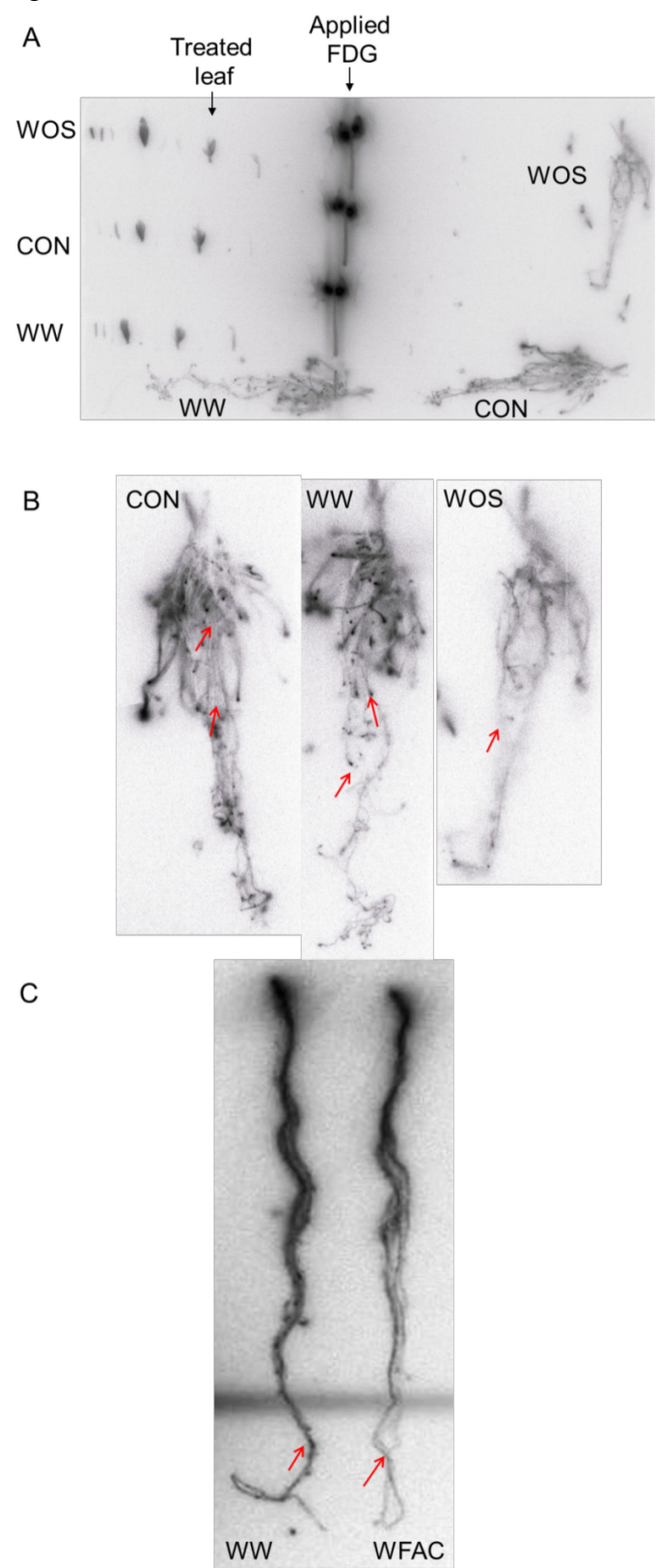
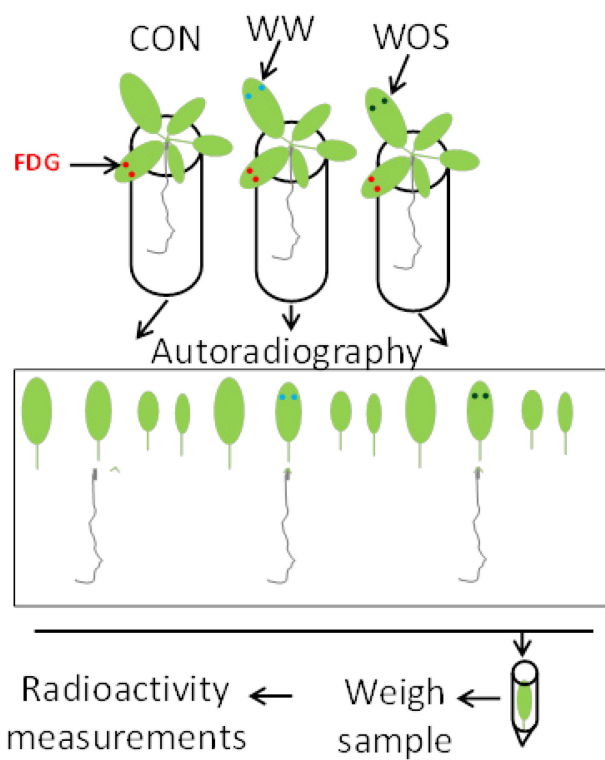
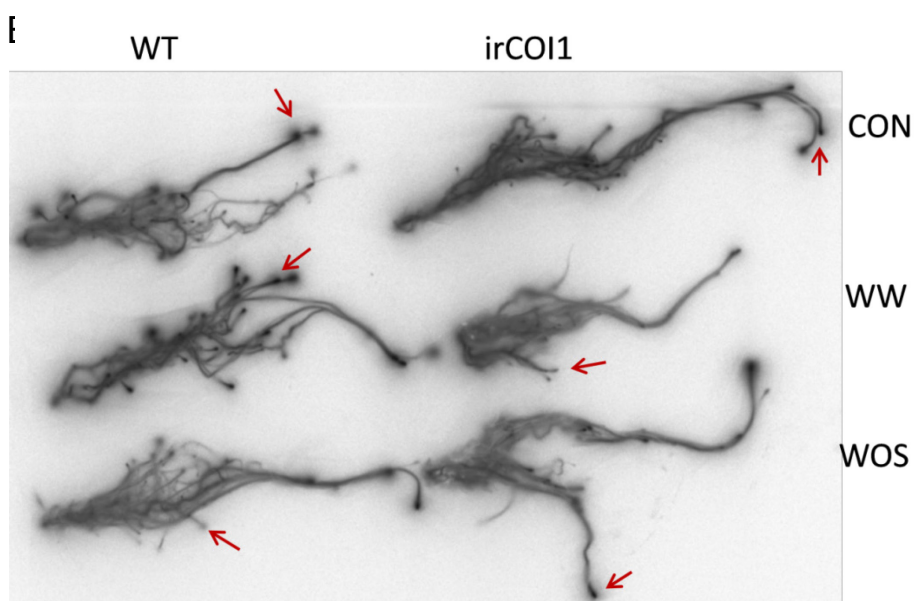


Figure :3

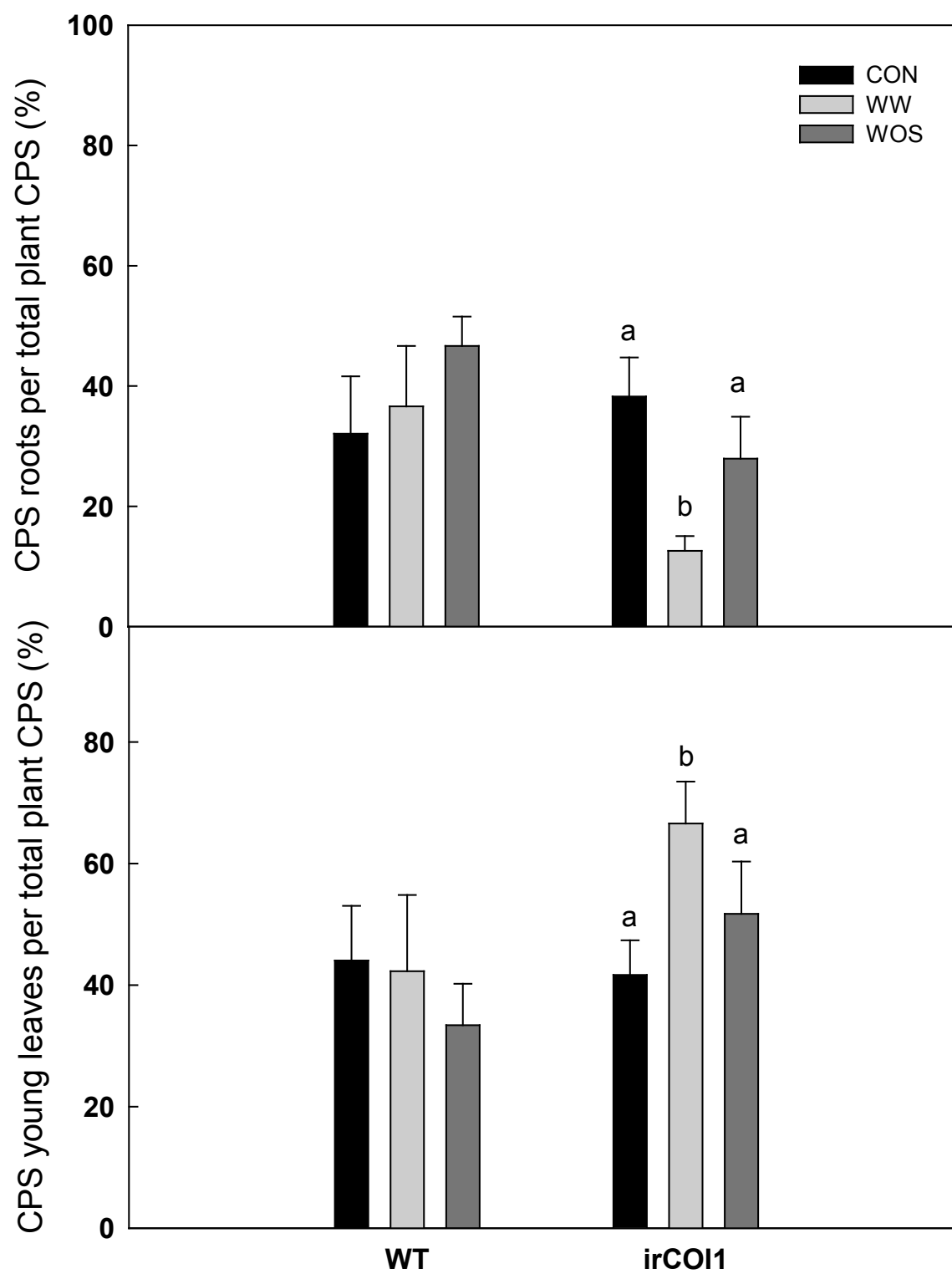
A



B



c



General Discussion

Plants are photoautotrophs. They photosynthesize sugars as primary metabolites, energy rich compounds which support whole ecological food chain. These energy-storing monosaccharides produced by photosynthesis are defined as photoassimilates. However, in broader context, photoassimilates encompass wide repertoire of energy rich anabolic end-products of photosynthesis such as ATP, triose phosphates, glucose, sucrose or starch etc. Photoassimilates can be stored locally or translocated to other plant parts such as fruits, root, or shoot for their storage or utilization. Photoassimilate translocation and partitioning are highly dynamic processes which are governed by current metabolic needs of the plant which in turn depend upon the plant physiology, age, growth stage, and environment [Zamski and Schaffer, 1996; Lemoine et al, 2013]. Growth rate and biomass productivity in plants is highly influenced by such photoassimilate dynamics. Current crop improvement strategies also heavily rely upon engineering of photoassimilate partitioning [Murillo et al, 2003; Van Camp W, 2005; Gómez-ariza et al, 2007, Jonik et al, 2012; Pandey et al, 2013, Ruan et al, 2013]. Thus, studying *in vivo* dynamics of photoassimilates partitioning under various environmental conditions is of significant interest in plant research [Ferrieri et al, 2013; Lemoine et al, 2013; Babst et al, 2013]. My research work in this thesis presents a possible methodology to elucidate *in vivo* dynamics of photoassimilate translocation and partitioning under various environmental conditions using FDG as a radiotracer.

Monitoring photoassimilate fluxes and FDG imaging:

Plant growth and fitness depends upon balanced allocation of carbon resources as per the need of various plant parts. Photosynthesizing plant parts such as mature green leaves fix atmospheric CO₂ into photoassimilate in excess of their need and make it available to other plant parts. Plant parts which contribute to central photoassimilate pool cumulatively constitute as sources [Turgeon R, 1989; Osorio et al, 2014]. Source strength determines how much of the fixed carbon will be available for translocation to other plant parts [Zamski and Schaffer, 1996; Wang and Nobel, 1996; Flore and Layne, 1999]. On the other hand, growing tissue, fruits, non-photosynthesizing tissue like root *etc.* derive their nutrition from available photoassimilate pool and constitute as sinks [Turgeon R, 1989]. Available resources are prioritized towards various plant parts as per their sink strength [Zamski and Schaffer, 1996; Minchin and Thorpe, 1996; Lemoine et al, 2013]. Thus, overall plant system could be looked as a regulated photoassimilate distribution system where source tissue (*eg.* photosynthesizing

mature leaves) acts as donor for photoassimilate which is strictly partitioned towards various sink tissues (eg. growing meristematic tissue, storage tissue, roots) as per their sink strength. Such source-sink relationship controls assimilated photoassimilate fluxes towards different plant parts.

Growing parts like shoot apex, young leaves and roots are primary sinks during early plant development stage however this balance tips in the direction of tubers, fruits and seeds during the later developmental stages such as fruiting or reproductive stages [Wardlaw IF, 1990; Ho LC, 1992]. *Arabidopsis* plants used in our experiments were of four week old and in early flowering stage [Boyes et al, 2001]. Thus, shoot apex and roots were expected to be the strongest sinks. Our results matched with the above hypothesis as we observed that the [^{18}F] radioactivity was mostly accumulated in shoot apex and roots. Very less of radioactivity was located in mature rosette leaves which are known to be sources of photoassimilate [Turgeon R, 1989]. Also, the route of radioactivity translocation was exclusively via phloem. However, we observed variability in plant replicates about relative amount of radioactivity accumulated in various plant parts. We think that plant stage, plant size, orthostichy and sectoriality have significant influence on the observed radioactivity distribution [Ferrieri et al, 2012; De schepper et al, 2013]. *Arabidopsis* depicts 3+5 phyllotaxis [Callos and Medford, 1994]. Leaf orthostichy and sectoriality may facilitate or hamper radioactivity passage among leaves and results in differential amounts of radioactivity accumulation in leaves of the same growth stage [Ferrieri et al, 2012]. We also observed that a large amount of [^{18}F] radioactivity was seen in ^{18}FDG applied leaf only. This may be because ^{18}FDG is locally sequestered and entrapped in leaf cells by its conversion to FDG-6-P [chapter-II]. Analysis of EDTA-mediated phloem exudate revealed intact ^{18}FDG as the transport form in which [^{18}F] radioactivity was translocated. This matched with previously reported result that ^{18}FDG persist as an intact sugar molecule during its translocation to other plant parts [Ferrieri et al, 2012]. This is contradictory to the literature that only sucrose, raffinose and sugar alcohol such as galactinol have been reported as translocated sugar forms in phloem of *Arabidopsis* [Ziegler H, 1975; Haritatos et al, 2000]. However, all imaging studies had showed profound pattern similarity between the [^{18}F] radioactivity and photoassimilates allocation [Hattori et al, 2008; Ferrieri et al, 2012]. Furthermore, Ferrieri et al (2012) showed that wounding or methyl jasmonate application to *Arabidopsis* leaf increased ^{18}FDG transport into elicited leaf. Wounding, methyl jasmonate application, or insect elicitation is known to increase local sink strengths [Quilliam et al, 2006; Ferrieri et al, 2013], increasing carbon allocation to elicited

leaf [Arnold and Schultz, 2002; Arnold et al, 2004; Ferrieri et al, 2013]. We think that upon feeding, major fraction of FDG is being taken up and sequestered locally in the plant tissue but small fraction of FDG is able to enter into phloem via apoplastic loading mechanism. Once inside the phloem, it will be translocated as a phloem sugar entity and partitioned to various plants parts similar to photoassimilates. This hypothesis should be tested using PET. Being non-invasive technique, PET could allow for the comparison of radioactivity distributions in a single plant using both $^{11}\text{CO}_2$ and ^{18}FDG as radiotracers. This comparison will conclusively prove that the ^{18}F radioactivity distribution after ^{18}FDG feeding is similar to that of ^{11}C photoassimilate distribution or not.

Plants fix atmospheric CO_2 to produce photoassimilate. Gaseous CO_2 being the precursor for assimilated carbon, recently synthesized photoassimilate compounds could be readily labeled with feeding the plants with isotopically labeled carbon. Isotopic labeling has been traditionally used to study carbon assimilation in photosynthesis and its flux via long distance vascular network of xylem and phloem. Photoassimilate fluxes in plants have been monitored using stable ^{13}C isotope [Lu et al, 2002; Dickson et al, 1990], long-lived ^{14}C radioisotope [Webb and Gorham, 1964; Geiger et al, 1969; Fisher DB, 1970; Finazzo et al, 1994] or short-lived positron-emitting ^{11}C radioisotope labeled compounds [Moorby et al, 1963; Thorpe and Minchin, 1991; Thorpe et al, 1998; Matsushashi et al, 2006; Ferrieri et al, 2013]. Monitoring photoassimilate fluxes using ^{13}C , ^{14}C , or ^{11}C are well known techniques and certainly have their merits. However, each has its own drawbacks. ^{13}C labelled plants need to be harvested for ^{13}C label detection [Lu et al, 2002; Dickson et al, 1990]. Also, a single plant can not be used for multiple labeling experiments. ^{14}C has a long half life but the beta particle emitted after ^{14}C decays are of low energy and could not escape thick plant tissue. Thus it also requires destructive harvesting of plant tissue [Webb and Gorham, 1964; Margolis et al, 1991; Finazzo et al, 1994]. Moreover, it can not be employed for *in vivo* quantification studies where changes in carbon allocation are very dynamic. Thus, ^{14}C radiotracers are rarely used to study the photoassimilate translocation in an intact plant. *In vivo* carbon allocation dynamics in plants can be visualized using positron-emitting ^{11}C radioisotope labeled compounds; however, ^{11}C has half-life of 20.3 min [www.nndc.bnl.gov/chart/] which limits its applicability to short time-scale experiments. Also, in gaseous $^{11}\text{CO}_2$ application technique, photoassimilates have to be first synthesized by the plant leaf and then translocated to other plant parts where they are needed. Initial lag time and short half-life of $^{11}\text{CO}_2$ ($t_{1/2}=20.3$ min) radiotracer makes it difficult to monitor of photosynthetic pathways

over long duration [Minchin and Grusak, 1998; Ferrieri et al, 2013]. We overcome these limitations with ^{18}FDG ($t_{1/2}=109.8$ min) as a radiotracer for photoassimilate translocation studies. It effectively addressed concerns over long term photoassimilate translocation studies. Also, ^{18}FDG is directly introduced into plant leaf in its intact form so there is no lag time existed between ^{18}FDG application and its translocation. One more advantage is that we can monitor photoassimilate translocation dynamics in dark cycle when no CO_2 fixation or photosynthesis is occurring due to absence of light. This makes ^{18}FDG a suitable tracer for long term photoassimilate translocation studies.

FDG metabolism in plants:

In our first chapter, we have shown that *Arabidopsis* leaf is able to take up ^{18}FDG from the pricked leaf spot and radioactivity was differentially distributed to various plants parts [Fatangare et al, 2014]. However, FDG metabolism was only been speculated from literature from FDG metabolism in animal tissue [Hattori et al, 2008]. In second chapter, we elucidated FDG metabolism in *Arabidopsis* leaf cells in order to complement our imaging results. We identified the presence of four different fluorine containing metabolites *viz.* F-gluconic acid, FDG-6-P, F-maltose, and UDP-FDG on the basis of exact mono-isotopic masses for these compounds, MS/MS fragmentation, and NMR analysis. We have shown that FDG is taken up by plant cells though the transport system sensitive to HgCl_2 . We think that, being glucose analog, FDG is taken up via low-affinity, facilitated-diffusion process as similar to that of glucose [Conde et al, 2007]. Upon uptake, FDG is being metabolized via glycolysis pathways, likewise in animal tissue, to form FDG-6-P as one of the major metabolites of FDG metabolism in plant cells. However, FDG metabolism goes beyond FDG-6-P. Discovery of F-gluconic acid, F-maltose, and UDP-FDG as FDG metabolites was unexpected and still unreported outcome of FDG metabolism in *Arabidopsis*. Here, we try to shed some light on the possible pathways which might be involved in this process.

Biosynthesis of FDG-6-P occurs via the glycolytic pathway [Miller and Kiney, 1981; Reivich et al, 1985; Suolinna et al, 1986]. Hexokinase catalyzes first reaction of glycolytic pathways and thus determines the flux of carbon going into energy production [Bouny and Saglio, 1996; Marín-Hernández et al, 2006]. It catalyzes conversion of glucose into glucose-6-phosphate. This step adds negative charge on influxed glucose and leads to its trapping inside the cell thus maintaining the downhill concentration gradient which favours the facilitated transport of glucose into the cell [Printz et al, 1993]. Broad substrate specificity of

hexokinase has already been noted as it could accommodate FDG, 2-deoxy-2-D-glucose or other glucose analogs [la Fuente et al, 1958; Machado de Domenech and Sols, 1980; www.brenda-enzymes.org/enzyme.php?ecno=2.7.1.1]. FDG is a known substrate for hexokinase [Machado de Domenech and Sols, 1980; Muzi et al, 2001]. Thus, FDG uptake which occurs via facilitated diffusion process will follow the similar kinetics as that of glucose in which FDG enters the cell via passive glucose transporter and will be converted to FDG-6-P thus effectively blocking its efflux. This step will further favour uptake of external FDG into the cell resulting in localized high radioactivity spots. We observed that FDG-6-P was the most abundant metabolites of FDG in the plants cells. However, not all FDG is converted to FDG-6-P. Hexokinase activity is highly regulated via reverse feedback mechanism in which accumulation of reaction product FDG-6-P allosterically inhibits the enzyme action [Lampidis et al, 2006; Kurtoglu et al, 2007a]. Build-up of intracellular FDG-6-P concentration will result in shutting down of glycolytic pathway. This explains why FDG acts as a glycolytic inhibitor [Lampidis et al, 2006; Kurtoglu et al, 2007a]. In animal studies, it has been reported that FDG-6-P further metabolized to FDG-1-P and FDG-1,6-biP [kanazawa et al, 1996; Mcsheehy et al, 2000; Southworth et al, 2003], however, we could not detect these metabolites. FDG-6-P reversibly epimerizes to 2-deoxy-2-fluoromannose-6-phosphate (FDM-6-P) under the action of phosphoglucose isomerase [Kanazawa et al., 1986; Kojima et al., 1988; Pouremad and Wyrwicz, 1991; O'Connell and London, 1995]. FDM-6-P will lead to formation of 2-deoxy-2-fluoromannose (FDM) or other FDM metabolites in the cell. FDM has been shown to cause cytotoxicity by inhibiting *N*-linked glycosylation [Datema et al, 1980; Kurtoglu et al, 2007a; Kurtoglu et al, 2007b]. Thus, FDG might be involved in not only glycolytic inhibition but also in indirect inhibition of *N*-linked glycosylation.

Formation of F-gluconic acid requires spontaneous or enzymatic oxidation of FDG. Buriova et al (2001) showed formation of F-gluconic acid upon oxidation of FDG mediated by $\text{FeSO}_4(\text{NH}_4)_2\text{SO}_4 \cdot 6\text{H}_2\text{O}$ and H_2O_2 [Buriova et al, 2001]. In one of our experiments, we checked possibility of spontaneous oxidation of free FDG into F-gluconic acid during the solvent extraction process. Results showed that there is no formation of F-gluconic acid in the final extracts. This removes the possibility that F-gluconic acid originated as an artefact arising due to spontaneous oxidation process during the solvent extraction procedure. In such case, enzymatic dehydrogenation and spontaneous hydration seems to be plausible way to explain formation of F-gluconic acid. Glucose oxidase (enzyme: 1.1.3.4) or Glucose

dehydrogenase (EC 1.1.5.9) could convert glucose to glucono-lactone which upon enzymatic hydration by gluconolactonase (EC 3.1.1.17) can transform into gluconic acid [www.brenda-enzymes.org/enzyme.php?ecno=3.1.1.17]. However, none of the above enzymes have been reported in *Arabidopsis*. At this moment, we could not comment upon the plausible mechanism for biosynthesis of F-gluconic acid. Thus, we have noted both enzymatic and spontaneous oxidation processes as possible routes [Fig. 3].

Discovery of F-maltose was very interesting and surprising outcome. Cytosolic component of transitory starch breakdown pathway seems to be most the plausible mechanisms leading to F-maltose biosynthesis *in vivo*. Maltose metabolism in *Arabidopsis* depends upon a disproportionating enzyme and α -glucan phosphorylase [Lu et al, 2006]. In *Arabidopsis*, cytosolic maltose is mainly metabolized via glucosyltransfer reaction catalyzed by cytosolic glucosyltransferase disproportionating enzyme 2 (DPE2) (EC 2.4.1.25) which transfers one of the glucosyl units of maltose as free glucose and transfers the other to glycogen [Lu and Sharkey, 2004; Chia et al, 2004] or highly branched, soluble heteroglycan [Lu et al, 2006]. Reversibly, DPE2 is able to catalyze the transfer of a segment of a (1-4)- α -D-glucan to a new position in an acceptor, which may be glucose, a (1-4)- α -D-glucan [Kaper et al, 2004; Lin and Preiss, 1988; Lu and Sharkey, 2004; Lu et al, 2006; Steichen et al, 2008] or FDG [Tantanarat et al, 2012]. FDG could be converted into the F-maltose *in vitro* using DPE2-mediated trans-glycosylation reaction with glycogen acting as a glucosyl donor [Tantanarat et al, 2012]. We hypothesize that similar DPE2-mediated trans-glycosylation reaction mechanism must have been involved in biosynthesis of F-maltose.

We found UDP-FDG as the only nucleotide-FDG conjugates form in the plant extract. UDP-FDG and GDP-FDG biosynthesis has been reported in yeast and chick embryo cells [Schmidt et al, 1978]. Kanazawa et al (1997) showed that FDG-6-P is metabolized further to produce nucleotide bound form of FDG [Kanazawa et al, 1997]. As per the proposed biosynthesis of UDP-FDG biosynthesis occurs via FDG-1-P though we could not detect it. We might have failed to detect presence of FDG-1-P due to low abundance or low chromatographic separation between FDG-6-P and FDG-1-P. UDP-FDG acts as a glucosyl moiety donor in various biosynthetic pathways such as starch, anthocyanin or flavonoid biosynthesis etc. Considering UDP-FDG role in diverse pathways, it's hard to imagine which the possible biosynthetic compounds it leads to. We think that UDP-FDG may have been involved in biosynthesis of fluorinated anthocyanin [Ferrieri et al, 2012].

Deciphering “Why FDG metabolism is directed towards formation of above mentioned end products” is still our challenge. We think, FDG, upon intracellular uptake, will be considered as energy source by the cell and will be fluxed into glycolytic pathway leading to synthesis of FDG-6-P. However, all taken-up FDG could not be metabolized into FDG-6-P as building-up concentration of FDG-6-P inside the cell slow down this bio-transformation through feedback inhibition of hexokinase. FDG-6-P will actually become a catabolic block brining glycolysis to halt. This has already been shown in hypoxic animal tissue [Lampidis et al, 2006; Kurtoglu et al, 2007a]. This may lead to rest of the free FDG pushed into F-maltose or F-gluconic acid biosynthetic pathways [Fig. 3]. FDG-6-P may be further transformed into FDG-1-P and finally to UDP-FDG as depicted in Fig. 3. Formation of various fluorine-metabolites in plants can be a way of plants to cope up with high intracellular concentration of FDG which is known glycolytic inhibitor. Thus, biosynthesis of various fluorine-metabolites could also be viewed as utilization of FDG as energy source and a corrective-protective mechanism in the plant cells to counteract its consequences.

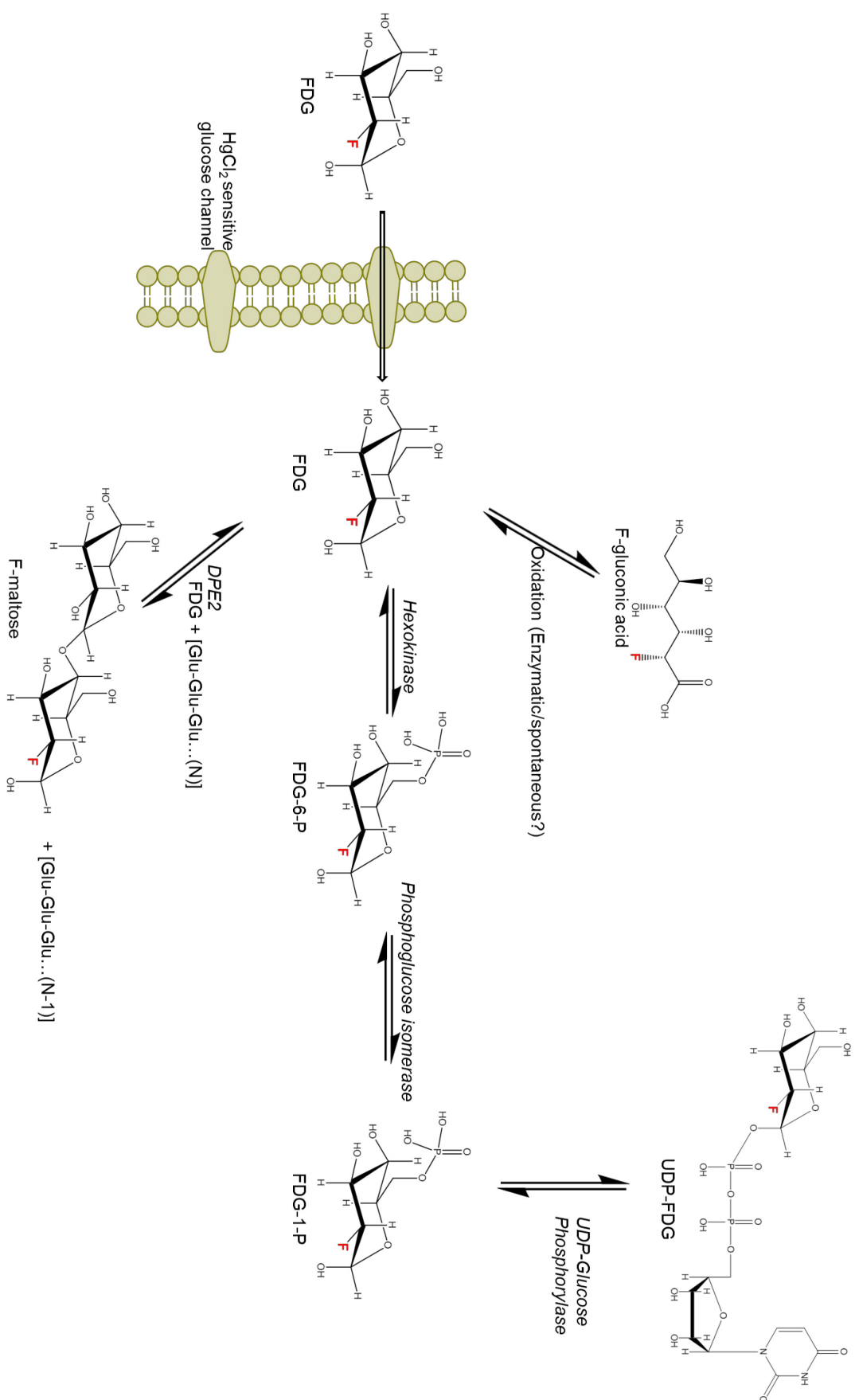


Figure 3. Schematic of the potential routes of FDG metabolism in plant cell. FDG, 2-fluoro-2-deoxyglucose; FDG-6-P, 2-fluoro-2-deoxy-D-glucose-6-phosphate; FDG-1-P, 2-fluoro-2-deoxyglucose-1-phosphate; F-gluconic acid, 2-deoxy-2-fluorogluconic acid; UDP, Uridine-diphosphate; F-maltose, 2-deoxy-2-fluoromaltose; Glu, glucose; *DPE2*, *Arabidopsis* cytosolic glucosyltransferase disproportionating enzyme 2.

FDG to study carbon allocation in plants after herbivore attack

In previous chapters, we illustrated FDG imaging and metabolism in plants. We saw *in planta* incorporation of FDG into different metabolites and [^{18}F] radioactivity distribution which was similar to photoassimilates distribution. In this chapter we discuss how FDG could be used to study carbon allocation dynamics in plants after particular biotic/abiotic stresses, here exemplified in the case of herbivory.

Plant fitness to herbivory depends upon how plants respond to herbivore attack [Núñez-Farfán et al, 2007; Lankau RA, 2007; Schwachtje and Baldwin, 2008; Carmona and Farnoni, 2013]. Generalist herbivores induce the plant defense pathways in which primary resources are directed towards production of toxic or deterrent secondary metabolites [Heil and Baldwin, 2002; Zavala and Baldwin, 2006; Schwachtje and Baldwin, 2008; Bolton MD, 2009; Ferrieri et al, 2013]. Induction of secondary defense pathways are costly and result in low fitness however they help survive the plant from extensive damage due to herbivory [Redman et al, 2001; Heil and Baldwin, 2002; Halitschke and Baldwin, 2003; Schwachtje and Baldwin, 2008; Meldau et al, 2012]. On the other hand, specialist herbivores are well adapted to host-specific defense metabolites and could tolerate or even benefit from feeding on such host plants [Pasteels et al, 1983; Pentzold et al, 1995; Zagrobelny et al, 2007; Kumar et al, 2014]. In such case, plant strategy to tolerate the herbivory emerges as the best solution [Schwachtje and Baldwin, 2008]. Tolerance mechanism allows plant to relocate resources into protected tissue from which they can be re-claimed for regrowth at later stage [Dyer et al, 1991; Briske et al, 1996; Schwachtje et al., 2006; Gómez et al, 2010]. Specialist herbivore *M. sexta* feeding reconfigures carbon allocation dynamics in *Nicotiana* [Schwachtje et al., 2006; Hummel et al, 2007; Machado et al, 2013]. It's shown that upon herbivory, carbon allocation towards roots increased [Schwachtje et al, 2006] and however total carbohydrate pool in root remained constant or even depleted [Gómez et al, 2012; Machado et al, 2013]. These results were counterintuitive. In our observations, we have seen that significant fraction of recently assimilated carbon was translocated to roots however, simulated herbivory reduced the amount of carbon allocated to root tips. Our results explain how herbivory increased carbon allocation towards roots [Holland et al, 1996; Babst et al, 2005; Schwachtje et al, 2006; Gómez et al, 2012] but still reduction in root growth rate is observed [Hummel et al, 2007]. Upon herbivory, various defense pathways are induced. It leads to increased sink strength in roots assisting upregulated nicotine production in roots. Increased

carbon allocation towards roots may not be used for storage but rather utilized into production of secondary defense metabolites such as nicotine [Shoji et al, 2000; Machado et al, 2013]. This may also lead to utilization of previously existing carbohydrate pool leading to its depletion. Thus, we come to think that *Nicotiana* does not “bunker” carbon resources in root after leaves are attacked but rather that allocation within the root is altered.

Carbon allocation dynamics vary as per the plant species and how the damage is perceived [Schwachtje et al 2006; Quilliam et al, 2006]. For e.g. In *Arabidopsis* upon herbivory, carbon allocation towards damaged leaves is increased [Quilliam et al, 2006; Arnold and Schultz, 2002; Arnold et al, 2004]. Whereas in several other plants like *Zea mays* [Holland et al, 1996] or *Nicotiana* [Schwachtje et al, 2006; Babst et al, 2005; Gómez et al, 2010; Holland et al, 1996], recently allocated carbon is directed towards roots. Plants perceive damage caused by wounding different than that caused by larval infestation. Leaf wounding increases JA levels which, in turn, stimulate root nicotine synthesis [Baldwin et al, 1997]. Leaf damage caused by mechanical wounding will be compensated by increased branching [Schwachtje et al, 2006] and increased photosynthetic activity in other leaves [Nowak and Caldwell, 1984; Quillum et al, 2006; Schwachtje and Baldwin, 2008]. Mechanical damage also increases sink strength in the vicinity of damaged tissue [Quillum et al, 2006]. Whereas leaf damage caused by herbivory will be perceived differently and result in induction of JA-mediated defense pathways which in turn suppresses regrowth and contribute to apical dominance [Zavala and Baldwin, 2006]. It appears that JA signaling is involved in regulation of resource allocation to growing parts. In *Nicotiana*, application of Fatty acid-amino acid conjugates (FACs) resulted in 10% more photoassimilate being partitioned to roots independent of JA signalling [Schwachtje et al, 2006]. This response is mediated via a β -subunit of an SNF1-related kinase, GAL83, which is induced via herbivore specific elicitors. SNF1-related kinase has been shown to regulate root–shoot partitioning of carbohydrates after herbivore attack independently of JA signaling. Schwachtje et al (2006) showed that just wounding reduced the carbon allocation to roots but wounding of sink-leaves increased carbon allocation to roots. This is somewhat contrary to what we observed. Our observations suggested that in wild type plants, resource allocation towards roots increased after leaf wounding treatment. Simulated herbivory also increased resource allocation towards roots but at the same time reduced carbon translocated to root meristems. However, in JA-insensitive *irCOII* plant, we observed that carbon allocation to roots is decreased significantly only in leaf wounding treatment but not in simulated herbivory. COII is a key player in controlling processes

downstream of JA biosynthesis. *irCOII* plants accumulate 75% less JA compared with wild-type plants upon wounding and oral secretion treatment [Paschold et al, 2008]. However, COII is also involved in regulatory feedback function to enhance JA-Ile turnover rate. Thus, *irCOII* plants accumulate higher and prolonged concentration of JA-Ile [Paschold et al, 2008]. JA-Ile has been demonstrated to be essential for herbivore-induced defense signaling in *Nicotiana* [Kang et al. 2006, Wang et al. 2008]. Thus, in *irCOII* plants, JA level decreases but JA-Ile level increases. This may have important consequences on cross-talk between JA and other phytohormones in regulating resource allocation.

Regulation of growth and resource allocation is mainly controlled by phytohormones. Role of JA in plant response to wounding and herbivory is well established, however, other compounds, such as systemin, oligosaccharides, and phytohormones such as auxins, cytokinin (CK), abscisic acid (ABA) and ethylene also play a role in wound signaling [Titarenko et al, 1997; León et al, 2000; Onkokesung et al, 2010]. Mechanical damage alone causes an increase in ABA which in turn activates biosynthesis of JA [Dammann et al, 1997]. Yang et al, (2012) proposed that cross talk between JA and gibberellic acid (GA) may reduce plant growth by interfering with the GA-mediated promotion of internode elongation [Yang et al, 2012]. Also, indole acetic acid (IAA) rapidly accumulates in the leaves and roots of herbivore-attacked *Nicotiana* plants and root auxin response was prolonged in JA deficient plant line [Machado et al, 2013]. Auxin maintains apical dominance and is supplied via shoot meristems. Herbivory could strongly influence the auxin from the shoot to the root system [Mcsteen et al, 2005] resulting in transient changes in auxin levels. It has been shown that external auxin applications changes herbivory-induced carbohydrate and re-growth patterns [Machado et al, 2013]. It has been proposed that auxins could act as a negative regulator of JA [Baldwin et al, 1997; Shi et al, 2006; Onkokesung et al, 2010] and play important role in plant tolerance against herbivory [Machado et al, 2013].

Auxin acts in concert with cytokinins to regulate plant growth. It's shown that leaf miners and gall forming insects, modulate plant CK levels to autumnal formation of 'green islands' presumably to attract primary resources [Larson and Whitham, 1991; Giron et al, 2007; Bartlett and Connor, 2014]. In *Nicotiana*, CK-related genes strongly regulated by FACs elicitors [Hui et al, 2003; Gilardoni et al, 2010], suggesting that JA-CK cross-talk in defense mediated pathways induction. Cytokinins have been shown to play profound roles in stress-induced growth responses [Argueso et al, 2009] and regulate root growth and development

Discussion

[Dello et al, 2008; Werner et al, 2003]. Along with JA, various phytohormones such as auxin, CK, ABA etc also play critical role in growth regulation and biotic stress response. Thus, carbon allocation and growth response in stress treatment may be a result of complex interplay between various phytohormones in co-ordination with the JA signaling.

Summary

The aim of this thesis is to explore and expand applications of FDG in plant imaging. FDG is a structural glucose analog and has been routinely used in clinical, diagnostic or animal studies to trace glucose metabolism. However, established FDG applications in animal imaging could not be directly extrapolated to plant imaging. FDG application in plant imaging necessitates successful radiotracer kinetics model which involves establishing FDG translocation in plants and unravelling underlying biochemistry which explains the observed radioactivity distribution pattern. In present work, I analyzed FDG translocation and elucidated FDG metabolism in model plant species *Arabidopsis*. In collaboration with Dr. Meldau, I demonstrated that FDG could be employed as radiotracer to study carbon allocation in *Nicotiana* upon herbivory.

Plants photosynthesize sugars and transport them as photoassimilates. In previous studies, [^{18}F] radioactivity distribution upon FDG feeding was found similar to photoassimilates distribution pattern in plants. Thus, it was proposed that FDG could be used as a tracer for photoassimilates. However, the question remained- whether the observed [^{18}F] radioactivity pattern is an outcome of chemical nature of radiotracer, of plant vasculature or the way in which radiotracer was applied to plants. I compared radioactivity distribution pattern of two chemical distinct radiotracers, viz. FDG and Ga-citrate. I showed that the resultant [^{18}F] and [^{68}Ga] radioactivity patterns were significantly different. Thus, chemical nature of the radiotracer played important role in determining its distribution and not the plant vasculature. Vasculature affected the [^{18}F] radioactivity distribution to some extent but not the overall distribution pattern. [^{18}F] radioactivity distribution pattern was similar to photoassimilates and [^{18}F] radioactivity was translocated exclusively via phloem. Observed [^{18}F] translocation and distribution pattern was consistent with the hypothesis that FDG could be used as radiotracer for photoassimilates distribution.

I analyzed FDG metabolism in *Arabidopsis* to unravel underlying biochemical pathways. FDG metabolism in plant cells is not well characterized till yet. Plants are photoautotrophs and specialist in sugar metabolism. Due to inherent physiological differences, FDG metabolism in plant cells can be very different than animal cells. To elucidate FDG metabolism in plant cells, I fed ^{19}F FDG, a non-radioactive form of FDG, to leaf tissue and analyzed polar extract using LCMS and NMR. On the basis of exact mono-isotopic masses, MS/MS fragmentation, and NMR data; I identified F-gluconic acid, FDG-6-P, F-maltose, and

UDP-FDG as four major end products of FDG metabolism. In plants, glycolysis and starch degradation pathway seems to be the important pathways for FDG metabolism. FDG was taken up by the cells via HgCl_2 -sensitive passive uptake process similar to that of glucose. It was directed into glycolysis via hexokinase leading to formation of FDG-6-P. However, FDG-6-P is not preferred substrate for subsequent enzymatic steps and known to accumulate inside the cell. Fraction of FDG-6-P further transformed into UDP-FDG presumably via FDG-1-P as an intermediate. Formation of UDP-FDG hints towards possible incorporation of FDG into starch or other glycosylated molecules like anthocyanins. High FDG-6-P concentration is known to inhibit hexokinase activity via feedback inhibition. Thus, fraction of FDG may be directed into formation of F-gluconic acid via enzymatic or spontaneous oxidation and into F-maltose via DPE2 mediated catalysis. FDG metabolism in plants goes beyond FDG-6-P and it is considerably different than animal cells.

Being a PET-radiotracer, FDG could be used in *in vivo* imaging. However, the scope of potential applications of FDG has not been fully explored. In collaboration with Dr. Meldau, I have exemplified how FDG could be used to study carbon allocation in *Nicotiana* upon herbivory. We fed FDG to *Nicotiana* and analyzed systemic tracer allocation using imaging plates. We observed that herbivory increased carbon allocation towards below ground parts such as roots but away from growing parts such as root tips. It matched with the previous literature that *Nicotiana* directs resources away from the damaged parts and these directed resources are most likely to be used in production of defense compounds and not in growth. Experiments with JA-insensitive *irCOII* plant showed that the resultant carbon allocation is dependent upon JA which may be acting in co-ordination with other phytohormones to regulate plant defense response and plant growth.

In conclusion, my thesis provides a basic foundation for establishing FDG as a radiotracer for plant imaging and presents a methodology to trace carbon allocation in plant using FDG. I hope this work will generate interest in wide range of scientists to employ FDG to analyze carbon allocation dynamics in plants *in vivo* and to explore new novel applications of FDG in plant imaging.

Zusammenfassung

Das Ziel dieser Arbeit war Anwendungen von FDG für das Imaging von Pflanzen zu untersuchen. FDG ist ein strukturelles Analogon zur Glucose und wird routinemäßig in klinischen und diagnostischen Studien sowie in Tierversuchen eingesetzt, um den Glucosestoffwechsel zu untersuchen. Diese Ansätze sind jedoch nicht auf den pflanzlichen Metabolismus übertragbar. Stattdessen ist es erforderlich erfolgreiche kinetische Modelle für radioaktive Tracerverbindungen durch Aufklärung der Translokation von FDG in Pflanzen und der zugrundeliegenden Biochemie zu erschließen. In der vorliegenden Arbeit untersuchte ich am Modellorganismus *Arabidopsis thaliana* die Translokation von FDG und klärte dessen Stoffwechsel auf. In Zusammenarbeit mit Dr. Meldau konnte ich zeigen, dass FDG als radioaktive Tracer dafür geeignet ist, die Kohlenstoffaufteilung in *Nicotiana* bei Fraßbefall zu analysieren.

Pflanzen sind in der Lage Zuckerverbindungen durch Photosynthese herzustellen und sie dann als Photoassimilate zu transportieren. In vorhergehenden Studien ähnelte die Verteilung der Radioaktivität des [^{18}F]-Isotops nach Zuführung von [^{18}F]-markierten FDG dem Verteilungsmuster von Photoassimilaten in Pflanzen. Daher wurde angenommen, dass FDG als Tracer für Photoassimilate geeignet ist. Es blieb jedoch ungeklärt, ob der Aufbau des pflanzlichen Gefäßsystems, die chemischen Eigenschaften oder der Zuführungsweg des Tracers Einfluss auf die Radioaktivitätsverteilung nehmen. In dieser Arbeit habe ich das Verteilungsmuster der Radioaktivität von zwei chemisch verschiedenen Radiotracern, FDG und Ga-citrat, miteinander verglichen und zeigen können, dass sich die resultierenden Verteilungsmuster der [^{18}F]-Radioaktivität und der [^{68}Ga]-Radioaktivität signifikant voneinander unterscheiden. Daraus folgt, dass die chemische Eigenschaft des Radiotracers eine wichtige Rolle bei seiner Verteilung spielt und nicht das Gefäßsystem der Pflanze. Zwar hatte das Gefäßsystem bis zu einem gewissen Grad Einfluß auf die Verteilung der [^{18}F]-Radioaktivität, das gesamte Verteilungsmuster blieb jedoch gleich. Zudem stimmte die [^{18}F]-Radioaktivitätsverteilung mit der von Photoassimilaten überein und [^{18}F]-Translokation fand ausschließlich über das Phloem statt. Die beobachteten Ergebnisse bestätigen erneut die Hypothese, dass FDG als Radiotracer für die Verteilung von Photoassimilaten geeignet ist.

Da in der Literatur zum FDG-Metabolismus in Pflanzenzellen keine Informationen vorliegen, erfolgte seine Untersuchung in *Arabidopsis*. Nach Inkubation des Pflanzengewebes mit ^{19}F FDG wurden dessen polare Extrakte mittels LC-MS und NMR analysiert. So gelang es, F-

Gluconsäure, FDG-6-P, F-Maltose und UDP-FDG als die vier wesentlichen Endprodukte des FDG-Metabolismus zu identifizieren. Dies weist darauf hin, dass Glycolyse und Stärkeabbau die bedeutenden Stoffwechselwege bei der Metabolisierung von FDG sind. Zunächst wird FDG, ähnlich wie bei Glucose, über einen passiven HgCl_2 -empfindlichen Prozess in die Zellen aufgenommen. Via Hexokinase erfolgt anschließend die Einbindung in die Glykolyse, was zur Bildung von FDG-6-P führt. Dies reichert sich in der Zelle an, da FDG-6-P kein geeignetes Substrat für die nachfolgenden enzymatischen Schritte ist. Ein Teil des FDG-6-P wird weiter zu UDP-FDG umgewandelt, wahrscheinlich über FDG-1-P als Zwischenstufe. Die Bildung von UDP-FDG weist darauf hin, dass FDG in Stärke oder andere glykosilierte Verbindungen, wie zum Beispiel Anthocyane, eingebaut wird. Bei hohen FDG-6-P-Konzentrationen kommt es aufgrund von Rückkopplungseffekten zur Inhibierung von Hexokinase. Daher könnte es sein, dass ein Teil des FDGs, entweder durch spontane oder enzymatische Oxidation, zu F-Gluconsäure umgewandelt wird. Danach würde sich die DPE2-vermittelte Katalyse zu F-Maltose anschließen. Der Stoffwechsel von FDG in Pflanzen geht über FDG-6-P hinaus und unterscheidet sich daher beträchtlich von dem in tierischen Zellen.

Als Radiotracer könnte sich FDG auch für *in vivo* Imaging-Analysen eignen. Jedoch wurde die Bandbreite an potentiellen Anwendungen von FDG hierfür nicht vollständig erforscht. In Zusammenarbeit mit Dr. Meldau konnte ich veranschaulichen wie FDG dafür eingesetzt werden kann, die Kohlenstoffaufteilung in *Nicotiana* bei Fraßbefall zu analysieren. Nach Zugabe von FDG zu *Nicotiana* untersuchten wir die systemische Verteilung des Tracers mittels Imaging-Bildplatten. Dabei beobachteten wir, dass bei Fraßbefall Kohlenstoffverbindungen an unter der Erde befindliche Pflanzenbereiche z.B. Wurzeln zugeführt und von wachsendem Gewebe z.B. Wurzelspitzen abgezogen wird. Diese Ergebnisse stimmen mit der bestehenden Literatur überein, der zufolge *Nicotiana* die Ressourcen aus verletzten Bereichen abzieht, um sie höchstwahrscheinlich für die Produktion von Abwehrstoffen einzusetzen und nicht für Wachstum. Experimente mit der JA-unempfindlichen *irCOII*-Pflanze ergaben, dass die Kohlenstoffverteilung von JA abhängt, welche womöglich in Koordination mit anderen Phytohormonen die Verteidigungsreaktionen und das Pflanzenwachstum regulieren.

Meine Arbeit liefert daher eine Grundlage für Etablierung von FDG als Radiotracer für das Imaging von Pflanzen und bietet eine Methodik um die Kohlenstoffverteilung mittels FDG zu

verfolgen. Ich hoffe dass, diese Arbeit das Interesse von verschiedenen Wissenschaftlern weckt, die Dynamiken der Kohlenstoffverteilung in Pflanzen mittels FDG *in vivo* zu untersuchen und neuartige Anwendungsgebiete von FDG für das Imaging von Pflanzen zu finden.

References

- [1] Alavi A, Reivich M, Jones S, Greenberg J, and Wolf A. Functional imaging of the brain with positron emission tomography. *Nuclear medicine annual* 1982; 1982.
- [2] Argueso CT, Ferreira FJ, and Kieber JJ. Environmental perception avenues: the interaction of cytokinin and environmental response pathways. *Plant, cell & environment* 2009;32:1147-60.
- [3] Arnold T, Appel H, Patel V, Stocum E, Kavalier A, and Schultz J. Carbohydrate translocation determines the phenolic content of *Populus* foliage: a test of the sink–source model of plant defense. *New Phytologist* 2004;164:157-64.
- [4] Arnold TM and Schultz JC. Induced sink strength as a prerequisite for induced tannin biosynthesis in developing leaves of *Populus*. *Oecologia* 2002;130:585-93.
- [5] Babst BA, Ferrieri RA, Gray DW, Lerdau M, Schlyer DJ, Schueller M, et al. Jasmonic acid induces rapid changes in carbon transport and partitioning in *Populus*. *New Phytologist* 2005;167:63-72.
- [6] Babst BA, Karve AA, and Judt T. Radio-metabolite analysis of carbon-11 biochemical partitioning to non-structural carbohydrates for integrated metabolism and transport studies. *Plant and Cell Physiology* 2013;54:1016-25.
- [7] Baldwin IT, Zhang Z-P, Diab N, Ohnmeiss TE, McCloud ES, Lynds GY, et al. Quantification, correlations and manipulations of wound-induced changes in jasmonic acid and nicotine in *Nicotiana sylvestris*. *Planta* 1997;201:397-404.
- [8] Barrio J, Huang S, Melega W, Yu D, Hoffman J, Schneider J, et al. 6-[18F] Fluoro-L-DOPA probes dopamine turnover rates in central dopaminergic structures. *Journal of neuroscience research* 1990;27:487-93.
- [9] Barrio JR, Satyamurthy N, Huang S-C, Keen RE, Nissenson CH, Hoffman JM, et al. 3-(2'-[18 F] fluoroethyl) spiperone: in vivo biochemical and kinetic characterization in rodents, nonhuman primates, and humans. *Journal of Cerebral Blood Flow & Metabolism* 1989;9:830-9.
- [10] Bartlett L and Connor EF. Exogenous phytohormones and the induction of plant galls by insects. *Arthropod-Plant Interactions* 2014:1-10.
- [11] Bessell E, Foster A, and Westwood J. The use of deoxyfluoro-D-glucopyranoses and related compounds in a study of yeast hexokinase specificity. *Biochemical Journal* 1972;128:199.
- [12] Bessell EM and Thomas P. The effect of substitution at C-2 of d-glucose 6-phosphate on the rate of dehydrogenation by glucose 6-phosphate dehydrogenase (from yeast and from rat liver). *Biochemical Journal* 1973;131:83.

References

- [13] Bolton MD. Primary metabolism and plant defense-fuel for the fire. *Molecular Plant-Microbe Interactions* 2009;22:487-97.
- [14] Borisjuk L, Rolletschek H, and Neuberger T. Surveying the plant's world by magnetic resonance imaging. *The Plant Journal* 2012;70:129-46.
- [15] Bouny JM and Saglio PH. Glycolytic flux and hexokinase activities in anoxic maize root tips acclimated by hypoxic pretreatment. *Plant Physiology* 1996;111:187-94.
- [16] Boyes DC, Zayed AM, Ascenzi R, McCaskill AJ, Hoffman NE, Davis KR, et al. Growth stage-based phenotypic analysis of Arabidopsis a model for high throughput functional genomics in plants. *The Plant Cell Online* 2001;13:1499-510.
- [17] Briske D, Boutton T, and Wang Z. Contribution of flexible allocation priorities to herbivory tolerance in C4 perennial grasses: an evaluation with ¹³C labeling. *Oecologia* 1996;105:151-9.
- [18] Brown RS, Leung JY, Kison PV, Zasadny KR, Flint A, and Wahl RL. Glucose transporters and FDG uptake in untreated primary human non-small cell lung cancer. *Journal of Nuclear Medicine* 1999;40:556-65.
- [19] Buriova E, Medová M, Macášek F, and Brúder P. Separation and detection of oxidation products of fluorodeoxyglucose and glucose by high-performance liquid chromatography-electrospray ionisation mass spectrometry. *Journal of Chromatography A* 2004;1034:133-7.
- [20] Callos JD and Medford JI. Organ positions and pattern formation in the shoot apex. *The Plant Journal* 1994;6:1-7.
- [21] Carmona D and Fornoni J. Herbivores can select for mixed defensive strategies in plants. *New Phytologist* 2013;197:576-85.
- [22] Chia T, Thorneycroft D, Chapple A, Messerli G, Chen J, Zeeman SC, et al. A cytosolic glucosyltransferase is required for conversion of starch to sucrose in Arabidopsis leaves at night. *The Plant Journal* 2004;37:853-63.
- [23] Conde C, Silva P, Agasse A, Tavares RM, Delrot S, and Gerós H. An Hg-sensitive channel mediates the diffusional component of glucose transport in olive cells. *Biochimica et Biophysica Acta (BBA)-Biomembranes* 2007;1768:2801-11.
- [24] Conrad C, Fokt I, Hsu S, Lampidis T, Priebe W, and Szymanski S. Hexose Compounds to Treat Cancer. Google Patents; 2007.
- [25] Converse A, Ahlers E, Bryan T, Williams P, Barnhart T, Engle J, et al. Positron emission tomography (PET) of radiotracer uptake and distribution in living plants: methodological aspects. *Journal of Radioanalytical and Nuclear Chemistry* 2013;297:241-6.

References

- [26] Dammann C, Rojo E, and Sánchez-Serrano JJ. Absciscic acid and jasmonic acid activate wound-inducible genes in potato through separate, organ-specific signal transduction pathways. *The Plant Journal* 1997;11:773-82.
- [27] Datema R, Schwarz R, and Jankowski A. Fluoroglucose-inhibition of protein glycosylation in vivo. Inhibition of mannose and glucose incorporation into lipid-linked oligosaccharides. *European journal of biochemistry/FEBS* 1980;109:331.
- [28] De Geyter N, Gholami A, Goormachtig S, and Goossens A. Transcriptional machineries in jasmonate-elicited plant secondary metabolism. *Trends in plant science* 2012;17:349-59.
- [29] De Schepper V, Bühler J, Thorpe M, Roeb G, Huber G, van Dusschoten D, et al. ¹¹C-PET imaging reveals transport dynamics and sectorial plasticity of oak phloem after girdling. *Frontiers in plant science* 2013;4.
- [30] Dello Ioio R, Linhares FS, and Sabatini S. Emerging role of cytokinin as a regulator of cellular differentiation. *Current opinion in plant biology* 2008;11:23-7.
- [31] Dhondt S, Vanhaeren H, Van Loo D, Cnudde V, and Inzé D. Plant structure visualization by high-resolution X-ray computed tomography. *Trends in plant science* 2010;15:419-22.
- [32] Dickson RE, Isebrands J, and Tomlinson PT. Distribution and metabolism of current photosynthate by single-flush northern red oak seedlings. *Tree physiology* 1990;7:65-77.
- [33] Dyer M, Acra M, Wang G, Coleman D, Freckman D, McNaughton S, et al. Source-sink carbon relations in two *Panicum coloratum* ecotypes in response to herbivory. *Ecology* 1991:1472-83.
- [34] Fatangare A, Gebhardt P, Saluz H, and Svatoš A. Comparing 2-[¹⁸F] fluoro-2-deoxy-D-glucose and [⁶⁸Ga] gallium-citrate translocation in *Arabidopsis thaliana*. *Nuclear medicine and biology* 2014;41:737-43.
- [35] Ferrieri A, Appel H, Ferrieri R, and Schultz J. Novel application of 2-[(¹⁸F)] fluoro-2-deoxy-D-glucose to study plant defenses. *Nuclear medicine and biology* 2012;39:1152.
- [36] Ferrieri AP, Agtuca B, Appel HM, Ferrieri RA, and Schultz JC. Temporal changes in allocation and partitioning of new carbon as ¹¹C elicited by simulated herbivory suggest that roots shape aboveground responses in *Arabidopsis*. *Plant physiology* 2013;161:692-704.
- [37] Finazzo SF, Davenport TL, and Schaffer B. Partitioning of photoassimilates in avocado (*Persea americana* Mill.) during flowering and fruit set. *Tree Physiology* 1994;14:153-64.
- [38] Fisher DB. Kinetics of C-14 translocation in soybean I. Kinetics in the stem. *Plant physiology* 1970;45:107-13.
- [39] Flore J and Layne DR. Photoassimilate production and distribution in cherry. *HortScience* 1999;34:1015-9.

References

- [40] Geiger DR, Saunders M, and Cataldo DA. Translocation and accumulation of translocate in the sugar beet petiole. *Plant physiology* 1969;44:1657-65.
- [41] Gilardoni PA, Schuck S, Jüngling R, Rotter B, Baldwin IT, and Bonaventure G. SuperSAGE analysis of the *Nicotiana attenuata* transcriptome after fatty acid-amino acid elicitation (FAC): identification of early mediators of insect responses. *BMC plant biology* 2010;10:66.
- [42] Giron D, Kaiser W, Imbault N, and Casas J. Cytokinin-mediated leaf manipulation by a leafminer caterpillar. *Biology letters* 2007;3:340-3.
- [43] Gómez S, Ferrieri RA, Schueller M, and Orians CM. Methyl jasmonate elicits rapid changes in carbon and nitrogen dynamics in tomato. *New Phytologist* 2010;188:835-44.
- [44] Gómez S, Steinbrenner AD, Osorio S, Schueller M, Ferrieri RA, Fernie AR, et al. From shoots to roots: transport and metabolic changes in tomato after simulated feeding by a specialist lepidopteran. *Entomologia Experimentalis et Applicata* 2012;144:101-11.
- [45] Gómez-Ariza J, Campo S, Rufat M, Estopà M, Messeguer J, Segundo BS, et al. Sucrose-mediated priming of plant defense responses and broad-spectrum disease resistance by overexpression of the maize pathogenesis-related PRms protein in rice plants. *Molecular plant-microbe interactions* 2007;20:832-42.
- [46] Halitschke R and Baldwin IT. Antisense LOX expression increases herbivore performance by decreasing defense responses and inhibiting growth-related transcriptional reorganization in *Nicotiana attenuata*. *The Plant Journal* 2003;36:794-807.
- [47] Haritatos E, Medville R, and Turgeon R. Minor vein structure and sugar transport in *Arabidopsis thaliana*. *Planta* 2000;211:105-11.
- [48] Hattori E, Uchida H, Harada N, Ohta M, Tsukada H, Hara Y, et al. Incorporation and translocation of 2-deoxy-2-[18F] fluoro-D-glucose in *Sorghum bicolor* (L.) Moench monitored using a planar positron imaging system. *Planta* 2008;227:1181-6.
- [49] Heidelberger C, Chaudhuri N, Danneberg P, Mooren D, Griesbach L, Duschinsky R, et al. Fluorinated pyrimidines, a new class of tumour-inhibitory compounds. 1957.
- [50] Heil M and Baldwin IT. Fitness costs of induced resistance: emerging experimental support for a slippery concept. *Trends in plant science* 2002;7:61-7.
- [51] Higashi T, Tamaki N, Torizuka T, Nakamoto Y, Sakahara H, Kimura T, et al. FDG Uptake, GLUT-i Glucose Transporter and Cellularity in Human Pancreatic Tumors. 1998.
- [52] Ho L. Fruit growth and sink strength. *Fruit and Seed Production. Aspects of Development, Environmental Physiology and Ecology* 1992:101-24.

References

- [53] Holland JN, Cheng W, and Crossley Jr D. Herbivore-induced changes in plant carbon allocation: assessment of below-ground C fluxes using carbon-14. *Oecologia* 1996;107:87-94.
- [54] Hui D, Iqbal J, Lehmann K, Gase K, Saluz HP, and Baldwin IT. Molecular Interactions between the Specialist Herbivore *Manduca sexta* (Lepidoptera, Sphingidae) and Its Natural Host *Nicotiana attenuata*: V. Microarray Analysis and Further Characterization of Large-Scale Changes in Herbivore-Induced mRNAs. *Plant physiology* 2003;131:1877-93.
- [55] Hummel GM, Naumann M, Schurr U, and Walter A. Root growth dynamics of *Nicotiana attenuata* seedlings are affected by simulated herbivore attack. *Plant, cell & environment* 2007;30:1326-36.
- [56] Jahnke S, Menzel MI, Van Dusschoten D, Roeb GW, Bühler J, Minwuyelet S, et al. Combined MRI–PET dissects dynamic changes in plant structures and functions. *The Plant Journal* 2009;59:634-44.
- [57] Jonik C, Sonnewald U, Hajirezaei MR, Flügge UI, and Ludewig F. Simultaneous boosting of source and sink capacities doubles tuber starch yield of potato plants. *Plant biotechnology journal* 2012;10:1088-98.
- [58] Kaarstad K, Bender D, Bentzen L, Munk OL, and Keiding S. Metabolic fate of 18F-FDG in mice bearing either SCCVII squamous cell carcinoma or C3H mammary carcinoma. *Journal of Nuclear Medicine* 2002;43:940-7.
- [59] Kanazawa Y, Momozono Y, Ishikawa M, Yamada T, Yamane H, Haradahira T, et al. Metabolic pathway of 2-deoxy-2-fluoro-D-glucose studied by F-19 NMR. *Life sciences* 1986;39:737-42.
- [60] Kanazawa Y, Umayahara K, Shimmura T, and Yamashita T. 19F NMR of 2-deoxy-2-fluoro-D-glucose for tumor diagnosis in mice. An NDP-bound hexose analog as a new NMR target for imaging. *NMR in Biomedicine* 1997;10:35-41.
- [61] Kanazawa Y, Yamane H, Shinohara S, Kuribayashi S, Momozono Y, Yamato Y, et al. 2-Deoxy-2-Fluoro-d-Glucose as a Functional Probe for NMR: The Unique Metabolism Beyond Its 6-Phosphate. *Journal of neurochemistry* 1996;66:2113-20.
- [62] Kang J-H, Wang L, Giri A, and Baldwin IT. Silencing threonine deaminase and JAR4 in *Nicotiana attenuata* impairs jasmonic acid–isoleucine–mediated defenses against *Manduca sexta*. *The Plant Cell Online* 2006;18:3303-20.
- [63] Kaper T, van der Maarel M, Euverink G, and Dijkhuizen L. Exploring and exploiting starch-modifying amylomaltases from thermophiles. *Biochemical Society Transactions* 2004;32:279-82.
- [64] Kiser MR, Reid CD, Crowell AS, Phillips RP, and Howell CR. Exploring the transport of plant metabolites using positron emitting radiotracers. *HFSP journal* 2008;2:189-204.

References

- [65] Kojima M, Kuribayashi S, Kanazawa Y, Haradahira T, Maehara Y, and Endo H. Metabolic pathway of 2-deoxy-2-fluoro-D-glucose and 2-deoxy-2-fluoro-D-mannose in mice bearing sarcoma 180 studied by fluorin-19 nuclear magnetic resonance. *Chemical & pharmaceutical bulletin* 1988;36:1194.
- [66] Kumar P, Rath P, Schöttner M, Baldwin IT, and Pandit S. Differences in Nicotine Metabolism of Two *Nicotiana attenuata* Herbivores Render Them Differentially Susceptible to a Common Native Predator. *PloS one* 2014;9:e95982.
- [67] Kume T, Matsushashi S, Shimazu M, Ito H, Fujimura T, Adachi K, et al. Uptake and transport of positron-emitting tracer (^{18}F) in plants. *Applied radiation and isotopes* 1997;48:1035-43.
- [68] Kurtoglu M, Gao N, Shang J, Maher JC, Lehrman MA, Wangpaichitr M, et al. Under normoxia, 2-deoxy-D-glucose elicits cell death in select tumor types not by inhibition of glycolysis but by interfering with N-linked glycosylation. *Molecular cancer therapeutics* 2007;6:3049-58.
- [69] Kurtoglu M, Maher JC, and Lampidis TJ. Differential toxic mechanisms of 2-deoxy-D-glucose versus 2-fluorodeoxy-D-glucose in hypoxic and normoxic tumor cells. *Antioxidants & redox signaling* 2007;9:1383-90.
- [70] la Fuente D, Gertrudis AS, Villar-Palasi C, and Asensio C. Substrate specificity and some other properties of baker's yeast hexokinase. *Biochimica et biophysica acta* 1958;30:92-101.
- [71] Lampidis TJ, Kurtoglu M, Maher JC, Liu H, Krishan A, Sheft V, et al. Efficacy of 2-halogen substituted D-glucose analogs in blocking glycolysis and killing "hypoxic tumor cells". *Cancer chemotherapy and pharmacology* 2006;58:725-34.
- [72] Lankau RA. Specialist and generalist herbivores exert opposing selection on a chemical defense. *New phytologist* 2007;175:176-84.
- [73] Larson KC and Whitham TG. Manipulation of food resources by a gall-forming aphid: the physiology of sink-source interactions. *Oecologia* 1991;88:15-21.
- [74] Lemoine R, La Camera S, Atanassova R, Dédaldéchamp F, Allario T, Pourtau N, et al. Source-to-sink transport of sugar and regulation by environmental factors. *Frontiers in plant science* 2013;4.
- [75] León J, Rojo E, and Sánchez-Serrano JJ. Wound signalling in plants. *Journal of Experimental Botany* 2001;52:1-9.
- [76] Lin T-P and Preiss J. Characterization of D-enzyme (4- α -glucanotransferase) in *Arabidopsis* leaf. *Plant physiology* 1988;86:260-5.
- [77] Lu Y and Sharkey TD. The role of amylomaltase in maltose metabolism in the cytosol of photosynthetic cells. *Planta* 2004;218:466-73.

References

- [78] Lu Y, Steichen JM, Yao J, and Sharkey TD. The role of cytosolic α -glucan phosphorylase in maltose metabolism and the comparison of amylomaltase in *Arabidopsis* and *Escherichia coli*. *Plant physiology* 2006;142:878-89.
- [79] Lu Y, Watanabe A, and Kimura M. Input and distribution of photosynthesized carbon in a flooded rice soil. *Global biogeochemical cycles* 2002;16:32-1--8.
- [80] Machado de Domenech EE and Sols A. Specificity of hexokinases towards some uncommon substrates and inhibitors. *FEBS letters* 1980;119:174-6.
- [81] Machado RA, Ferrieri AP, Robert CA, Glauser G, Kallenbach M, Baldwin IT, et al. Leaf-herbivore attack reduces carbon reserves and regrowth from the roots via jasmonate and auxin signaling. *New Phytologist* 2013;200:1234-46.
- [82] Margolis HA, Delaney S, Vézina L-P, and Bellefleur P. The partitioning of ^{14}C between growth and differentiation within stem-deformed and healthy black spruce seedlings. *Canadian journal of botany* 1991;69:1225-31.
- [83] Marín-Hernández A, Rodríguez-Enríquez S, Vital-González PA, Flores-Rodríguez FL, Macías-Silva M, Sosa-Garrocho M, et al. Determining and understanding the control of glycolysis in fast-growth tumor cells. *FEBS Journal* 2006;273:1975-88.
- [84] Matsushashi S, Fujimaki S, Uchida H, Ishioka NS, and Kume T. A new visualization technique for the study of the accumulation of photoassimilates in wheat grains using $[^{14}\text{C}] \text{CO}_2$. *Applied radiation and isotopes* 2006;64:435-40.
- [85] Matwiyoff N and Ott D. Stable isotope tracers in the life sciences and medicine. *Science* 1973;181:1125-33.
- [86] McSheehy PM, Leach MO, Judson IR, and Griffiths JR. Metabolites of 2'-fluoro-2'-deoxy-D-glucose detected by ^{19}F magnetic resonance spectroscopy in vivo predict response of murine RIF-1 tumors to 5-fluorouracil. *Cancer research* 2000;60:2122-7.
- [87] McSteen P and Leyser O. Shoot branching. *Annu. Rev. Plant Biol.* 2005;56:353-74.
- [88] Meldau S, Ullman-Zeunert L, Govind G, Bartram S, and Baldwin IT. MAPK-dependent JA and SA signalling in *Nicotiana attenuata* affects plant growth and fitness during competition with conspecifics. *BMC plant biology* 2012;12:213.
- [89] Miller A and Kiney C. Metabolism of $[^{14}\text{C}]$ fluorodeoxyglucose by rat brain in vivo. *Life sciences* 1981;28:2071.
- [90] Minchin P and GRUSAK MA. Continuous in vivo measurement of carbon partitioning within whole plants. *Journal of experimental botany* 1988;39:561-71.

References

- [91] Minchin P and Thorpe M. What determines carbon partitioning between competing sinks? *Journal of Experimental Botany* 1996;47:1293-6.
- [92] Moorby J, Ebert M, and Evans N. The translocation of ^{11}C -labelled photosynthate in the soybean. *Journal of Experimental Botany* 1963;14:210-20.
- [93] Murillo I, Roca R, Bortolotti C, and Segundo BS. Engineering photoassimilate partitioning in tobacco plants improves growth and productivity and provides pathogen resistance. *The Plant Journal* 2003;36:330-41.
- [94] Muzi M, Freeman SD, Burrows RC, Wiseman RW, Link JM, Krohn KA, et al. Kinetic characterization of hexokinase isoenzymes from glioma cells: implications for FDG imaging of human brain tumors. *Nuclear medicine and biology* 2001;28:107-16.
- [95] Myers W. Georg Charles de Hevesy: the father of nuclear medicine. *Journal of nuclear medicine: official publication, Society of Nuclear Medicine* 1979;20:590.
- [96] Nour-Eldin HH and Halkier BA. The emerging field of transport engineering of plant specialized metabolites. *Current opinion in biotechnology* 2013;24:263-70.
- [97] Nowak R and Caldwell M. A test of compensatory photosynthesis in the field: implications for herbivory tolerance. *Oecologia* 1984;61:311-8.
- [98] Núñez-Farfán J, Fornoni J, and Valverde PL. The evolution of resistance and tolerance to herbivores. *Annual Review of Ecology, Evolution, and Systematics* 2007:541-66.
- [99] O'Connell T and London R. Identification of 2-fluoro-2-deoxy-D-glucose metabolites by ^{19}F (1H) hetero-RELAY. *Journal of magnetic resonance. Series B* 1995;109:264.
- [100] Onkokesung N, Gális I, von Dahl CC, Matsuoka K, Saluz H-P, and Baldwin IT. Jasmonic acid and ethylene modulate local responses to wounding and simulated herbivory in *Nicotiana attenuata* leaves. *Plant physiology* 2010;153:785-98.
- [101] Osorio S, Ruan Y-L, and Fernie AR. An update on source-to-sink carbon partitioning in tomato. *Frontiers in plant science* 2014;5.
- [102] Pandey M, Srivastava AK, D'Souza SF, and Penna S. Thiourea, a ROS scavenger, regulates source-to-sink relationship to enhance crop yield and oil content in *Brassica juncea* (L.). *PloS one* 2013;8:e73921.
- [103] Partelová D, Uhrovčík J, Lesný J, Horník M, Rajec P, Kováč P, et al. Application of positron emission tomography and 2- ^{18}F fluoro-2-deoxy-D-glucose for visualization and quantification of solute transport in plant tissues. *Chemical Papers* 2014;68:1463-73.

References

- [104] Paschold A, Bonaventure G, Kant MR, and Baldwin IT. Jasmonate perception regulates jasmonate biosynthesis and JA-Ile metabolism: the case of COI1 in *Nicotiana attenuata*. *Plant and cell physiology* 2008;49:1165-75.
- [105] Paschold A, Halitschke R, and Baldwin IT. Co (i)-ordinating defenses: NaCOI1 mediates herbivore-induced resistance in *Nicotiana attenuata* and reveals the role of herbivore movement in avoiding defenses. *The Plant Journal* 2007;51:79-91.
- [106] Pasteels JM, ROWELL-RAHIER M, Braekman JC, and Dupont A. Salicin from host plant as precursor of salicylaldehyde in defensive secretion of chrysomeline larvae. *Physiological Entomology* 1983;8:307-14.
- [107] Pentzold S, Zagrobelny M, Rook F, and Bak S. How insects overcome two-component plant chemical defence: plant β -glucosidases as the main target for herbivore adaptation. *Biological Reviews* 2013.
- [108] Phelps ME. PET: molecular imaging and its biological applications: Springer, 2004.
- [109] Pouremad R and Wyrwicz AM. Cerebral metabolism of fluorodeoxyglucose measured with ^{19}F NMR spectroscopy. *NMR in biomedicine* 1991;4:161-6.
- [110] Printz RL, Magnuson MA, and Granner DK. Mammalian glucokinase. *Annual review of nutrition* 1993;13:463-96.
- [111] Quilliam RS, Swarbrick PJ, Scholes JD, and Rolfe SA. Imaging photosynthesis in wounded leaves of *Arabidopsis thaliana*. *Journal of experimental botany* 2006;57:55-69.
- [112] Redman AM, Cipollini Jr DF, and Schultz JC. Fitness costs of jasmonic acid-induced defense in tomato, *Lycopersicon esculentum*. *Oecologia* 2001;126:380-5.
- [113] Reivich M, Alavi A, Wolf A, Fowler J, Russell J, Arnett C, et al. Glucose metabolic rate kinetic model parameter determination in humans: the lumped constants and rate constants for ^{18}F fluorodeoxyglucose and ^{11}C deoxyglucose. *Journal of Cerebral Blood Flow & Metabolism* 1985;5:179-92.
- [114] Ruan Y-L, Patrick JW, Shabala S, and Slewinski TL. Uptake and regulation of resource allocation for optimal plant performance and adaptation to stress. *Frontiers in plant science* 2013;4.
- [115] Sanchez-Crespo A, Andreo P, and Larsson SA. Positron flight in human tissues and its influence on PET image spatial resolution. *European journal of nuclear medicine and molecular imaging* 2004;31:44-51.
- [116] Schieferstein H and Ross TL. ^{18}F -labeled folic acid derivatives for imaging of the folate receptor via positron emission tomography. *Journal of Labelled Compounds and Radiopharmaceuticals* 2013;56:432-40.
- [117] Schmidt M, Biely P, Krátký Z, and Schwarz R. Metabolism of 2-deoxy-2-fluoro-D-[^3H] glucose and 2-deoxy-2-fluoro-D-[^3H] mannose in yeast and chick-embryo cells. *European journal of biochemistry/FEBS* 1978;87:55.

References

- [118] Schwachtje J and Baldwin IT. Why does herbivore attack reconfigure primary metabolism? *Plant Physiology* 2008;146:845-51.
- [119] Schwachtje J, Minchin PE, Jahnke S, van Dongen JT, Schittko U, and Baldwin IT. SNF1-related kinases allow plants to tolerate herbivory by allocating carbon to roots. *Proceedings of the National Academy of Sciences* 2006;103:12935-40.
- [120] Shi Q, Li C, and Zhang F. Nicotine synthesis in *Nicotiana tabacum* L. induced by mechanical wounding is regulated by auxin. *Journal of experimental botany* 2006;57:2899-907.
- [121] Shoji T, Yamada Y, and Hashimoto T. Jasmonate induction of putrescine N-methyltransferase genes in the root of *Nicotiana sylvestris*. *Plant and Cell Physiology* 2000;41:831-9.
- [122] Smith T. The rate-limiting step for tumor [18F] fluoro-2-deoxy-D-glucose (FDG) incorporation. *Nuclear medicine and biology* 2001;28:1.
- [123] Sols A and Crane RK. Substrate specificity of brain hexokinase. *Journal of Biological Chemistry* 1954;210:581-95.
- [124] Som P, Ansari A, Atkins H, Casella V, Fowler J, Gallagher B, et al. Biodistribution in normal and tumor bearing animals of F-18-2-deoxy-2-fluoro-D-glucose (F-18-DG)- new agent for measuring myocardial glucose-transport and metabolism. *J Nucl Med* 1977: p. 618.
- [125] Som P, Atkins H, Bandoypadhyay D, Fowler J, MacGregor R, Matsui K, et al. A fluorinated glucose analog, 2-fluoro-2-deoxy-D-glucose (F-18): nontoxic tracer for rapid tumor detection. *J Nucl Med* 1980;21:670-5.
- [126] Southworth R, Parry CR, Parkes HG, Medina RA, and Garlick PB. Tissue-specific differences in 2-fluoro-2-deoxyglucose metabolism beyond FDG-6-P: a ¹⁹F NMR spectroscopy study in the rat. *NMR in Biomedicine* 2003;16:494-502.
- [127] Steichen JM, Petty RV, and Sharkey TD. Domain characterization of a 4- α -glucanotransferase essential for maltose metabolism in photosynthetic leaves. *Journal of Biological Chemistry* 2008;283:20797-804.
- [128] Steppuhn A and Baldwin IT. Resistance management in a native plant: nicotine prevents herbivores from compensating for plant protease inhibitors. *Ecology Letters* 2007;10:499-511.
- [129] Suolinna E, Haaparanta M, Paul R, Härkönen P, Solin O, and Sipilä H. Metabolism of 2-[18F] fluoro-2-deoxyglucose in tumor-bearing rats: chromatographic and enzymatic studies. *International journal of radiation applications and instrumentation. Part B, Nuclear medicine and biology* 1986;13:577.
- [130] Tantanarat K, Rejzek M, O'Neill E, Ruzanski C, Hill L, Fairhurst SA, et al. An expedient enzymatic route to isomeric 2-, 3-and 6-monodeoxy-monofluoro-maltose derivatives. *Carbohydrate research* 2012;358:12-8.

References

- [131] Thorpe M and Minchin P. Continuous monitoring of fluxes of photoassimilate in leaves and whole plants. *Journal of experimental botany* 1991;42:461-8.
- [132] Thorpe M, Walsh K, and Minchin P. Photoassimilate partitioning in nodulated soybean I. ¹¹C methodology. *Journal of experimental botany* 1998;49:1805-15.
- [133] Thorpe MR, Ferrieri AP, Herth MM, and Ferrieri RA. ¹¹C-imaging: methyl jasmonate moves in both phloem and xylem, promotes transport of jasmonate, and of photoassimilate even after proton transport is decoupled. *Planta* 2007;226:541-51.
- [134] Titarenko E, Rojo E, Leon J, and Sanchez-Serrano JJ. Jasmonic acid-dependent and-independent signaling pathways control wound-induced gene activation in *Arabidopsis thaliana*. *Plant Physiology* 1997;115:817-26.
- [135] Tsuji A UH, Yamashita T, Matsuhashi S, Ito T, Mizuniwa C, Ishioka NS, Watanabe S, Sekine T. Uptake of ¹⁸F¹⁸FDG and ¹³N¹³NO₃⁻ in tomato plants. In: TIARA Annu Rep 2001. Japan: Japan Atomic Energy Research Institute, 2002;035:103-4.
- [136] Turgeon R. The sink-source transition in leaves. *Annual review of plant biology* 1989;40:119-38.
- [137] Uchida H, Okamoto T, Ohmura T, Shimizu K, Satoh N, Koike T, et al. A compact planar positron imaging system. *Nuclear Instruments and Methods in Physics Research Section A: Accelerators, Spectrometers, Detectors and Associated Equipment* 2004;516:564-74.
- [138] Ung YC, Maziak DE, Vanderveen JA, Smith CA, Gulenchyn K, Lacchetti C, et al. ¹⁸F-fluorodeoxyglucose positron emission tomography in the diagnosis and staging of lung cancer: a systematic review. *Journal of the National Cancer Institute* 2007;99:1753-67.
- [139] Van Camp W. Yield enhancement genes: seeds for growth. *Current opinion in biotechnology* 2005;16:147-53.
- [140] Wang L, Allmann S, Wu J, and Baldwin IT. Comparisons of LIPOXYGENASE3-and JASMONATE-RESISTANT4/6-silenced plants reveal that jasmonic acid and jasmonic acid-amino acid conjugates play different roles in herbivore resistance of *Nicotiana attenuata*. *Plant Physiology* 2008;146:904-15.
- [140] Wang N and Nobel PS. Doubling the CO₂ concentration enhanced the activity of carbohydrate-metabolism enzymes, source carbohydrate production, photoassimilate transport, and sink strength for *Opuntia ficus-indica*. *Plant Physiology* 1996;110:893-902.
- [142] Wardlaw IF. Tansley Review No. 27 The control of carbon partitioning in plants. *New phytologist* 1990;116:341-81.
- [143] Webb J and Gorham P. Translocation of photosynthetically assimilated C¹⁴ in straight-necked squash. *Plant physiology* 1964;39:663.

References

- [144] Werner T, Motyka V, Laucou V, Smets R, Van Onckelen H, and Schmülling T. Cytokinin-deficient transgenic *Arabidopsis* plants show multiple developmental alterations indicating opposite functions of cytokinins in the regulation of shoot and root meristem activity. *The Plant Cell Online* 2003;15:2532-50.
- [145] Wheeler D and Power I. Comparison of plant uptake and plant toxicity of various ions in wheat. *Plant and Soil* 1995;172:167-73.
- [146] Wolfe RR and Chinkes DL. Isotope tracers in metabolic research: principles and practice of kinetic analysis: John Wiley & Sons, 2005.
- [147] Yang D-L, Yao J, Mei C-S, Tong X-H, Zeng L-J, Li Q, et al. Plant hormone jasmonate prioritizes defense over growth by interfering with gibberellin signaling cascade. *Proceedings of the National Academy of Sciences* 2012;109:E1192-E200.
- [148] Yen T-C, See L-C, Lai C-H, Yah-Huei CW, Ng K-K, Ma S-Y, et al. 18F-FDG uptake in squamous cell carcinoma of the cervix is correlated with glucose transporter 1 expression. *Journal of Nuclear Medicine* 2004;45:22-9.
- [149] Zagrobelny M, Bak S, Ekstrøm C, Olsen C, and Møller B. The cyanogenic glucoside composition of *Zygaena filipendulae* (Lepidoptera: Zygaenidae) as effected by feeding on wild-type and transgenic lotus populations with variable cyanogenic glucoside profiles. *Insect biochemistry and molecular biology* 2007;37:10.
- [150] Zamski E and Schaffer AA. Photoassimilate distribution in plants and crops: source-sink relationships: Marcel Dekker Inc., 1996.
- [151] Zavala JA and Baldwin IT. Jasmonic acid signalling and herbivore resistance traits constrain regrowth after herbivore attack in *Nicotiana attenuata*. *Plant, cell & environment* 2006;29:1751-60.
- [152] Ziegler H. Nature of transported substances. *Transport in Plants I*: Springer; 1975, p. 59-100.
- [153] Zissen MH, Kunz P, Subbarayan M, Chin FT, Conti PS, Fisher GA, et al. 18F-5-fluorouracil dynamic positron emission tomography/computed tomography shows decreased tracer activity after bevacizumab in colorectal metastases. *Nuclear medicine communications* 2011;32:343-7.

Aknowledgements

Aha! Finally I reach ‘Writing Aknowledgements’ point. I like writing aknowledgements because it reminds me that I must be in the end of completing my *painful scientific writing endeavor* and at the same time, it brings up the most cherishable memories I shared with all the people during that journey.

Thus, Thanks to all who, knowingly or unknowingly, helped me to get to this stage of 100+ page document.

After said so, my first and foremost thanks goes to my boss, **Dr. Aleš Svatoš**. He is a constant source of motivation and support during my study. I was quite a novice student when I started my doctoral research. Now, at the verge of finishing my studies, I look back and say thanks to Aleš for his guidance and constant encouragement, for it helped me survive or rather thrive through this tedious PhD journey. In addition to his excellent scientific profile, he is very generous, kind and supportive mentor and I feel privileged having had opportunity to work with him.

I am very grateful to my co-supervisors, **Prof. Dr. Hans Peter Saluz**, and **Dr. Marco Kai** for their constructive suggestions (criticisms!), encouragement and support that were invaluable in my research.

I would like to thank **Dr. Peter Gebhardt** for helping me out with plant radiotracer experiments, **Dr. Marco Kai** for MS measurements, his patience with me and teaching me about MS troubleshooting (I caused so many trouble, you (I) know! but thus allowing possibility for troubleshooting), **Dr. Stefan Meldau** for collaboration on ‘FDG application in *N. att.*’ project, **Dr. Christian Paetz** for his indispensable help in elucidating F-compounds using NMR, **Prof. Sebastian Böcker** and **Kerstin Scheubert** for their cooperation on *A. thaliana* metabolomics project, **Klaus** and **Thomas** for letting me use IP for radiotracer imaging experiments. I also thank **Riya, Mayuri, Dong** and **Filip** for all the help and nice company in the lab. I would like thank **Dr. Jerrit Weißflog** for all the scientific help (~theoretical and practical chemistry vol I) and also for scientific and (particularly) non-scientific discussions about science, life, universe and everything...

Aknowledgements

I would specially thank **Sybille Lorenz** for all the help and endless support from scientific to administrative stuff. Also for nice conversations and and putting good restraint on our office jokes. I thank **Natalie, Yvonne** and **Antje** for their help and support.

I appreciate **Dr. Karin Groten** for her always ‘ready to help’ persona and invaluable advices which helped me to tackle the problems I faced during my stay in Jena. I thank **Ms. Ellen Hascher** for her patience and tireless efforts in improving my Deutsch skills.

I sincerely aknowledge International Max Planck Research School and the Max Planck Society for providing me with a PhD fellowship and a excellent platform with state of the art MS laboratory facilities for my research work.

I would like to thank all the administrative staff, green-house people (especially, **Andreas**), IT department (especially **Martin**) and workshop team at the Max Planck Institute for Chemical Ecology for helping me in various ways during my studies.

My social life in Jena would not have been enjoyable without all my friends, I’ve met. Special thanks to **Ilka, Anna, Radek, Catarina** for all their time they shared with me. I also thank **Prashant, Abu, Suyog, Pavan, Sneha, Vijay, Amol-2, Joy, Raja, Rakesh, Karen, Madhunita, Kirti** for their time and support in numerous ways throughout my stay in Jena. Also I thank Baldwin’s (**Felipe, Michi, Mariana, Vari, Arne, Martin, Matthias**) for enjoyable Mahlzeit and coffee times. I would like to specially mention my friends **Claudia** and **Julia** for being there for me during all these years.

Curriculum Vitae

Mr. Amol Fatangare. (M.Sc., M.Tech.)

Mass spectrometry/Proteomics research Group,

Max Planck Institute for Chemical Ecology. Hans-Knöll-Straße 8, 07745, Jena.

Email : afatangare@ice.mpg.de

Education:

2011-present: PhD student, Friedrich-Schiller-University, Jena, Germany.

2009-2010: M.Tech. (Biotechnology), University of Pune, Pune, India.

2004-2009: M.Sc. (Biotechnology), University of Pune, Pune, India.

Research Experience:

PhD Thesis: Elucidating 2-deoxy-2-fluoro-D-glucose translocation, metabolism, and application in plants.

Duration: 2011 – till date. Supervisor: Dr. Aleš Svatoš.

Mass spectrometry/Proteomics research group, Max Planck Institute for Chemical Ecology, Hans-Knöll-Straße 8, D-07745, Jena, Germany.

M.Tech. dissertation: Protease Inhibitors (PI) formulation conferring resistance against *Helicoverpa armigera*.

Duration: 2009 – 2010. Supervisor: Dr. Ashok Giri.

Biochemical Science Department, National Chemical Laboratory, Pune-411008, India.

M.Sc. dissertation: Heterologous Expression, Purification and Characterization of recombinant β -Glucosidase from *Leucaena leucocephala*.

Duration: 2008 – 2009. Supervisor: Dr. Bashir Khan.

Biochemical Science Department, National Chemical Laboratory, Pune-411008, India.

B.Sc. research project: Study of Polymorphism in honeybee species *Apis cerana* with reference to LDH allozyme variation, wing morphometric indices and chromosomal compliments.

Duration: 2006 – 2007. Supervisor: Dr. Baban Nath.

Department of Zoology, University of Pune, Pune-411007, India.

Research Interest:

- Identification and characterization of plant metabolites.
- Mass spectrometry based metabolomics.

Publications:

1. **Fatangare A**, Paetz C, Schneider B, Saluz HP, Svatoš A. 2-deoxy-2-fluoro-D-glucose metabolism in *Arabidopsis thaliana*. (Manuscript in preparation)
2. Meldau S, Woldemariam MG, **Fatangare A**, Svatoš A, Galis I. Using 2-deoxy-2-[¹⁸F]fluoro-D-glucose ([¹⁸F]FDG) to study carbon allocation in plants after herbivore attack. (Submitted to BMC research notes)
3. **Fatangare A**, Gebhardt P, Saluz HP, Svatoš A. (2014). Comparing 2-[¹⁸F]fluoro-2-deoxy-D-glucose and [⁶⁸Ga]gallium-citrate translocation in *Arabidopsis thaliana*. *Nucl Med Biol.* 2014 Oct;41(9):737-43.
4. Shaik NM, Misra A, Singh S, **Fatangare AB**, Ramakumar S, Rawal SK, Khan BM. (2013). Functional characterization, homology modeling and docking studies of β -glucosidase responsible for bioactivation of cyanogenic hydroxynitrile glucosides from *Leucaena leucocephala* (subabul). *Molecular biology reports*, 40(2), 1351-1363.

Selected posters presentation and Talks:

1. Poster: “A combined XCMS and automated fragmentation trees alignment approach for rapid characterization of differentially induced metabolites.” International Mass Spectrometry Conference (IMSC)-2014, Geneva, Switzerland.
2. Talk: “High throughput analysis of differentially induced metabolites using metaXCMS and automated fragmentation tree alignment.” Plant science student conference (PSSC)-2013, Halle, Germany.
3. Talk: “Application of 2-[¹⁸F]fluoro-2-Deoxy-D-glucose (¹⁸FDG) in *in vivo* plant imaging.” Annual IMPRS Symposium-2013, MPI for Chemical Ecology, Jena, Germany.
4. Poster: “Analysis of FDG (2-deoxy-2-fluoro-D-glucose) fate in the plant cells”, Joint Conference of the Polish Mass Spectrometry Society (PTSM) and the German Mass Spectrometry Society (DGMS)- 2012, Poznan, Poland.
5. Poster: “FluoroDeoxyGlucose (FDG) radiotracer distribution and metabolism in plants.” Annual IMPRS Symposium-2012, MPI for Chemical Ecology, Jena, Germany.

Honours, Awards, Fellowships:

1. Member of IMPRS and JSMC (2011).
2. CSIR-UGC NET (Dec. 2009): qualified for National Eligibility Test for Junior Research Fellowship & LectureShip.
3. CSIR-UGC NET (Dec. 2008): qualified for LectureShip.
3. GATE (2008): Percentile - 99.97, All India Rank: 26. (Graduate Aptitude Test in engineering-Equivalent to subject GRE).

Declaration of independent work:

I hereby declare that I have written this thesis independently using mentioned resources, personal communications and cited literature. All the people involved in experimental implementation, data analysis or manuscript writing are listed as coauthors in the respective manuscripts. I was not assisted by anyone in completion of this thesis. The thesis has not been previously submitted to the Friedrich Schiller University, Jena or to any other university.

Eigenständigkeitserklärung

Die zurzeit gültige Promotionsordnung der Biologisch-Pharmazeutischen Fakultät der Friedrich-Schiller-Universität Jena ist mir bekannt. Die vorliegende Arbeit wurde von mir selbst und nur unter Verwendung der angegebenen Hilfsmittel erstellt und all benutzten Quellen angegeben. All Personen, die an der experimentellen Durchführung, Auswertung des Datenmaterials oder bei der Verfassung der Manuskripte beteiligt waren, sind benannt. Es wurde weder bezahlte noch unbezahlte Hilfe eines Promotionsberaters in Anspruch genommen. Die vorliegende Arbeit wurde bisher weder als Prüfungsarbeit für eine staatliche oder andere wissenschaftliche Prüfung noch bei einer anderen Hochschule als Dissertation eingereicht.



Jena, den 06.08.2015

Fatangare, Amol